# INVESTIGATION OF STRETCH AND CURVATURE EFFECTS ON FLAMES

By

Peiyong Wang

Dissertation

Submitted to the Faculty of the

Graduate School of Vanderbilt University

in partial fulfillment of the requirements

for the degree of

DOCTOR OF PHILOSOPHY

in

Mechanical Engineering

August, 2006

Nashville, Tennessee

Approved:

Professor Robert W. Pitz

Professor Mark A. Stremler

Professor Deyu Li

Professor Joseph A. Wehrmeyer

Professor Kenneth A. Debelak

*Dedicated*

*to*

*Rachel and Qiong*

## ACKNOWLEDGEMENTS

I would like to thank Dr. Robert W. Pitz and Dr. Joseph A. Wehrmeyer for their guidance and encouragement of this work and throughout my studies at Vanderbilt. I would also like to thank the other committee members, Dr. Deyu Li, Dr. Mark A. Stremler, and Dr. Kenneth A. Debelak, for their comments and suggestions for this dissertation. Special appreciation is given to fellow graduate student Shengteng Hu for his assistance in the experiments. I would like to express my appreciation to National Science Foundation for funding this research through Grant CTS-0314704. Finally, I would like to express my gratitude to my family. Without their support and love, I would never have succeeded.

## TABLE OF CONTENT

## LIST OF FIGURES

# CHAPTER I

# INTRODUCTION

## Motivation

The most elementary premixed flame is the one-dimensional planar premixed flame as shown in Fig. 1.1 ($S$ is the flame speed; $T$ is the temperature; $y$ is the species mass fraction; subscript $u$ and $b$ mean unburned and burned side respectively; superscript 0 means the one-dimensional unstretched planar flame); its study provides the understanding of basic flame characteristics including flame temperature, flame speed, extinction, etc. A further step is the study of the stretched planar flame with the opposed jet burner as shown in Fig. 1.2 which provides the information on the interaction of flow field and combustion. The preferential diffusion caused by stretch generates differences in flame temperature from the adiabatic equilibrium value and the differences depend on Lewis number, i.e., $Le$ and stretch rate ($Le=\alpha/D$ where $\alpha$ is the thermal diffusivity of the mixture and $D$ is the mass diffusivity of the deficient reactant). The one-dimensional planar flame is an ideal model and it is hard to apply its knowledge directly to practical flames. The stretched planar flame resembles practical flames more and an enormous amount of research has been done on it. However, most practical flames are not only stretched but also curved and it is necessary to extend the elementary study to the curved and stretched flames. The tubular burner shown in Fig. 1.3 applies to premixed flames and the opposed tubular burner shown in Fig. 1.4 applies to both premixed flames and diffusion flames. These burners are excellent tools to study curvature effects on flames. The tubular flames formed by these burners possess uniform curvature throughout the

flame front that is easy to characterize. The study of them will provide deeper understanding and better prediction of practical flames.

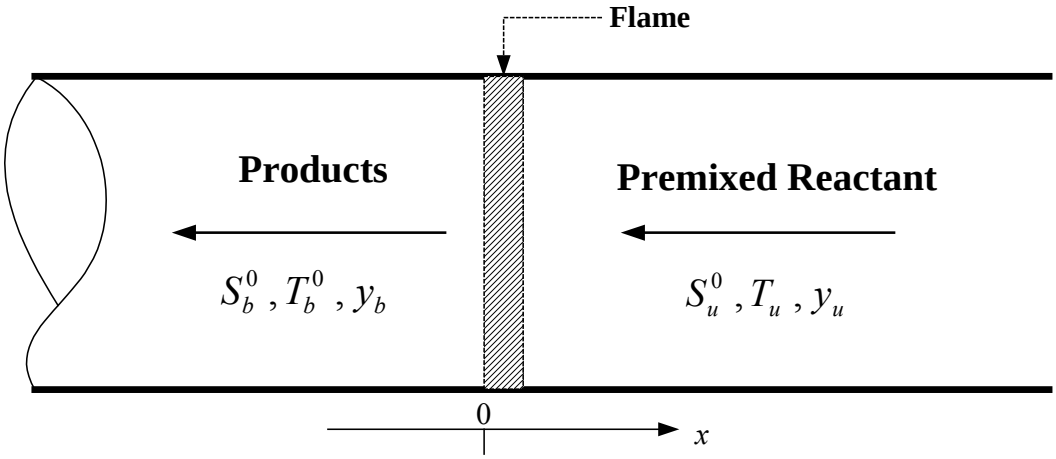


**Fig. 1.1**. Schematic of one-dimensional planar flame.

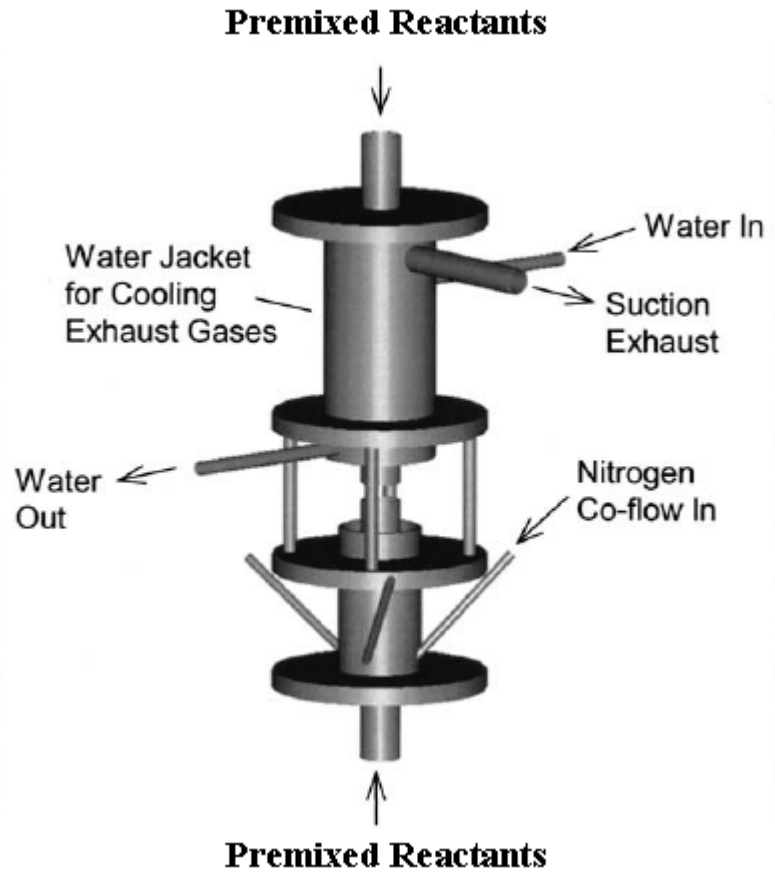


**Fig. 1.2**. Opposed jet burner.

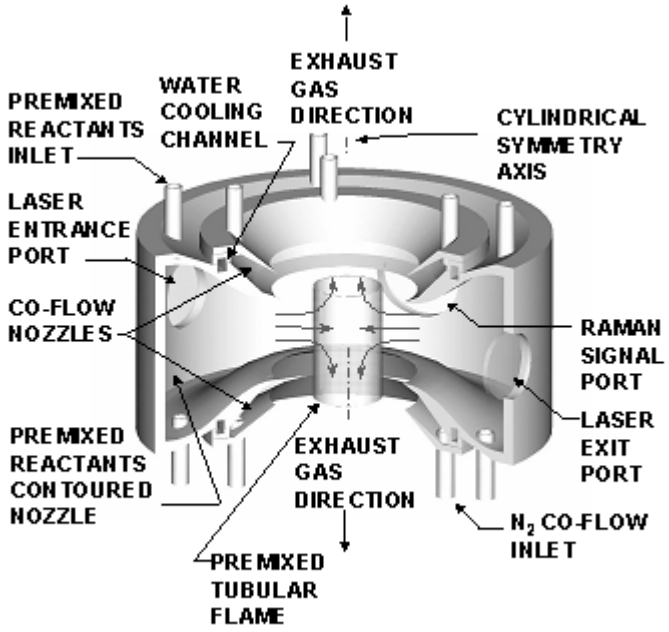


**Fig. 1.3**. Tubular burner.

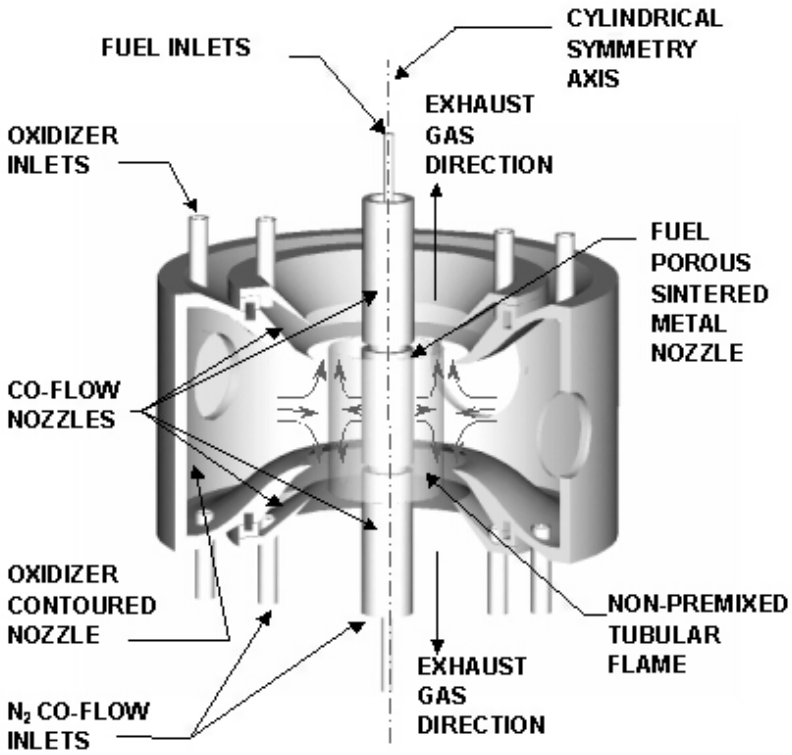


**Fig. 1.4**. Opposed tubular burner.

Most of the practical flames in engines and industry furnaces are turbulent flames. Turbulent flow is so complicated (i.e., 3D, unsteady) that it is generally described statistically. Combustion is also a complicated phenomenon involving convection, diffusion and chemical reactions. The coupling of these two phenomena makes it very hard to model and predict turbulent combustion. The DNS (direct numerical simulation) can model the turbulent flow field and combustion process simultaneously; however, it requires so much calculation time that it is not possible for real devices now. A popular modeling method for turbulent combustion is to separate the coupling of the flow field and combustion: give the statistical distribution of flow parameters of turbulent flow field (for example, the statistical distribution of stretch rate) and use the flame parameters responding to the flow parameters in laminar flames (for example, the flame speed and flame temperature obtained in the stretched laminar flames). The laminar flame responses to stretch such as flame speed and extinction stretch rate have been used in turbulent modeling (Peters, 2000). The turbulent flow field is a stretched flow field and the flamelets in it are generally curved. To understand and model turbulent combustion, the knowledge about flame responses to stretch and curvature is necessary. The direct motivation for studying the responses of laminar flames to stretch and curvature is the existence of stretched and curved flamelets in the turbulent combustion region when the flame thickness is less than Kolmogorov length (applies to most of the engines and furnaces).

## Previous Work

Williams (1975) gave the definition of stretch as $k = dA/dt/A$, which reflects the nonuniformity of the flow field relative to the flame. The area $A$ consists of the points that stay on the flame surface, that have the same normal velocity as the flame surface and that have the same tangential velocity with local fluid particles. So two parts cause the stretch rate: the local nonuniform flow field and the movement of a curved flame surface.

The laminar flame responses on premixed flames to stretch have been studied in detail for a long time by many researchers; it is almost fully understood. The typical negatively stretched flames are the tip of the Bunsen burner flame and the inwardly propagating spherical flame. The typical positively stretched flames are the opposed jet flame and the outwardly propagating spherical flame. Among these burners, the opposed jet burner creates steady and uniformly stretched flames; the stretch rate is well defined; the similarity solution can be obtained and the flame structure is one-dimensional. Because of these merits, it has been used extensively to study the stretch effect on flame temperature, flame speed, extinction, pollution formulation and so on. Two review papers by Law (1988), and Law and Sung (2000) have investigated these flames numerically and experimentally and analytical results with the integral method were given.

Sivashinsky (1976) and Buckmaster (1977) started asympotic studies on the stretch effects of premixed flames, followed by Clavin and Williams (1982), and Matalon and Matkowsky (1982). They are reviewed in Clavin (1985). Sivashinsky (1976) and Buckmaster (1977) indicated that the flame speed would increase with stretch rate when *Le* is less than one and decrease with stretch rate when *Le* is more than one. Clavin and

Williams (1982), and Matalon and Matkowsky (1982) indicated that the flame speed would increase with stretch rate when the *Le* is less than some critical value that is less than one. All of them agreed that the flame temperature increases with stretch rate if *Le* is less than one and vice versa. The disadvantage of the asymptotic analyses is that they only apply to small stretch rate and small deviation of Lewis number from unity. They also assume that the flame is infinitely thin, so there is no useful flame structure information provided and only the flame speed at product side is given.

Chung and Law (1988), and Sun et al. (1999) recognized the finite thickness of premixed flames and gave an integral analysis of premixed flame structure and properties. Since the flame has finite thickness, they obtained two flame speed expressions: one is defined at the product side and the other one is defined at fresh mixture side. They showed that the flame speed at the fresh mixture side increases with stretch rate if *Le* is less than one. The conclusion about the flame speed at product side is consistent with Clavin and Williams (1982), and Matalon and Matkowsky (1982). The conclusion about flame temperature is also consistent with those obtained by the asymptotic method.

All the above theoretical works both with the asymptotic and integral methods are based on the general flow field. Specifically, Tien and Matalon (1991) analyzed the flame speeds of the opposed jet flame with the asymptotic method. They showed that the flame speed at the fresh mixture side will increase with stretch rate when *Le* is less than some critical value that is more than one; and that the flame speed at the product side will increase with stretch rate when *Le* is less than some critical value that is less than one.

The physical explanation of the flame temperature response to stretch can be found in Law (1988). It showed a control volume bounded by the streamlines as shown in Fig. 6 of

Law (1988). There is heat loss from conduction out of the control volume and chemical energy gain from the species diffusion into the control volume. The flame temperature depends on the relative rates of mass and heat diffusions. For Lewis number less than one, mass diffusion coefficient is larger and the chemical energy gain is more than the heat loss, the flame temperature increases. For Lewis number more than one, the opposite effect appears. This phenomenon on flame temperature is called the preferential diffusion or Lewis number effect. The difference of flame temperature from its adiabatic value does not contradict the energy conservation law. Law (1988) explained this paradox as shown in Fig. 7 of Law (1988). The energy gain in product zone is balanced by the energy loss in preheat zone.

The physical explanation of the flame speed response is not given clearly in the literature. Some helpful information is found in Clavin (1985) where the control volume that is shown in its Fig. 9 comprises the preheat zone of a stretched flame, it is explained that the heat conduction from the reaction zone should be balanced by the convection since there is no temperature gradient at the fresh mixture boundary. With positive stretch, the transverse convection is added to the normal convection which means the flame speed (defined at the product side) is lowered for a given diffusion heat flux. However, since the heat conduction depends on the flame temperature that depends on the Lewis number; it is hard to determine the overall effect of stretch on flame speed. Only for unity Lewis number, it is safe to say that the flame speed at the product side is lowered by positive stretch. Clavin (1985) claimed that the flame speed would be lowered for most reactive mixtures and a possible exception is for lean hydrogen flames whose Lewis number is much less than one.

The numerical simulation of the opposed jet flames is first conducted by Kee et al. (1988) to study the extinction of $CH_4$/air premixed flames. It adopted the similarity solution to reduce the problem to a one-dimensional problem. A commercial code, OPPDIF of CHEMKIN originated from Kee et al. (1988) has been extensively used by combustion scientists. Other codes were used in Guo et al. (1997), Ju et al. (1997), and Giovangigli and Smooke (1987), which use the potential boundary conditions, i.e. no nozzles, and the stretch rate is constant everywhere outside the flame zones. Given appropriate definition of stretch rate, two kinds of codes with different boundary conditions could predict almost the same results. With complex chemistry, Ju et al. (1997), Sung and Law (1996), and Giovangigli and Smooke (1987) simulated the extinction of opposed jet flames. It is shown that the flames have two extinction limits; one is at very low stretch rate caused by radiation, the other one is at high stretch rate caused by stretch rate. For $CH_4$/air premixed flames whose Lewis number is close to one, when the stretch rate increases, the distance between the twin flames decreases; the residence time of reactants in the reaction zone becomes shorter. When this time is less than the chemical reaction time, the chemical reactions are incomplete and the flame temperature starts to decrease until it finally reaches extinction. The incompleteness of chemical reactions is the extinction mechanism for $CH_4$/air premixed flames and the flames will be extinguished at the center of the burner. For lean $C_3H_8$/air premixed flame whose *Le* is larger than one, increasing of stretch rate will decrease the flame temperature continuously due to Lewis number effect until extinction; the flame is extinguished at a certain distance away from the center of the burner. The combination of Lewis number effect and incompleteness of chemical reactions is the extinction mechanism. As pointed

out in Law (1988), the incompleteness of chemical reactions in the opposed jet burner is not the intrinsic character of stretch effects, it comes from the symmetry of the burner. In real flames, the flames may propagate freely; the extinction caused by the incompleteness of chemical reactions is invalidated. However, the extinction caused by preferential diffusion effect is an intrinsic character of stretch effects; the extinction stretch rate predicted or measured from the opposed jet flame can be used in real flames.

The experimental works using an opposed jet burner are enormous; combustion scientists used it to study all kind of flame phenomena such as flame stability, NOx formation, flame speed measurement, etc. Wu and Law (1984) measured the premixed flame speed and flame temperature variations with stretch rate for several mixtures. The experimental results showed that the flame speed at the fresh mixture side increases with stretch rate for lean $CH_4$/air, $C_3H_8$/air, $C_4H_{10}$/air, and lean and rich $H_2$/air flames. However, for $C_4H_{10}$/He/$O_2$ mixture whose Lewis number is much larger than one, the flame speed decreases with stretch rate. This result is consistent with the theoretical analysis by Tien and Matalon (1991). The measured flame temperature for lean $C_3H_8$/air $C_4H_{10}$/air and $C_4H_{10}$/He/$O_2$ flames whose Lewis number are more than one, decreases with stretch rate. This is consistent with the preferential diffusion effect. Law et al. (1986) measured the flame speed over a wide range of stretch rate and equivalence ratio for $CH_4$/air and $C_3H_8$/air flames. They also measured the extinction stretch rate over the full range of equivalence ratio for these flames. The results showed that the extinction stretch rate increases with equivalence ratio first, and then decreases. For $CH_4$/air flames, it peaks at the equivalence ratio 0.95; For $C_3H_8$/air flames, it peaks at the equivalence ratio 1.17. This result can be explained with the preferential diffusion effect. Since the Lewis

numbers of lean $CH_4$/air and rich $C_3H_8$/air flames are less than one, the preferential diffusion effect causes the flame temperature to peak at the equivalence ratio less than one for $CH_4$/air flame and more than one for $C_3H_8$/air flame (higher temperature means higher reaction rate and heat release rate, and so higher resistance to extinction). As for the flame structure, Law et al. (1994) and Sung et al. (1996) measured the opposed jet premixed flame structure with visible Raman scattering. Although the stretch rate tends to decrease the flame thickness, the freely standing premixed flame has an ability to relocate its position. For the freely standing premixed flame with Lewis number close to unity, the flame structure, flame thickness and flame speed are insensitive to stretch rate. The thickness of the freely standing flame tends to increase with stretch rate for Lewis number more than one and vice versa; however, the increase ratio is much smaller than that of stretch rate. Osborne et al. (1996) studied the flame structure of a partially premixed $CH_4$/air flame versus air with UV Raman scattering. Wehrmeyer et al. (2002) measured the flame structure of $C_3H_8$/air flame versus hot product with visible Raman scattering. Cheng et al. (2004) measured stretched lean $CH_4$/air flame versus hot products; one nozzle supplies the $CH_4$/air mixture and the other one supplies the $H_2$/air mixture that burned to products away from the $CH_4$/air flame. At moderate stretch rate, a normal premixed $CH_4$/air is observed; at high stretch rate or for very lean mixture, a diffusion-controlled weak flame is observed; the transition between the two states is very sensitive to chemical kinetics numerically. Similar phenomena are observed for the lean $C_3H_8$/air flame versus hot product in Wehrmeyer et al. (2002).

The stretch effects on premixed flames have almost been fully understood. The curvature effects and the interaction between curvature and stretch have caught the

attention of combustion scientists for a long time since the flamelets in turbulent flow field undergo both stretch and curvature. Tubular flames are good tools to study the curvature effects since the curvature is uniform around the whole flame. However, there is little literature reported on the theoretical study of tubular premixed flames. Ishizuka (1984,1989) and Yamamoto et al. (1994) studied the tubular premixed flame with rotation experimentally which is formed by injecting the fresh mixture tangentially from a slit on the tube wall into a long tube. The boundary conditions are not cylindrically symmetric. Although a tubular shape flame can be obtained with this burner, the flow field, the flame structure and the flame properties may be substantially different from the tubular flame without rotation. Especially, it is really hard to identify the stretch rate on this kind of tubular flame. However, in the theoretical study of the tubular flames with rotation, Takeno and Ishizuka (1986a), Nishioka et al. (1988, 1991), Yamamoto et al. (1996) and Libby et al. (1989) assumed that the mixture is injected into the tube with uniform radial and tangential velocities around the tube wall. In this case, the tubular flame with rotation is equivalent to that without rotation since the circumferential flow field can be uncoupled and solved separately. Takeno and Ishizuka (1986a) solved the flow field of the tubular flame with the constant density assumption. It is shown that ignoring the viscous term in the axial momentum conservation only gives a very tiny error if the Reynolds number is more than 10. A numerical simulation is also given with the assumptions of constant density, unity Lewis number and one-step chemistry. Numerical results indicated that the tubular flame could be extinguished by the incompleteness of chemical reactions; this phenomenon is consistent with that of the opposed jet flame. However, unlike the opposed jet flame where the incompleteness of

reactions is not the intrinsic character of stretch effects, the incompleteness of reactions is part of the intrinsic character of curved flames since the curvature restrains the flame movement (at least, it cannot propagate to a radius less than zero). Takeno et al. (1986b) solved the tubular flame asymptotically, the solution agreed well with the numerical solution by Takeno and Ishizuka (1986a). For non-unity Lewis number, the preferential diffusion effect also exists. Nishioka et al. (1988) modeled the rotating tubular flame with variable density. Compared to the constant density simulation, the combustion accelerates the axial and radial velocity due to thermal expansion seriously and decelerates the circumferential velocity due to increased viscosity; the expansion also increases the local stretch rate in the flame and extinguished the flame with less nozzle exit velocity. Libby et al. (1989) also did the asymptotic analysis on the tubular flame with variable density and non-unity Lewis number. In the above four papers, similar phenomena are observed and similar conclusions are drawn as the opposed jet flame; no specific results about the curvature effects are reported. Ishizuka (1993) reviewed the research on the tubular flames with and without rotation.

Klimov and Lebedev (1983) first studied the tubular premixed flames without rotation numerically for the incompleteness of chemical reactions in turbulent combustion. The potential boundary condition, one-step chemistry, constant heat and mass transport properties, and constant density are assumed. Kobayashi et al. (1988) carried out a similar numerical study based on the same assumptions. It is shown that the curvature of the tubular flame tends to enhance the preferential diffusion effect: For Lewis number less than one, the tubular flame has a higher flame temperature than the opposed jet flame; for Lewis number greater than one, the tubular flame has a lower flame temperature. As for

the extinction, the curvature of the tubular flame tends to weaken the flame and the tubular flame extinguishes at lower stretch rate when Lewis number is close to or more than one; when Lewis number is less than one but more than some critical value, the tubular flame has higher flame temperature, but it is extinguished at lower stretch rate.

The assumptions used by the above two authors are not physically realistic and more accurate simulation is needed. Dixon-Lewis (1990) modeled the tubular flame with plug boundary condition, dedicated heat and mass transport model, and complex chemistry for the first time. It discussed the relationship of chemical reactions and flame structure. The simulation of stoichiometric $CH_4$/air flames showed that the tubular flame is extinguished at lower stretch rate than the opposed jet flame. Dixon-Lewis et al. (1991) showed that the extinction stretch rate of the stoichiometric $CH_4$/air flame is remarkably sensitive to reaction kinetics. The extinction pressure eigenvalue for the stoichiometric $CH_4$/air is about 35% of that for the opposed jet flame at identical chemistry and other conditions. Smooke and Giovangigli (1990) also solved the tubular flames numerically with complex chemistry for the $CH_4$/air and $C_3H_8$/air premixed flames. The numerical results indicated that the tubular flames have lower extinction stretch rate and higher extinction diameter over the whole range of equivalence ratio for both flames. The comparison of extinction stretch rate between the numerical result by Smooke and Giovangigli (1990) and experimental result by Kobayshi and Kitano (1989) showed a good agreement. Ju et al. (1999) studied the radiation effect on tubular flames numerically with potential boundary conditions; its simulation for $CH_4$/air flames with the equivalence ratio from about 0.5 to 1.0 indicated that the tubular flame and the opposed jet flame has almost the same extinction stretch rate. Most of the above numerical simulations are concerned about the

extinction stretch rate, and the conclusions are diverse. Three major reasons might contribute to the problem: 1), the extinction of the flames is very sensitive to reaction kinetics; 2), the definition of stretch rate is not consistent among these papers; 3), the difference between the plug boundary conditions and the potential boundary conditions.

As for the flame structure, Mosbacher et al. (2002) used a modified version of the OPPDIF code to simulate the tubular $H_2$/air premixed flames. At low stretch rate, the simulation and experiment data agree very well on temperature and species structure; at high stretch rate close to extinction, the prediction has higher flame temperature and much higher extinction stretch rate than the experiment. They also showed that flame temperature and flame structure is sensitive to the transport properties.

Most of the experimental work on tubular flames comes from Kobayashi et al. (1989, 1991, 1993) and Mosbacher et al. (2002). Kobayashi and Kitano (1989) first introduced the tubular burner and measured the extinction stretch rate of the $CH_4$/air and $C_3H_8$/air premixed flames. For the $CH_4$/air flames, the tubular flame is extinguished at almost the same stretch rate as the opposed jet flame when the mixture is very lean; the tubular flame has lower extinction stretch rate for equivalence ratio more than about 0.75. For the $C_3H_8$/air flames, the tubular flame has lower extinction stretch rate for the equivalence ratio less than about 1.4 and has higher extinction stretch rate for the equivalence ratio more than about 1.4. Kobayashi and Kitano (1991) measured the flow field of the tubular flame. The axial velocity is confirmed to be a linear function of axial coordinate, which provides the experimental basis for the similarity method used in the numerical solutions. Kobayashi and Kitano (1993) measured and compared the extinction between the tubular flames and the opposed jet flames based on a different choice of stretch rates. In this

paper, the stretch rate is defined as the local stretch rate at the stagnation center (the maximum stretch rate). The measured extinction stretch rates of the premixed $CH_4$/air tubular flames are much higher than those of the opposed jet flames. The measured extinction stretch rates of the premixed $C_3H_8$/air tubular flames are much higher than those of the opposed jet flames up to an equivalence ratio of about 1.6. Part of the discrepancy between their two measurements (Kobayashi and Kitano, 1989,1993) might come from the definition of stretch rates and velocity measurement uncertainty in the high temperature zone. Mosbacher et al. (2002) measured the species and temperature structure in the tubular $H_2$/air flame with visible Raman scattering. The measured local equivalence ratio is consistent with the differential diffusion caused by stretch; $H_2$ diffuses faster than $O_2$; so the local equivalence ratio at the burner center is higher than that of the fresh mixture; as a balance, the local equivalence ratio in part of the preheat zone is less than that of the fresh mixture.

As for the diffusion flames, the opposed jet diffusion flames have been studied broadly. The earliest theoretical work is the asymptotic analysis by Linan (1974). He studied the extinction of the opposed jet flame; an explicit extinction expression on Damköhler number was given. The Damköhler number is defined as the ratio of diffusion time to chemical reaction time and it reflects the completeness of chemical reactions. As the stretch rate increases, the Damköhler number decreases, eventually the incompleteness of chemical reactions extinguishes the flame. Peters (1983) also studied the extinction of diffusion flames by stretch in turbulent flames. Both papers showed that the scalar dissipation rate (inversely proportional to diffusion time) is proportional to stretch rate. Both papers assumed unity Lewis numbers, no preferential diffusion effect is reported.

Law and Chung (1982), Chung and Law (1984), and Cuenot and Poinsot (1996) analyzed opposed jet diffusion flames with infinitely fast chemistry (Burke-Schumann assumption) and non-unity Lewis numbers. In this case, the preferential diffusion effect is emphasized. It is shown that the preferential diffusion effect exists on both the fuel side and the oxidizer side of the flame. For example, when the Lewis number of the fuel or oxidizer is less than one, the flame temperature is higher than its adiabatic equilibrium temperature. The adiabatic equilibrium temperature is the temperature with unity Lewis numbers assumptions, i.e. $Le_f = Le_o = 1$; it is a constant under the infinitely fast chemistry assumption, Glassman (1996). If the Lewis number of the fuel or oxidizer is more than one, the flame temperature is less than its adiabatic equilibrium value. However, the preferential diffusion effect just gives a constant temperature change under infinitely fast chemistry, that is, the temperature increase or decrease is independent of stretch rate. With one-step high-activation-energy finite rate chemistry, Chung and Law (1983), and Cuenot and Poinsot (1996) gave the flame temperature and extinction expressions with stretch rate and Lewis numbers. Sung et al. (1995) studied the opposed jet diffusion flame structure numerically and experimentally. Unlike the premixed flame that can relocate its position upon stretch rate variation, the position of the diffusion flame is fixed and the thickness of diffusion flame decreases with stretch rate monotonically, which is consistent with the result of Cheng et al. (2006). The experimental data has a good agreement with the numerical data in Sung et al (1995); it is shown that the flame thickness is proportional inversely to the square root of stretch rate. As stretch rate increases, the intensive heat release increases because of higher flow rate; the specific heat release rate decreases because of lower Damköhler number. Sung et al

(1995) also showed the influence of chemical mechanism on the structure of the opposed jet flame. Brown et al. (1997) studied the flame structure and preferential diffusion for the opposed jet hydrogen diffusion flame. It is also shown that the flame thickness is inversely proportional to the square root of stretch rate.

The study of curvature effects on diffusion flames basically focused on two flames: the flame tip of the Burke-Schumann flames (Ishizuka, 1983; Ishizuka and Sakai, 1986; Im et al., 1990; Katta et al., 1994; Takagi et al., 1994, 1996a) and the perturbed opposed jet flames (Takagi et al., 1996b; Finke and Grünefeld, 2000; Yoshida and Takagi, 1998, 2003; Lee et al., 2000; Katta et al., 1998). Ishizuka and Sakai (1983, 1986) studied the extinction at the curved flame tip of the Burke-Schumann flame experimentally. The local extinction at the tip was observed with the mixture of hydrogen and carbon dioxide as the fuel stream. Im et al. (1990) also studied the flame tip theoretically and experimentally. The flame tip is negatively stretched (higher curvature causes higher negative stretch rate) which increases the residential time of reactants in reaction zone, it makes the flame tip stronger and harder to extinguish. For fuel stream with Lewis number less than one, preferential diffusion results in lower fuel concentration, lower temperature and possible extinction at the flame tip. Katta et al. (1994) and Takagi et al. (1994, 1996a) also studied similar flames numerically. In Takagi et al. (1996a), the flame tip temperature is much lower than the adiabatic equilibrium temperature if the fuel ($H_2/N_2$) comes from the inner nozzle, i.e. the flame is concave to the fuel stream and vice versa if the flame comes from the outer nozzle; detailed numerical analysis on flame structure substantiated the preferential diffusion effect. Takagi et al. (1996b), and Finke and Grünefeld (2000) perturbed the opposed jet flow field to form curved flames with

positive stretch. The experimental results are consistent with those from Burke-Schumann flames. When the flame is concave to the fuel stream ($H_2/N_2$) whose Lewis number is less than one, the flame is weak and the local extinction is observed and vice versa. The interesting negatively stretched flame surrounded by the positively stretched flame was formed at the center of the opposed jet burner by sucking the flow out at the center of the opposed jet burner in Yoshida and Takagi (2003). They studied the interactions among curvature, negative stretch and positive stretch. For the planar flame, the flame temperature increases as the stretch rate decreases from positive to negative values. With the same stretch rate, the flame has a higher temperature if the flame is convex to the $H_2/N_2$ fuel stream and lower temperature if the flame is concave to the fuel stream. The temperature differences increase as the stretch rate decreases.

However, for the above diffusion flames including both the flame tip of Burke-Schumann flame and the perturbed opposed jet flames, the flames are multidimensional and it is hard to identify the value of stretch rate; and sometimes, it is hard to separate the effects of stretch and curvature since stretch and curvature vary simultaneously when the operational conditions are varied. To overcome these difficulties, the opposed tubular burner was built and tested by Wehrmeyer et al. (2001). The main advantages of this burner are: 1), the flame structure is one-dimensional; 2), the flame is uniformly stretched and curved; 3), the stretch rate and curvature can be varied independently; 4), it has well established flow field. However, these kinds of opposed tubular diffusion flames have not been studied in detail.

## Objectives

Turbulent premixed flamelets are stretched and curved. Although the stretch effects on premixed flames are almost fully revealed, more work is needed to reveal the curvature effects on premixed flames. The current research is aimed at studying curvature effects on premixed flame responses including flame properties (such as flame temperature, flame speed and extinction stretch rate) and flame structure (such as temperature and species distributions) in stretched flow fields. The comparisons between tubular flames and opposed jet flames are used to reveal the curvature effects on stretched premixed flames. The physical analysis and numerical simulation are carried out to explain and prove the mechanism of curvature effects. An asymptotic analysis is also given to confirm the curvature effects obtained from the physical analysis. Based on the physical analysis, correlations on premixed flame temperature and flame speed are given and proved by asymptotic analysis. Premixed flame structures (lean $H_2$/air, $CH_4$/air, $C_3H_8$/air flames) are measured with visible Raman scattering and compared with the numerical results. Finally, the curvature theory on premixed flames is extended to apply for diffusion flames and the application is proved to be correct by numerical simulation.

## Organization

The dissertation includes 6 chapters. Chapter I describes the motivation and related background. It also briefly reviews the previous work about stretch and curvature effects on flames. Chapter II ~ Chapter V mainly concentrate on the analysis and numerical simulation. Chapter II derives the stretch rate expression for the tubular flames; which provides a basis for comparison between the opposed jet flame and the tubular flame.

Chapter III reveals the curvature effects on premixed flames by comparing the opposed jet flame and the tubular flame numerically; it also analyzes the physical mechanism of curvature effects on premixed flames. Chapter IV analyzes the tubular flame asymptotically and gives correlations of flame speed and flame temperature for curved and stretched premixed flames. Chapter V studies the curvature effects on diffusion flames numerically. Chapter VI describes the measured flame structure of lean $H_2$/air, $CH_4$/air and $C_3H_8$/air premixed flames with visible Raman scattering and compares it with numerical simulations.

# CHAPTER II

# STRETCH RATE OF THE TUBULAR FLAMES


## Abstract

Following Seshadri and Williams (1978) solution describing the flow field for the opposed jet burner, the analytical solution is given for the flow field of two other burners: the opposed tubular burner and the tubular burner. Under plug flow boundary conditions, it is shown that the stretch rate at the stagnation surface of the opposed tubular burner is $k = \pi V /(R_2 - R_1)$ for the case of equal velocities and equal densities (i.e. $\rho_1 = \rho_2$ and $V_1 = -V_2 = V$). For the tubular burner, the stretch rate at the center of the burner is $k = \pi V / R_2$ . The comparison of the numerical simulation and analytical solution is carried out to verify the analytical solution.


## Introduction

The idea of a laminar stretched flamelet has been used in turbulent modeling for both premixed and diffusion flames (Peters, 1986; Hilbert et al., 2004). The planar stretched flamelet, which is realized by the opposed jet burner as schematized Fig. 2.1, has been fully studied analytically, numerically and experimentally as reviewed by Law (1988), Law and Sung (2000), and Clavin (1985). However, in turbulent combustion, the flamelets are generally curved and stretched. The tubular burner schematized in Fig. 2.2 (positively stretched and positively curved flame) applies to curved and stretched premixed flames. The opposed tubular burner schematized in Fig. 2.3 (positively stretched and positively curved flame outside, and positively stretched and negatively

curved flame inside) applies to both curved premixed and diffusion flames. These burners are excellent tools to study the combined effects of stretch and curvature. Tubular premixed flames have been studied analytically, numerically and experimentally by Klimov and Lebedev (1983); Dixon-Lewis et al. (1990,1991), Kobayashi et al. (1988,1989,1991,1993), Mosbacher et al. (2002), Takeno et al. (1986b), Ishizuka (1993), Ju et al. (1999), and Smooke and Giovangigli (1990). The opposed tubular burner can be realized by inserting a small tubular porous nozzle in the center of the tubular burner; it has been tested by Wehrmeyer et al. (2001).

Ishizuka (1984,1989), and Yamamoto et al. (1994) studied the tubular premixed flame with rotation experimentally which is formed by injecting the fresh mixture tangentially from a slit on the tube wall into a long tube. The boundary conditions are not cylindrically symmetric. Although a tubular shape flame can be obtained with this burner, the flow field, the flame structure and the flame properties may be substantially different from the tubular flame without rotation. However, in the theoretical study of the tubular flames with rotation, Takeno and Ishizuka (1986a), Nishioka et al. (1988, 1991), Yamamoto et al. (1996), and Libby et al. (1989) assumed that the mixture is injected into the tube with uniform radial and tangential velocities around the tube wall. In this case, the tubular flame with rotation is equivalent to that without rotation since the circumferential flow field is uncoupled and solved separately (Ishizuka, 1993; Takeno and Ishizuka, 1986a; Libby et al., 1989). The only property influenced by the vortex is the radial pressure gradient that is higher with rotation and could enhance the pressure diffusion in the radial direction. However, Yamamoto et al. (1996) has shown that the influence of the enhanced pressure diffusion on the flame position and flame temperature

is minimal. Ishizuka (1993) reviewed the research on the tubular flames with and without rotation.

Comparisons between the tubular flames and the opposed jet flames are generally used to understand how curvature affects the properties of stretched flames and these comparisons must be based on the same stretch rate on the flames. However, determining the correct values of stretch rate on these flames is a problem. Different scientists use different values based on different flow field assumptions; which could lead to different quantitative or qualitative conclusions. For example, Dixon-Lewis (1990) compared the extinction of the tubular and the opposed jet flames based on "applied stress" which is the square root of minus pressure eigenvalue divided by the fresh mixture density; Kobayashi and Kitano (1989) compared the extinction of the tubular and the opposed jet flames based on $2V/L$ as the stretch rate of the opposed jet flame and $-V_2/R_2$ as the stretch rate of the tubular flame; Kobayashi and Kitano (1993) used the local stretch rates at the stagnation line or the stagnation plane as the stretch rates of the tubular flame and the opposed jet flame. Ju et al. (1999) did the comparisons between the opposed jet flame and the tubular flame numerically with the potential flow boundary conditions; so it is hard to relate their definition of stretch rate to the geometry and nozzle velocity of the burners. Smooke and Giovangigli (1990) also did the comparisons numerically, but the definition of the stretch rate for the opposed jet flame is not stated clearly.

In this chapter, we solve the flow field of the tubular burner and the opposed tubular burner, and give the appropriate choice of stretch rates for comparison of different flames.

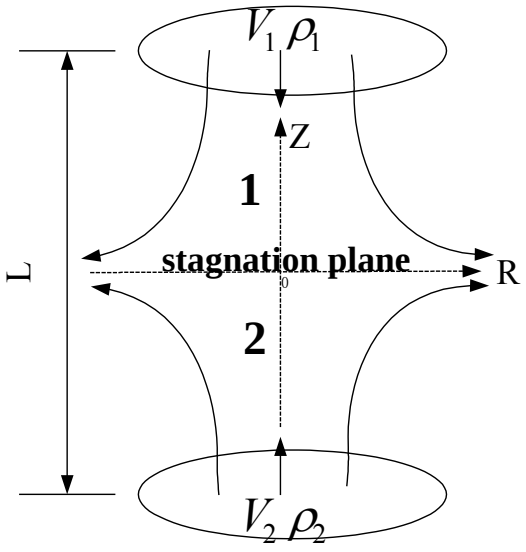


**Fig. 2.1**. Opposed jet burner schematic.

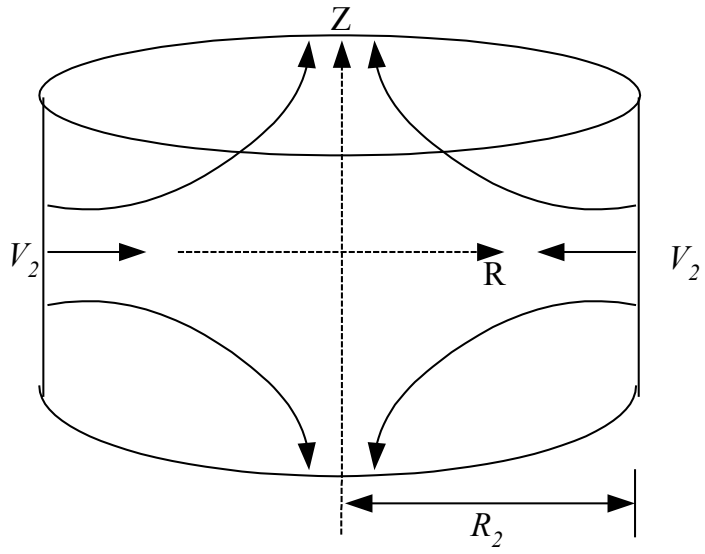


**Fig. 2.2**. Tubular burner schematic.

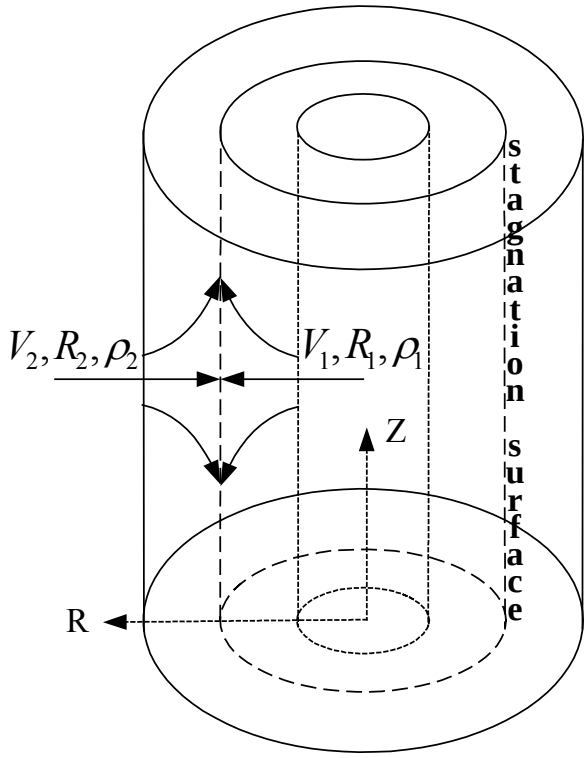


**Fig. 2.3**. Opposed tubular burner schematic

### Governing equations

Since we will compare the numerical solution with the analytical solution, this section will show the governing equations solved by the numerical code for the tubular flames and the opposed jet flame.

For the steady opposed tubular flame (Fig. 2.3), neglecting the buoyancy, the mass and momentum conservations are as in Dixon-Lewis (1991):

$$\frac{\partial(R\overline{\rho}U_Z)}{\partial Z}+\frac{\partial(R\overline{\rho}U_R)}{\partial R}=0 \tag{2.1}$$

$$\overline{\rho}U_Z\frac{\partial U_Z}{\partial Z}+\overline{\rho}U_R\frac{\partial U_Z}{\partial R}=-\frac{\partial p}{\partial Z}+\frac{\partial}{\partial Z}\left[\mu\left\{\frac{4}{3}\frac{\partial U_Z}{\partial Z}-\frac{2}{3R}\frac{\partial}{\partial R}\left(RU_R\right)\right\}\right]+\frac{1}{R}\frac{\partial}{\partial R}\left[\mu R\left(\frac{\partial U_R}{\partial Z}+\frac{\partial U_Z}{\partial R}\right)\right] \tag{2.2}$$

$$\overline{\rho}U_Z\frac{\partial U_R}{\partial Z}+\overline{\rho}U_R\frac{\partial U_R}{\partial R}=-\frac{\partial p}{\partial R}+\frac{\partial}{\partial R}\left[\mu\left\{2\frac{\partial U_R}{\partial R}-\frac{2}{3}\frac{\partial U_Z}{\partial Z}-\frac{2}{3R}\frac{\partial}{\partial R}\left(RU_R\right)\right\}\right] + \frac{\partial}{\partial Z}\left[\mu\left(\frac{\partial U_R}{\partial Z}+\frac{\partial U_Z}{\partial R}\right)\right]+\frac{2\mu}{R}\left(\frac{\partial U_R}{\partial R}-\frac{U_R}{R}\right) \tag{2.3}$$

Here, $p$ is the pressure; $\overline{\rho}$ is the density; $\mu$ is the dynamic viscosity; $U_R$ and $U_Z$ are the velocities in the radial and axial directions, respectively. As in Dixon-Lewis et al. (1991), Takeno and Ishizuka (1986a), and Yuan and Finkelstein (1956), a stream function $\psi(Z,R)=Zf(R)$ is assumed which satisfied the mass conservation exactly.

$$-\frac{\partial\psi}{\partial R}=R\overline{\rho}U_Z=-Z\frac{df}{dR}\ \text{and}\ \frac{\partial\psi}{\partial Z}=R\overline{\rho}U_R=f \tag{2.4}$$

Thus the radial velocity is a function only of $R$ and the axial velocity is a linear function of $Z$; this is the exact situation if the tubular nozzle's height is infinity. The height of real nozzle is finite. However, in the region where $Z$ is small such as it is within the height of the nozzle, the above stream function assumption is appropriate which has been demonstrated by the LDV measurement data of Kobayashi and Kitano (1991). Within this region, it is also appropriate to assume the temperature; species concentration, density and transport coefficients are functions of $R$ alone. The Mach number is very small (generally less than 0.05) in this region; the pressure is considered to be constant, but the pressure gradient terms still remain in the momentum equations and they are not zero. Neglecting the Dufour effect, the pressure diffusion and the work done by pressure and dissipation due to viscosity, the energy and species conservations are:

$$\overline{\rho}C_pU_R\frac{dT}{dR}+\frac{1}{R}\frac{d}{dR}\left(-R\lambda\frac{dT}{dR}\right)+\overline{\rho}\frac{dT}{dR}\left(\sum_i C_{pi}Y_iV_i'\right)+\sum_i h_i\varpi_i=0 \tag{2.5}$$

$$\overline{\rho}U_R\frac{dY_i}{dR}+\frac{1}{R}\frac{d}{dR}\left(R\overline{\rho}Y_iV_i'\right)-\varpi_i=0 \qquad (i=1\ldots K) \tag{2.6}$$

where $T$ is the temperature; $Y_i$ is the mass fraction of species $i$; $K$ is the number of species; $\lambda$ is the thermal conductivity; $C_p$ and $C_{p_i}$ are the average specific heat and specific heat of species $i$ respectively; $V_i^{'}$ is the diffusion velocity of species $i$; $h_i$ is the enthalpy per unit mass of species $i$ and $\varpi_i$ is the mass reaction rate per unit volume of species $i$.

The diffusion velocity are given by the mixture averaged formulation (Bird et al., 1960; CHEMKIN, 2000):

$$V_i' = -\frac{1}{X_i} D_{im} \frac{dX_i}{dR} - \frac{D_i^T}{\overline{\rho} Y_i} \frac{1}{T} \frac{dT}{dR} \quad \text{where} \quad D_{im} = \frac{1 - Y_i}{\sum_{j \neq i}^{K} X_j / D^{'}_{ji}} \tag{2.7}$$

or the multi-component formulation (Dixon-Lewis, et al., 1991; CHEMKIN, 2000):

$$V_i' = \frac{1}{X_i W} \sum_{j \neq i}^{K} W_j D_{i,j} \frac{dX_j}{dR} - \frac{D_i^T}{\overline{\rho} Y_i} \frac{1}{T} \frac{dT}{dR} \tag{2.8}$$

where $X_i$ is the molar fraction of species $i$; $W_j$ and $W$ are the molecular mass of the $j$-th species and the averaged molecular mass; $D_{i,j}$, $D_{im}$, $D^{'}_{ji}$ and $D^{T}_{i}$ are the multi-component, mixture averaged, binary and thermal diffusion coefficients, respectively. To satisfy the species conservation, a correction diffusion velocity $V_C = -\sum_i Y_i V_i'$ will be added to the diffusion velocities of all the species.

Applying Eq. (2.4) to momentum conservation equations:

$$\frac{1}{Z} \frac{\partial p}{\partial Z} = - \frac{(df / dR)^2}{\overline{\rho} R^2} + \frac{f}{R} \frac{d(df / dR \cdot 1 / \overline{\rho} R)}{dR} - \frac{1}{R} \frac{d(\mu R \cdot d(df / dR \cdot 1 / \overline{\rho} R) / dR)}{dR} = F_1(R) = J \tag{2.9}$$

$$\frac{\partial p}{\partial R} = F_2(R) \tag{2.10}$$

where $F_2(R)$ is a set of terms similar to the right hand side of Eq. (2.9). As discussed in Dixon-Lewis et al. (1991), from above equations, we can get $\partial[(1/Z)\partial p/\partial Z]/\partial Z = 0$ and $\partial[(1/Z)\partial p/\partial Z]/\partial R = 0$ (comes from $\partial^2 p/\partial Z\partial R = 0$) which means $(1/Z)\partial p/\partial Z$ is a constant for certain boundary conditions and is called the pressure eigenvalue *J*. Thus, one has,

$$\frac{dJ}{dR} = 0 \tag{2.11}$$

Defining

$$g = -\frac{1}{\overline{\rho}R}\frac{df}{dR} \tag{2.12}$$

the momentum conservation Eq. (2.9) is in the following form (Dixon-Lewis et al., 1991):

$$f\frac{dg}{dR} = \frac{d}{dR}\left(\mu R\frac{dg}{dR}\right) - R(J + \overline{\rho}g^2) \tag{2.13}$$

The boundary conditions are:

$R=R_1\neq 0 \quad f = R_1\rho_1 V_1 \quad g = 0 \quad T = T_1 \quad \overline{\rho}U_R Y_i + \overline{\rho}Y_i V_i' = \rho_1 V_1 Y_{i1}$

$R=R_1=0 \quad f = 0 \quad dg/dR = 0 \quad dT/dR = 0 \quad dY_i/dR = 0$

$R=R_2 \quad f = R_2\rho_2 V_2 \quad g = 0 \quad T = T_2 \quad \overline{\rho}U_R Y_i + \overline{\rho}Y_i V_i' = \rho_2 V_2 Y_{i2}$

The boundary conditions specify the total mass flux, including diffusion and convection, rather than the species mass fraction; hence concentration gradients can exist at the boundary allowing for diffusion into the nozzle.

The above equations have been previous solved for tubular flames (Dixon-Lewis et al., 1991; Dixon-Lewis, 1990; Mosbacher et al., 2002; Ju et al., 1999; Smooke and Giovangigli, 1990). Here we determine the solution for the opposed tubular flame as well. Using a modified version of the OPPDIF program (Mosbacher et al., 2002), we

numerically solve Eq. (2.5), Eq. (2.6), Eq. (2.7) or Eq. (2.8) (substitute $\overline{\rho}U_R = f / R$ in Eq. (2.5) and Eq. (2.6)) and Eq. (2.11) to Eq. (2.13) with perfect gas law, using complex chemistry and detailed transport properties (All the transport and thermodynamic properties are calculated by the transport and thermodynamic data package of CHEMKIN).

For the opposed jet flame, the OPPDIF program of CHEMKIN gives the numerical solution; it has similar assumptions and solves similar equations in which all the flame parameters are functions only of $Z$ and the pressure eigenvalue is defined as $(1/R)\partial p/\partial R$. The conservation equations can be found in Kee et al. (1988); which are listed below.

Recognizing that $U_R/R$ and other variables should be functions of $Z$ only, the following variables can be defined.

$$G(Z) = -\frac{\overline{\rho}U_R}{R} \quad \text{and} \quad F(Z) = \frac{\overline{\rho}U_Z}{2} \tag{2.14}$$

The mass conservation equation is reduced to:

$$G(Z) = \frac{dF(Z)}{dZ} \tag{2.15}$$

Axial velocity $U_Z$, $F$, $G$, $T$, $Y_i$, $\overline{\rho}$ are functions of $Z$ only.

Following the same procedure as the tubular flame, the following constant pressure eigenvalue and radial momentum conservation equation are deduced.

$$J = \frac{1}{R}\frac{\partial p}{\partial R} = \text{constant} \tag{2.16}$$

$$J - 2\frac{d}{dZ}\left(\frac{FG}{\overline{\rho}}\right) + \frac{3G^2}{\overline{\rho}} + \frac{d}{dZ}\left[\mu\frac{d}{dZ}\left(\frac{G}{\overline{\rho}}\right)\right] = 0 \tag{2.17}$$

Energy conservation:

$$\overline{\rho}C_p U_Z \frac{dT}{dZ} - \frac{d}{dZ}\left(\lambda \frac{dT}{dZ}\right) + \overline{\rho}\frac{dT}{dZ}\left(\sum_i C_{pi} Y_i V_i'\right) + \sum_i h_i \varpi_i = 0 \tag{2.18}$$

Species conservation:

$$\overline{\rho}U_Z \frac{dY_i}{dZ} + \frac{d}{dZ}\left(\overline{\rho}Y_i V_i'\right) - \varpi_i = 0 \tag{2.19}$$

The diffusion velocities can be calculated by Eq. (2.7) or Eq. (2.8) with the substitution of $R$ to $Z$.

Boundary conditions:

$Z$=0 $\quad F = \rho_2 V_2 / 2 \quad$ $G$=0 $\quad T = T_2 \quad \overline{\rho}U_Z Y_i + \overline{\rho}U_Z V_i' = \rho_2 V_2 Y_{i2}$

$Z$= $L$ $\quad F = \rho_1 V_1 / 2 \quad$ $G$=0 $\quad T = T_1 \quad \overline{\rho}U_Z Y_i + \overline{\rho}U_Z V_i' = \rho_1 V_1 Y_{i1}$

In the following numerical simulations for opposed jet flame and tubular flames, no gradients are observed at the boundaries and the mass flux boundary condition is equivalent to fixed mass fraction.

### Stretch rate definition

As suggested by Williams (1975), the definition of stretch rate is as follows.

$$k = \frac{1}{A}\frac{dA}{dt} \tag{2.20}$$

where $A$ consists of the points that stay on the flame surface, that have the same normal velocity as the flame surface and that have the same tangential velocity with local fluid particles. So the stretch rate includes two parts: the local flow divergence and the movement of a curved flame surface as indicated by Matalon (1983).

$$k = -[\nabla \times (\mathbf{U} \times \mathbf{n})] \cdot \mathbf{n} + v_n (\nabla \cdot \mathbf{n}) \tag{2.21}$$

where **U** is the local fluid velocity, **n** is the unit normal vector of flame surface, $v_n$ is the normal component of the velocity of flame surface and $\nabla \cdot \mathbf{n}$ is the flame curvature. For a steady flame, $v_n$ is 0, and the stretch rate just depends on flow field and flame shape.

We apply Eq. (2.21) to the opposed jet flame and the tubular flames.

Opposed jet flame;

$$k = \frac{1}{A}\frac{dA}{dt} = \frac{\partial U_R}{\partial R} + \frac{U_R}{R} = 2\frac{\partial U_R}{\partial R} \tag{2.22}$$

Tubular flames;

$$k = \frac{1}{A}\frac{dA}{dt} = \frac{\partial U_Z}{\partial Z} \tag{2.23}$$

**Analytical solutions for cold flow field**

Previously, Seshadri and Williams (1978) gave an analytical expression of stretch rate for the opposed jet burner and it is rewritten briefly below.

If we set the stagnation position as the origin of axial coordinate, i.e. $Z_s = 0$; the position of the nozzle 2 is $Z_2 = -L/[1 + |V_1 / V_2|(\rho_1 / \rho_2)^{0.5}]$ and the position of the nozzle 1 is $Z_1 = L + Z_2$.

The stretch rate in side 2:

$$k = 2 / L[|V_1|(\rho_1 / \rho_2)^{0.5} + |V_2|](1 - Z / Z_2) \qquad Z_2 < Z < 0 \tag{2.24}$$

The stretch rate in side 1:

$$k = 2 / L[|V_2|(\rho_2 / \rho_1)^{0.5} + |V_1|](1 - Z / Z_1) \qquad 0 < Z < Z_1 \tag{2.25}$$

For the case of $\rho_1 = \rho_2$ and $-V_1 = V_2 = V$, the above solution can be reduced to the following expression.

$$k = 4V(1 \pm 2Z / L) / L \tag{2.26}$$

where the plus sign is for $-L/2 < Z < 0$ and the minus sign is for $0 < Z < L/2$.

For the opposed tubular burner, if we normalize the distance, density and velocity by the values of the outer nozzle and assume constant dynamic viscosity and constant density, then the mass and axial momentum equations result in the following forms.

$$U_Z = uV_2 \quad U_R = vV_2 \quad R = rR_2 \quad Z = zR_2 \quad \overline{\rho} = \rho\rho_2 \tag{2.27}$$

$$\frac{\partial(r\rho u)}{\partial z} + \frac{\partial(r\rho v)}{\partial r} = 0 \tag{2.28}$$

$$\rho u\frac{\partial u}{\partial z} + \rho v\frac{\partial u}{\partial r} = -\frac{1}{\rho_2 V_2^2}\frac{\partial p}{\partial z} + \frac{1}{\mathrm{Re}}\nabla^2 u \tag{2.29}$$

$$\mathrm{Re} = \frac{\rho_2 V_2 R_2}{\mu} \tag{2.30}$$

$$r = 1 \qquad v = 1 \qquad u = 0 \quad \text{and} \quad \rho = 1 \tag{2.31}$$

$$r = R_1 / R_2 \quad v = V_1 / V_2 \quad u = 0 \quad \text{and} \quad \rho = \rho_1 / \rho_2 \tag{2.32}$$

In the inviscid layers outside the mixing layer, the Reynolds number is large enough such that the last term in the Eq. (2.29) is negligible. Since $u/z$ and $v$ are functions of $r$ only, we can express the velocities in the following form.

$$u = z\frac{m(r)}{r} \; ; \qquad v = \frac{n(r)}{r} \tag{2.33}$$

where $m$ and $n$ are functions of radial coordinate. For the cold flow field where the densities are constant, i.e. $\overline{\rho} = \rho_1$ on the inner side and $\overline{\rho} = \rho_2$ on the outer side, the density may be not continuous at the stagnation surface. The conservation equations now become:

$$m + \frac{dn}{dr} = 0 \tag{2.34}$$

$$\rho[(\frac{m}{r})^2 + \frac{n}{r}\frac{d(m/r)}{dr}] = -\frac{1}{\rho_2 V_2^2}\frac{\partial p}{z\partial z} = Q \tag{2.35}$$

The right hand side term of Eq. (2.35) is the normalized pressure eigenvalue $Q$ and is a constant in the flow field.

Substituting Eq. (2.34) into Eq. (2.35).

$$\rho[r(\frac{dn}{dr})^2 - rn\frac{d^2n}{dr^2} + n\frac{dn}{dr}] = Qr^3 \tag{2.36}$$

The boundary conditions are:

$$r = 1 \qquad n = 1 \quad \frac{dn}{dr} = 0 \text{ and } \rho = 1 \quad \text{for } r_s \le r \le 1 \tag{2.37}$$

$$r = R_1/R_2 \quad n = \frac{V_1 R_1}{V_2 R_2} \quad \frac{dn}{dr} = 0 \text{ and } \rho = \rho_1/\rho_2 \text{ for } R_1/R_2 \le r \le r_s \tag{2.38}$$

where $r_s$ is the value of $r$ at the stagnation surface.

The same equation as Eq. (2.36) with different boundary conditions can be found in Takeno and Ishizuka (1986a). Since the solution of the tubular flame with rotation is independent of the circumferential flow field if the boundary conditions are independent of azimuthal coordinate, it is a natural result that we got the same differential equation as in Takeno and Ishizuka (1986b). Eq. (2.36) has the solution form $n = a\sin(\sqrt{Q/\rho}r^2/a/2 + b)$ where $a$ and $b$ are constants which will be determined by the boundary conditions (As in Yuan and Finkelstein (1956), $n\cdot(d^2n/d\eta^2) - (dn/d\eta)^2 = -Q/(4\rho)$ results from substituting $\eta = r^2$, which has a solution form $n = a\sin(\sqrt{Q/\rho}\eta/a/2 + b)$ ).

Applying above solution form to Eq. (2.36) and boundary condition Eq. (2.37), the solution from $r$ = 1 to the stagnation surface $r_s$ is:

$$n = \sin(0.5Q^{0.5}r^2 + \pi/2 - 0.5Q^{0.5}) \tag{2.39}$$

The stretch rate is

$$k = \frac{\partial U_z}{\partial Z} = \frac{V_2}{R_2}\frac{\partial u}{\partial z} = -\frac{V_2}{R_2}\frac{dn}{rdr} = -\frac{V_2}{R_2}Q^{0.5}\cos(0.5Q^{0.5}r^2 + \pi/2 - 0.5Q^{0.5}) \tag{2.40}$$

At the stagnation surface where $n = 0$, $k = -\frac{V_2}{R_2}Q^{0.5}$

For Eq. (2.36) and boundary condition Eq. (2.38), the solution for $r = R_1/R_2$ to the stagnation surface $r_s$ is:

$$n = \frac{V_1R_1}{V_2R_2}\sin(\frac{V_2R_2}{V_1R_1}\sqrt{\frac{Q\rho_2}{4\rho_1}}r^2 + \frac{\pi}{2} - \frac{V_2R_1}{V_1R_2}\sqrt{\frac{Q\rho_2}{4\rho_1}}) \tag{2.41}$$

$$k = -\frac{V_2}{R_2}(\frac{\rho_2}{\rho_1}Q)^{0.5}\cos(\frac{V_2R_2}{V_1R_1}\sqrt{\frac{Q\rho_2}{4\rho_1}}r^2 + \frac{\pi}{2} - \frac{V_2R_1}{V_1R_2}\sqrt{\frac{Q\rho_2}{4\rho_1}}) \tag{2.42}$$

At the stagnation surface where $n = 0$, $k = -\frac{V_2}{R_2}(\frac{\rho_2}{\rho_1}Q)^{0.5}$

For $\rho_1 \neq \rho_2$, the stretch rate is not continuous at the stagnation surface, which comes from the assumption of a density jump at the stagnation surface. If $\rho_1 = \rho_2$, this problem disappears.

By matching the above two solutions for their respective regions at the stagnation surface where $n = 0$, we can obtain the value of $Q$ and stagnation radius $r_s$,

$$0.5Q^{0.5}r_s^2 + \pi/2 - 0.5Q^{0.5} = 0$$

$$\frac{V_2R_2}{V_1R_1}\sqrt{\frac{Q\rho_2}{4\rho_1}}r_s^2 + \frac{\pi}{2} - \frac{V_2R_1}{V_1R_2}\sqrt{\frac{Q\rho_2}{4\rho_1}} = 0$$

which leads to the following solution:

$$\sqrt{Q} = [(R_2/R_1 - \sqrt{\rho_1/\rho_2}V_1/V_2)/(R_2/R_1 - R_1/R_2)]\pi \tag{2.43}$$

$$r_s = [1-(R_2/R_1 - R_1/R_2)/(R_2/R_1 - \sqrt{\rho_1/\rho_2}V_1/V_2)]^{0.5} \quad (2.44)$$

Here, we define $R_r = R_2/R_1$ and $V_r = -V_2/V_1$; Fig. 2.4 shows how the pressure eigenvalue $Q$ and stagnation radius $r_s$ vary with $V_r$ for given $R_r$. As $V_r$ increases, the stagnation surface is pushed inside; both $r_s$ and $Q$ decreases; when $V_r \to \infty$; $r_s \to 1/R_r$, $Q^{0.5} \to \pi/(1-1/R_r^{\,2})$ and $k \to -\pi V_2 R_2/(R_2^{\,2} - R_1^{\,2})$ at the outer side of the stagnation surface. As $V_r$ decreases, the stagnation surface is pushed outside; both $r_s$ and $Q$ increases; when $V_r \to 0$ ; $r_s \to 1$ , $(Q\rho_2/\rho_1)^{0.5} \to \pi/[V_r R_r(1-1/R_r^{\,2})]$ and $k \to \pi V_1 R_1/(R_2^{\,2} - R_1^{\,2})$ at the inner side of the stagnation surface.

For the case of $\rho_1 = \rho_2$ and $V_1 = -V_2 = V$; the solution can be simplified as:

$$r_s = (R_1/R_2)^{0.5} \text{ i.e. } R_s = (R_1 R_2)^{0.5}$$

$Q = \dfrac{\pi^2}{(1-R_1/R_2)^2}$ which means: $k = \dfrac{\pi V}{R_2 - R_1}$ at the stagnation surface.

## Results and discussion

Fig. 2.5 shows the radial velocity and stretch rate comparisons of the numerical solution and the above analytical solution for cold air-to-air flow in the opposed tubular burner. The boundary conditions for this figure are: $R_1$ = 0.3cm, $R_2$ = 1.5cm, $V_1$ = -$V_2$ = 30cm/s. The analytical and numerical results are in excellent agreement that demonstrates the appropriateness of the above analysis.

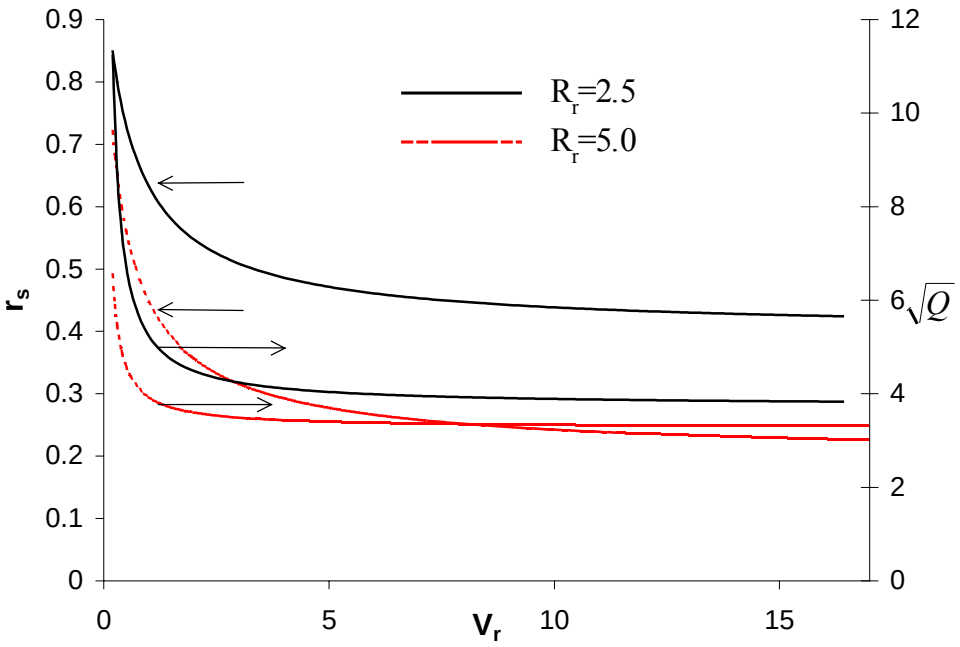


**Fig. 2.4**. Pressure eigenvalue and stagnation radius of the opposed tubular burner ( $\rho_1 = \rho_2$ ).

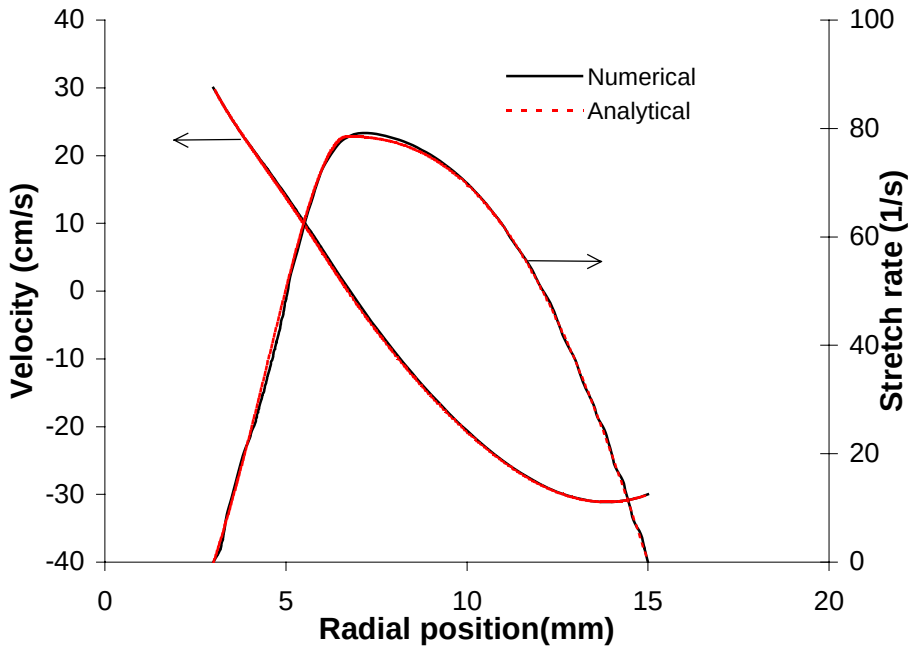


**Fig. 2.5**. Radial velocity and stretch rate variation with radial position of the opposed tubular burner (cold air flow, $R_1$=0.3cm, $R_2$=1.5cm, $V_1$=-$V_2$=30cm/s).

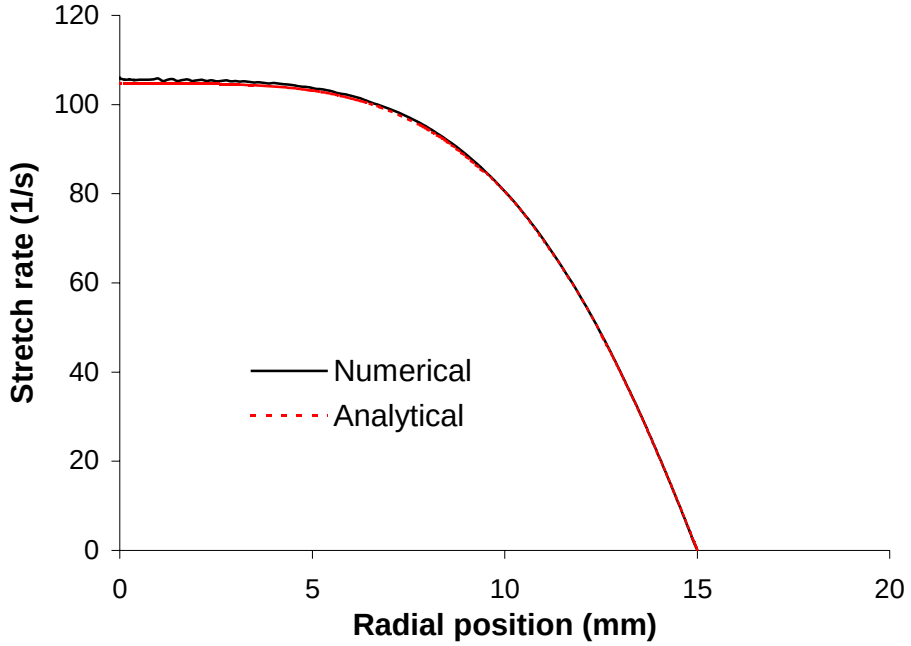


**Fig. 2.6**. Stretch rate variation with radial position of the tubular burner without flame (cold air flow, $V_2$=-50cm/s, $R_2$=1.5cm).

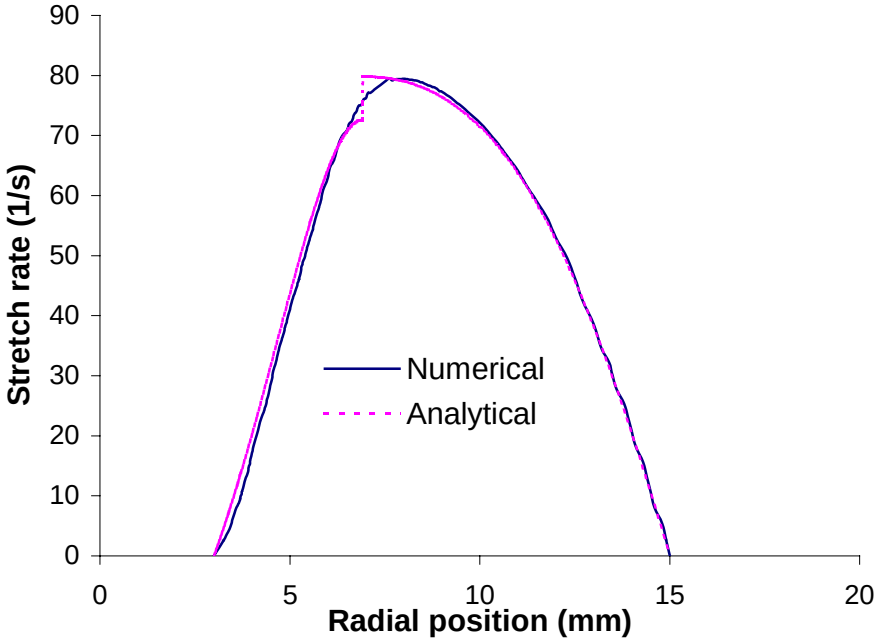


**Fig. 2.7**. Stretch rate variation with radial position for the opposed tubular burner (cold air-air/helium flow, $R_1$=0.3cm, $R_2$=1.5cm, $V_1$=-$V_2$=30cm/s, $\rho_2 = 0.99$ Kg/m$^3$, $\rho_1 = 1.2$ Kg/m$^3$).

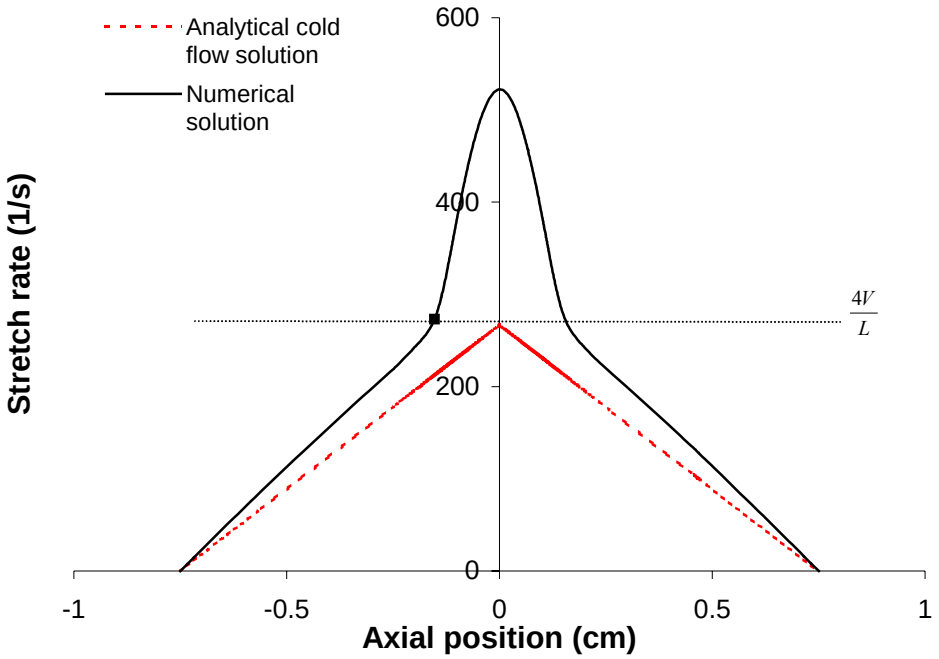


**Fig. 2.8**. Stretch rate variation with axial position for the opposed jet flame ($V$ = 100cm/s, $L$ = 1.5 cm, $H_2$/air twin premixed flame, equivalence ratio = 0.25).

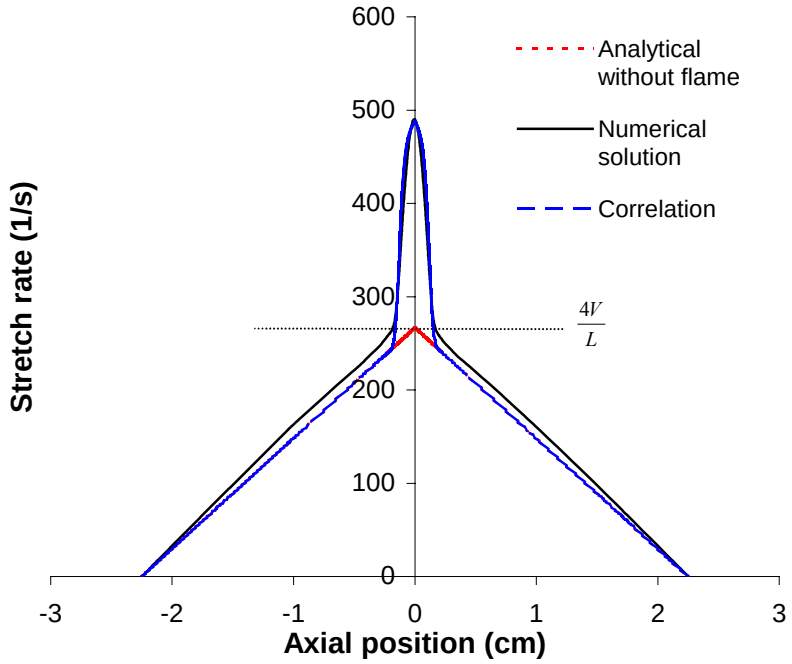


**Fig. 2.9**. Stretch rate variation with axial position for the opposed jet flame ($V$ = 300cm/s, $L$ = 4.5 cm, $H_2$/air twin premixed flame, equivalence ratio = 0.25).

If $R_1$ shrinks to 0, the opposed tubular burner becomes a tubular burner. The solution for the tubular burner follows from the opposed tubular burner solution where $Q^{0.5} = \pi$.

$$n = \sin(0.5\pi r^2) \tag{2.45}$$

$$k = -\frac{\pi V_2}{R_2}\cos(0.5\pi r^2) \quad \text{and} \quad k = -\pi V_2 / R_2 \text{ at the stagnation line, } r = 0. \tag{2.46}$$

In fact, for $R_1$ = 0, the above two equations recover the solution of Takeno and Ishizuka (1986a). The notable characteristic of the cosine function is that it is almost constant and equal to one when $r$ is small. For example, $r$ = 0.4, it is 0.97 and $r$ = 0, it is 1; Thus, the cold flow stretch rate in a large region around the center of the burner is constant, $-\pi V_2/R_2$. Fig. 2.6 shows that the numerical and analytical results have excellent agreement for $V_2$ = -50 cm/s, $R_2$ = 1.5cm. The stretch rate is almost constant of 105 $s^{-1}$ when $r$ is less than 0.6cm. So we can adjust $R_2$ to locate the flame in this constant stretch rate region in the calculation.

Fig. 2.7 shows a case of $\rho_2 / \rho_1 = 0.827$ for the opposed tubular burner, the agreement between numerical solution and analytical solution is very good except in the narrow mixing zone around the stagnation surface where there is a discontinuity of stretch rate at the stagnation surface in the analytical curve. When the ratio $\rho_2 / \rho_1$ is within 0.8~1.2, the above analytical solution can be used because the jump is small (within 10%).

When there is a flame in the flow field, the pressure eigenvalue changes from that of the cold flow field. The analytical solutions for the opposed jet burner and the tubular burners will still be valid in the following two situations:

1. If the distance between the twin flames is very small compared to $L$ for the opposed jet flame or the flame radius is tiny compared to the nozzle radius $R_2$ for the tubular flame

(i.e. the combustion region is tiny compared to the whole flow field), the combustion expansion has minor influence on the flow field of the fresh mixture and the eigenvalues almost do not change. Fig. 2.8 and Fig. 2.9 show the comparisons of stretch rate variation with axial distance between the lean $H_2$/air (numerical) premixed flame and the cold flow (no flame, analytical) for the opposed jet burner. The chemical reaction mechanism is from Mueller et al. (1999). For small $L$ as in Fig. 2.8, in the fresh mixture region, the numerical solution with the flame and the analytical solution without the flame are significantly different, i.e., the combustion expansion substantially changes the pressure eigenvalue and the flow field in the fresh mixture region. For larger $L$ as in Fig. 2.9, the numerical and analytical solutions are almost the same in the fresh mixture region, i.e., the combustion expansion only slightly changes the cold flow field.

2. For both of the opposed jet burner and the tubular burner, the flame structure and flame properties (i.e., flame temperature, flame speed, temperature and species concentration distribution, etc.) just depend on $V/L$ or $V_2/R_2$. Figures 2.10, 2.11 and 2.12 show the numerical predictions of temperature, axial velocity and stretch rate variation with axial position of the opposed jet flame for different $L$ (0.75cm, 1.5cm, 3.0cm and 4.5 cm) while keeping $V/L$ constant. From these figures, we can see that the flame structure does not depend on the value of $L$. Once the value of $V/L$ is set, the flame structure is determined. The same conclusion holds for the tubular flame as indicated from the numerical result in Figures 2.13, 2.14 and 2.15 ($R_2$= 4.5mm, 7.5mm, 15mm and 30mm). That means, no matter how large the flame region is, we can use large enough values of $L$ and $R_2$ to analyze the flame using the above analytical solutions.

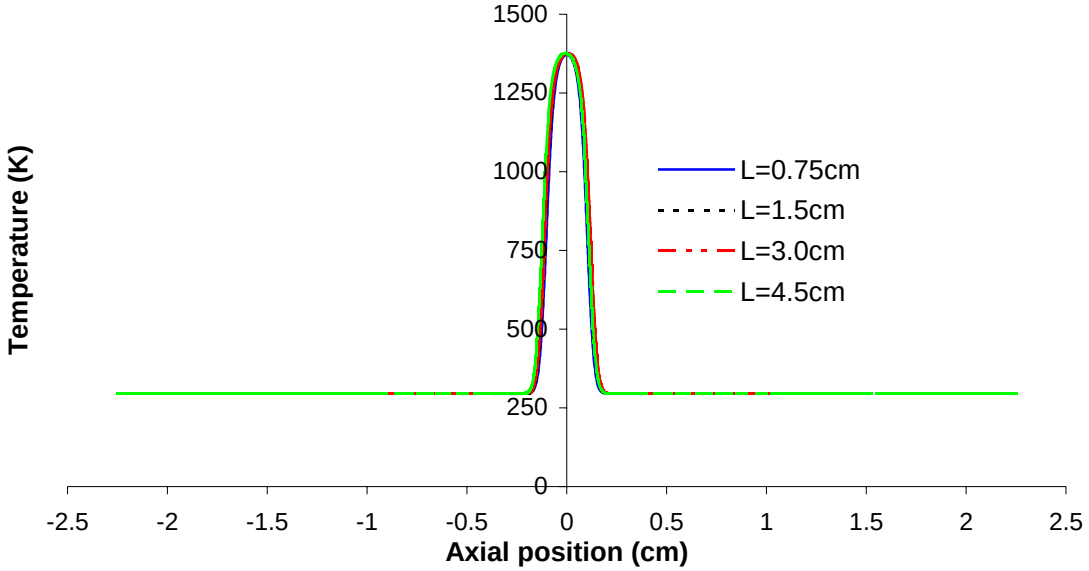


**Fig. 2.10**. Temperature variation with axial position for the opposed jet flames with different burner geometries (numerical solution, *V/L* = 66.67/s, $H_2$/air twin premixed flame, equivalence ratio = 0.25).

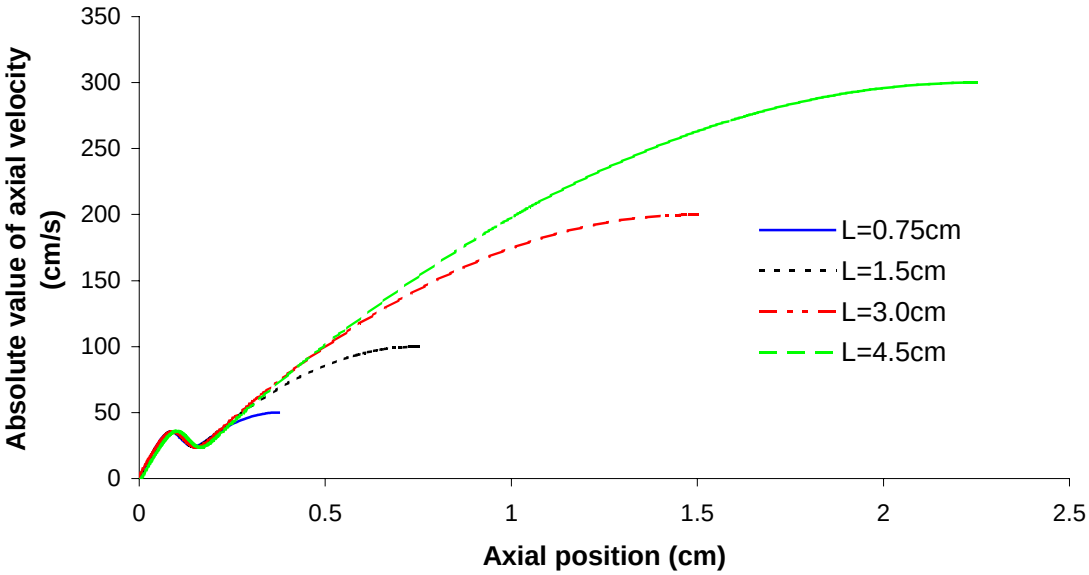


**Fig. 2.11**. Axial velocity variation with axial position for the opposed jet flames with different burner geometries (numerical solution, *V/L* = 66.67/s, $H_2$/air twin premixed flame, equivalence ratio = 0.25).

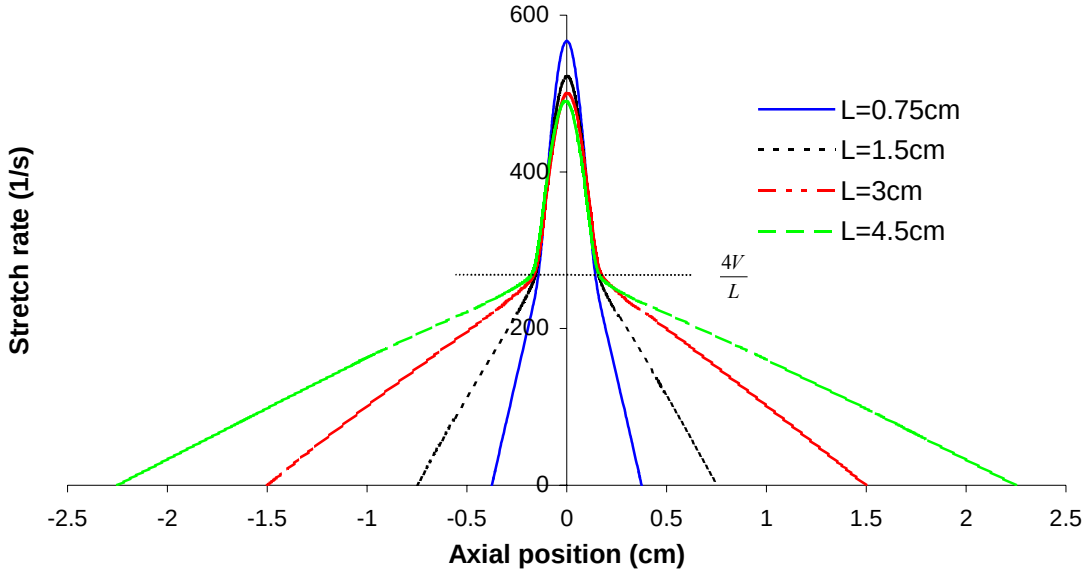


**Fig. 2.12**. Stretch rate variation with axial position for the opposed jet flames with different burner geometries (numerical solution, $V/L$ = 66.67/s, $H_2$/air twin premixed flame, equivalence ratio = 0.25).

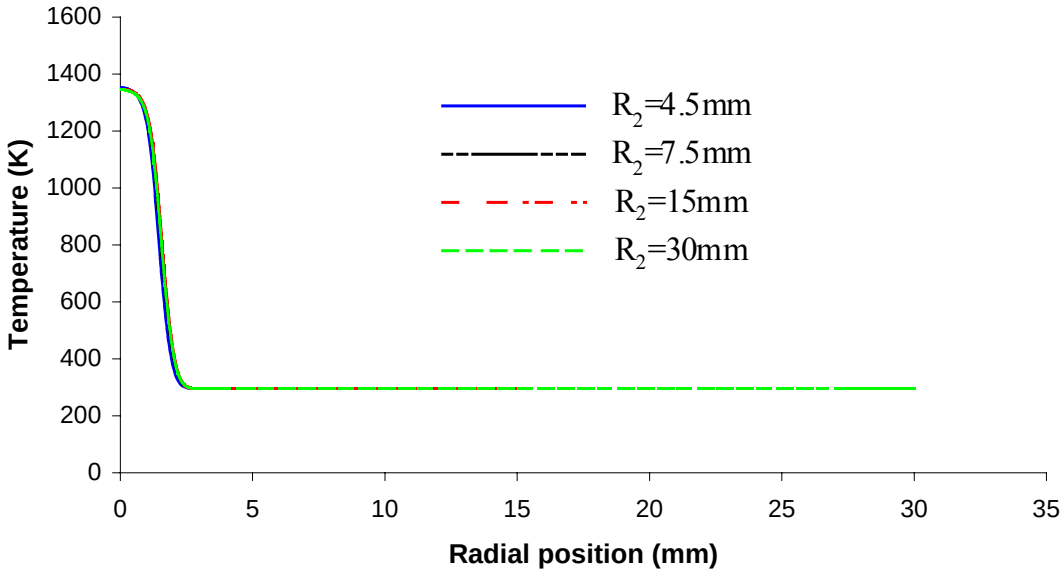


**Fig. 2.13**. Temperature variation with radial position for the tubular flames with different burner geometries (numerical solution, $-V_2/R_2$ = 66.67/s, $H_2$/air premixed flame, equivalence ratio = 0.18).

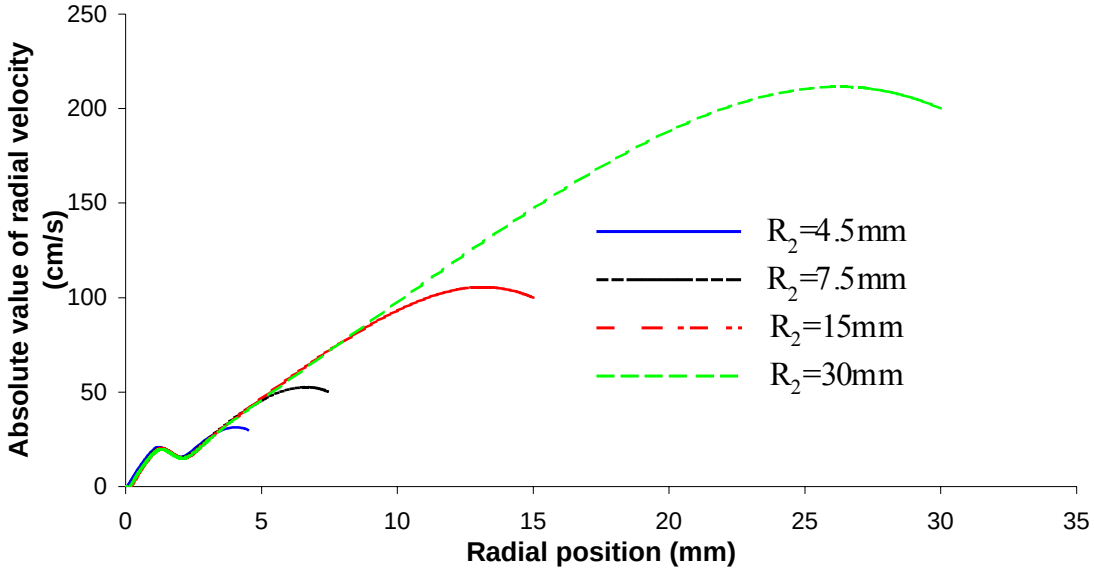


**Fig. 2.14**. Radial velocity variation with radial position for the tubular flames with different burner geometries (numerical solution, $-V_2/R_2$ = 66.67/s, $H_2$/air premixed flame, equivalence ratio = 0.18).

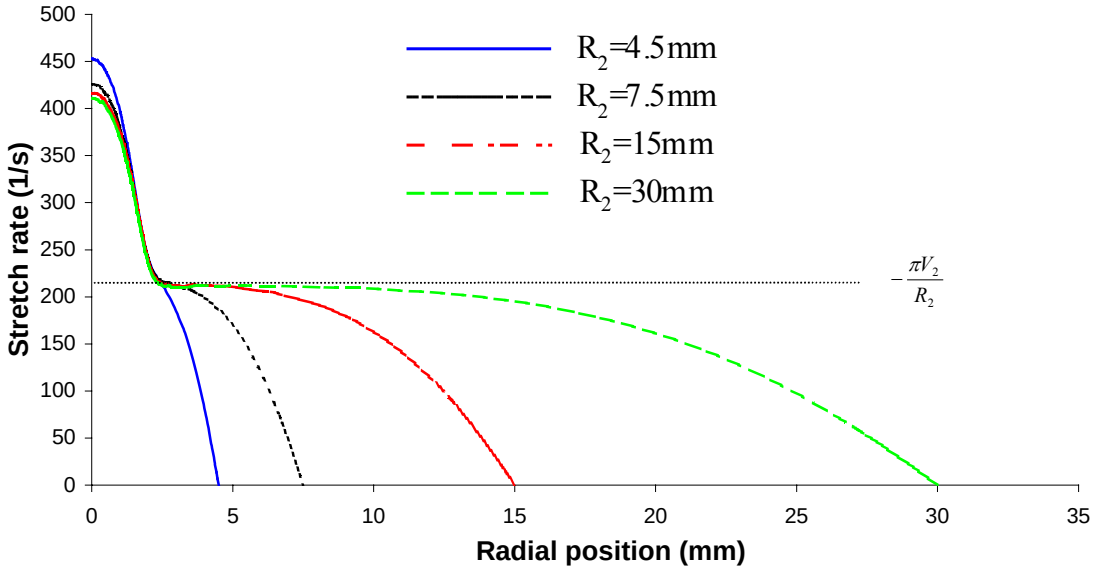


**Fig. 2.15**. Stretch rate variation with radial position for the tubular flames with different burner geometries (numerical solution, $-V_2/R_2$ = 66.67/s, $H_2$/air premixed flame, equivalence ratio = 0.18).

Besides the above advantages, there is another important reason to use large enough values of $L$ and $R_2$ in analysis. For the opposed jet flame, we know that the stretch rate without the flame is not a constant and it varies linearly with axial coordinate (see Fig. 2.8 and Fig. 2.12). When the flame region is very large, the cold flow stretch rate corresponding to the flame region is not a constant, it can change from the maximum value $4V/L$ to a small value; so it is hard to decide what value represents the stretch rate on the flame. However, if we use large enough $L$, the flame region is just a very tiny region around the symmetry plane where the cold flow stretch rate is almost constant with a value of $4V/L$. Thus, $4V/L$ is the stretch rate on the flame. Even with small $L$, while the cold flow field with flame is much different from the analytical cold flow solution, we can still see that the turning point of the stretch rate curve (black mark on Fig. 2.8) is the best choice representing the stretch on the flame. Here, the turning point of the stretch rate curve is very close to $4V/L$. In Fig. 2.12, we also showed that for different geometries, the turning points of all these flames are near $4V/L$. That means the value $4V/L$ best represents the stretch on the opposed jet flame.

For the tubular flame, because the flame structure does not depend on the value of nozzle radius $R_2$, in the analysis, we choose large enough $R_2$ to make the flame in a small region around the centerline where the cold flow stretch rate is constant at $-\pi V_2/R_2$. This value is the best choice to represent the stretch on the tubular flame (see Fig. 2.15).

The stretch rate defined in Dixon-Lewis et al. (1990,1991) is equivalent to above choice if the flames are small compared to the burner geometry. For the opposed jet flame, the applied stress is defined as $a_e = (-J/\rho_e)^{0.5}$ and the stretch rate is $k = 2a_e = 2(-J/\rho_e)^{0.5}$ where $J$ is the pressure eigenvalue and $\rho_e$ is the density of fresh

mixture. Without flames, $J = -4\rho_e V^2 / L^2$ (Seshadri and Williams, 1978), that means the stretch rate is $k = 2a_e = 4V / L$. For the tubular flame, the applied stress and stretch rate are defined as $k = a_e = (-J / \rho_e)^{0.5}$. From above analytical solution, $J = -\pi^2 \rho_e {V_2}^2 / {R_2}^2$, that means the stretch rate is $k = a_e = -\pi V_2 / R_2$. Since the eigenvalues with flames vary little from those values without flame (generally less than 10%) if the flames are small compared to the burner geometry, the applied stress defined by Dixon-Lewis is only slightly different from the choice in this paper (generally less than 5% since the stretch rate depends on the square root of the eigenvalue). However, if the flame is not small compared to the burner geometry, the pressure eignvalue *J* varies substantially with burner geometry when *V/L* or $V_2/R_2$ is constant. As we pointed out above, the flame properties just depend on *V/L* for the opposed jet flame and $V_2/R_2$ for the tubular flame. That means the definition of stretch rate with the pressure eignvalue works if the flame is small and not if the flame is large compared to the burner geometry.

The extinction curves of premixed $CH_4$/air flames are compared in Fig. 2.7 of Kobayashi and Kitano (1989) based on $2V/L$ as the stretch rate of the opposed jet flame and $-V_2/R_2$ as the stretch rate of the tubular flame. It is shown that the tubular flame extinguished at the almost same stretch rate as the opposed jet flame when the mixture is very lean and the tubular flame has lower extinction stretch rate for equivalence ratio more than about 0.75. If we apply the choice of stretch rates in this paper, the comparison is quite different: the tubular flame has a little bit higher extinction stretch rate than the opposed jet flame until the equivalence ratio is greater than about 1.3. Fig. 2.8 of Kobayashi and Kitano (1989) compared the extinction of premixed $C_3H_8$/air flames. It is shown that the tubular flame has lower extinction stretch rate for the equivalence ratio

less than about 1.4 and has higher extinction stretch rate for the equivalence ratio more than about 1.4. The same trend is shown with the stretch rate values defined in this paper; but the crossover equivalence ratio is about 1.1 instead of about 1.4.

For the opposed tubular flame, the stretch rate at the stagnation surface represents the stretch rate on the flame and the inverse of the stagnation radius represents the curvature on the flame when the flames are close to the stagnation surface (large enough stretch rate). Fig. 2.16 shows the comparison of the twin premixed flame temperature structure for the opposed tubular burner with different geometries. Geometry 1: $R_1$=0.3cm, $R_2$=1.5cm and $V$=40cm/s; Geometry 2: $R_1$=0.2cm, $R_2$=2.25cm and $V$=68.33cm/s; Geometry 3: $R_1$=0.4cm, $R_2$=1.125cm and $V$=24.17cm/s. These three geometries give the same stretch rate and curvature: $k = \pi V/(R_2 - R_1) = 105\,\mathrm{s}^{-1}$ and $R_s = (R_1 R_2)^{0.5} = 0.671$ cm. For the premixed flame, the flame structure depends on stretch rate and curvature. The same stretch rate and curvature should give the same flame structure and Fig. 2.16 is consistent with this argument. Fig. 2.17 shows the local stretch rate comparison of numerical, analytical and correlation solutions (described below); the turning point (black mark) of numerical solution is 110 $s^{-1}$ which is almost the same as the analytical value (105 $s^{-1}$).

Here, we want to discuss how the stretch rate varies with density due to thermal expansion in the flame zone. To obtain the exact formula of the stretch rate variation with thermal expansion requires a complete analytical solution of the flame equations. That is beyond the scope of this paper; however, we have found a good correlation.

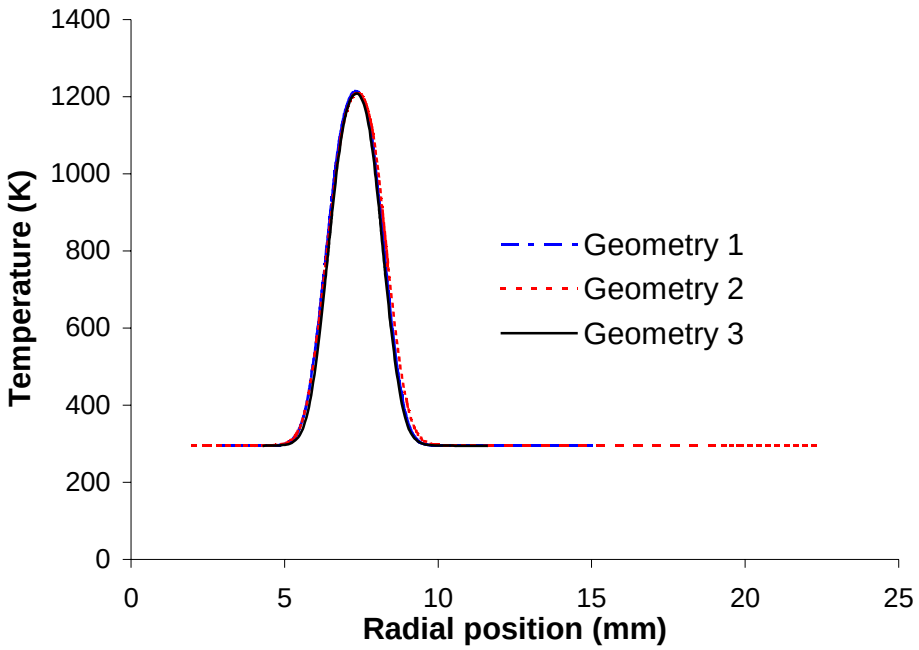


**Fig. 2.16**. Temperature variation with radial position for the opposed tubular flames with different burner geometries (numerical solution, $k = 105\,\mathrm{s}^{-1}$, $R_s = 0.671\,\mathrm{cm}$, $H_2$/air twin premixed flame, equivalence ratio = 0.18).

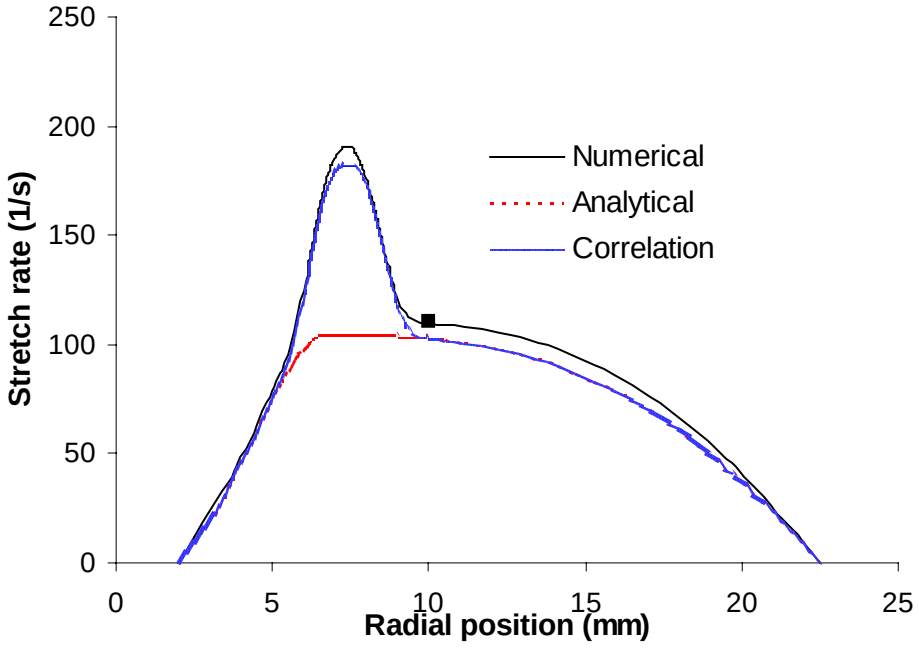


**Fig. 2.17**. Stretch rate variation with radial position for the opposed tubular flame ($V$ = 68.3cm/s, $R_1$=0.2cm, $R_2$=2.25cm, $H_2$/air twin premixed flame, equivalence ratio = 0.18).

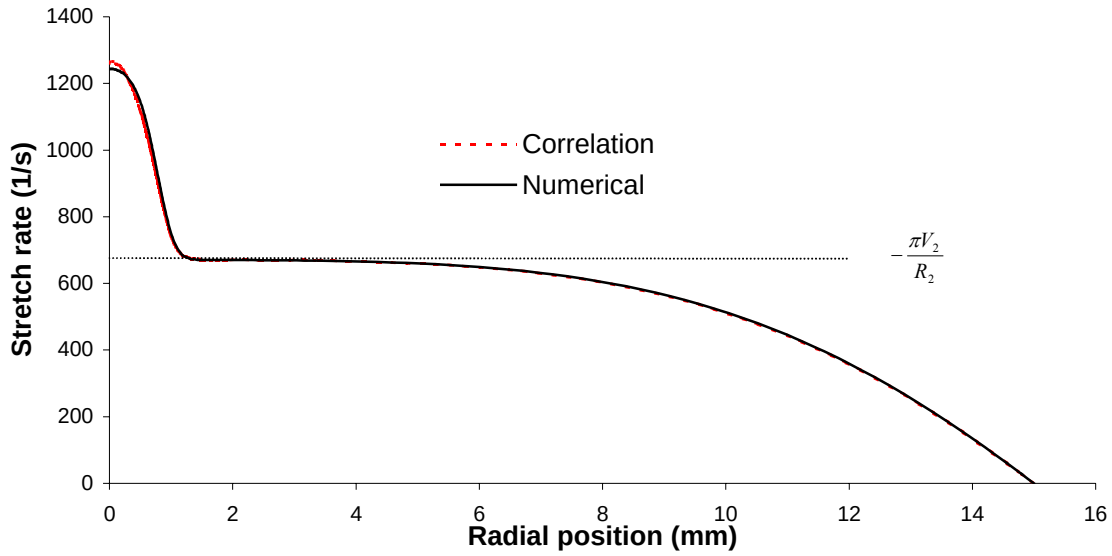


**Fig. 2.18**. Stretch rate variation with radial position in the hot flow field for the tubular flame ($V_2$ = -320 cm/s, $R_2$ = 15mm, $H_2$/air premixed flame, equivalence ratio = 0.18).

For the opposed jet flame ( $\rho_1 = \rho_2$ and $-V_1 = V_2 = V$), we have the correlation:

$$k \approx \left(\frac{\rho_u}{\rho}\right)^n \frac{4V}{L}\left(1 \pm \frac{2Z}{L}\right) \tag{2.47}$$

where $n$ is about 0.4~0.5. Fig. 2.9 shows the comparison of numerical solution and correlated solution with $n$ = 0.4; the agreement is nearly perfect.

For the tubular flame, we have the correlation:

$$k \approx -\left(\frac{\rho_u}{\rho}\right)^n \frac{\pi V_2}{R_2}\cos(0.5\pi r^2) \tag{2.48}$$

where $n$ is about 0.4~0.5. Fig. 2.18 shows the comparison of numerical solution and correlated solution with $n$ = 0.4; the agreement is also very good.

The opposed tubular flames ( $\rho_1 = \rho_2$ and $-V_1 = V_2 = V$) also follow the above power correlation using Eq. (2.40) and Eq. (2.42); which can be seen in Fig. 2.17 ($n$=0.4).

In fact, from Eq. (2.9), we have $k = [(-J - \overline{\rho} U_R \cdot dk/dR + 1/R \cdot d(\mu R \cdot dk/dR)/dR)/\overline{\rho}]^{0.5}$ where $k = U_Z / Z = -(df/dR)/\overline{\rho} R$. If the sum of the second term and third term is 0, then the stretch rate is a –0.5 power function of density; Dixon-Lewis et al. (1991) used $k = a_e(\rho_e/\rho)^{0.5} = (-J/\rho)^{0.5}$ as the local stretch rate. Since $-\overline{\rho} U_R \cdot dk/dR + 1/R \cdot d(\mu R \cdot dk/dR)/dR = (-\overline{\rho} U_R + d\mu/dR) \cdot dk/dR + \mu/R \cdot dk/dR + \mu \cdot d^2k/dR^2$, $dk/dR$ is zero at $R = 0$; $\mu \cdot d^2k/dR^2$ is negative and small compared to $-J$. Thus the local real stretch rate should be a little bit less than $k = a_e(\rho_e/\rho)^{0.5}$. Dixon-Lewis (1990) also has shown that the real stretch rate for the opposed jet flames is always a little less than $2(-J/\rho)^{0.5}$. If we want to express the stretch rate relation with density as a power function, the power number should be less than 0.5 and close to 0.5. Here, we found 0.4 is an appropriate value.

## Conclusion

We have solved the cold flow field for the opposed tubular burner (Eq. (2.39) ~ Eq. (2.44)) and the tubular burner (Eq. (2.45) and Eq. (2.46)) for the plug flow boundary conditions. For equal densities and nozzle velocities, the stretch rate and curvature of the opposed tubular flame can be represented by $\pi V/(R_2-R_1)$ and $R_s = (R_1 R_2)^{0.5}$. The stretch rate of the tubular flame can be represented by $\pi V/R$. To compare the flames in these three burners, $4V/L$ (equal densities, equal velocities) for the opposed jet flame, $\pi V/R$ for the tubular flame and $\pi V/(R_2-R_1)$ (equal densities, equal velocities) for the opposed tubular flame should be very good choices representing the stretch rates on these flames. Comparing flame phenomena using these choices of stretch rate should lead to improved

understanding of the effect of stretch and curvature on flame properties, structure and extinction.

# CHAPTER III

# PHYSICAL ANALYSIS OF STRETCH AND CURVATURE EFFECTS ON PREMIXED FLAMES


## Abstract

A physical analysis is carried out on the opposed jet premixed flame and the tubular premixed flame. The main conclusions about the stretch and curvature effects on premixed flames are recovered qualitatively. The most important difference between the classic one-dimensional planar flame and the opposed jet flame is that the latter has nonuniform transverse convection. The stretch effects on flame temperature and flame speed should be related to this convection. A flow divergence ratio is defined and it is proportional to Karlovitz number for the opposed jet flame. In the analysis on the tubular flame, it is shown that positive curvature strengthens the transverse convection and has a higher divergence ratio by one additional term that is proportional to the ratio of flame thickness to flame radius.


## Introduction

For stretched premixed flames, the flame temperature is higher than the adiabatic equilibrium value and increases with stretch rate if the Lewis number is less than one; the flame temperature is lower than the adiabatic equilibrium value and decreases with stretch rate if the Lewis number is more than one. This phenomenon is called the preferential diffusion effect or Lewis number effect. The popular explanation to the preferential diffusion effect by stretch is: The stretch thins the flame, both the species concentration and temperature gradients increase which enhances both mass and heat

diffusions. For the mixture with *Le* less than one, the gain of enthalpy by enhanced mass diffusion is more than the loss by heat diffusion; this results in a higher flame temperature; and vice versa for the mixture with *Le* more than one. However, if we increase the pressure for the one-dimensional unstretched planar flame, the flame is thinned and the gradients are increased, but the flame temperature is unchanged no matter how much *Le* is. So the flame thinning is not necessarily resulting in preferential diffusion effect. The basic difference between the stretched and unstretched flames is the nonuniform convection in the transverse direction, so the preferential diffusion effect must be related to this convection. The popular explanation to the curvature effect on premixed flames is: For the positively curved flame (the flame is convex to the fresh mixture), the curvature has a focusing effect to the mass diffusion and a defocusing effect to the heat diffusion; For *Le* less than one, the enthalpy gain from the focusing effect of mass diffusion is more than the loss from the heat defocusing; so the flame temperature is higher than the adiabatic flame temperature and vice versa for *Le* more than one. However, for the one-dimensional unstretched cylindrical or spherical premixed flames, the flame temperature is constant no matter how much the *Le* and curvature are. Another kind of physical explanation for the stretch and curvature effects is needed. Here we analyze the one-dimensional planar flame, the opposed jet flame and the tubular flame using basic energy conservation. The results recover the main conclusions about the stretch effects on premixed flames and reveal the physical mechanism of curvature effects for the first time.

**One-dimensional planar flame**

As we know, for the one-dimensional planar flame, Glassman (1996):

$$-\rho_u D_u (d^2 y / dx^2) - \rho_u S_u^0 (dy / dx) + \omega = 0 \tag{3.1}$$

$$-\lambda (d^2 T / dx^2) - \rho_u S_u^0 c_p (dT / dx) - \omega Q = 0 \tag{3.2}$$

$$x = 0,\ T = T_b^0,\ y = 0 \text{ and } x = \infty,\ T = T_u,\ y = y_u \tag{3.3}$$

$T$ is the temperature; $y$ is the mass fraction of deficient reactant; $\rho$ is the density; $D$ is the mass diffusivity; $\lambda$ is the thermal conductivity; $c_p$ is the specific heat; $S$ is the laminar flame speed; $\omega$ is the chemical reaction rate and $Q$ is the reaction heat of unit mass deficient reactant. Subscript $b$ and $u$ represent the burned and unburned mixtures respectively and superscript 0 indicates the one-dimensional planar adiabatic flame. Assuming an infinitely thin reaction zone, the solution for temperature and mass fraction of deficient reactant is:

$$T = T_u + (T_b^0 - T_u) e^{-\frac{x}{\delta_T^0}}; \qquad y = y_u (1 - e^{-\frac{x}{\delta_M^0}}) = y_u (1 - e^{-\frac{xLe}{\delta_T^0}}) \tag{3.4}$$

$$\delta_T^0 = \lambda / (\rho_u S_u c_p); \qquad \delta_M^0 = \rho_u D_u / (\rho_u S_u) = \delta_T^0 / Le \tag{3.5}$$

The enthalpy term $e$ that includes thermal and chemical enthalpies is given as

$$e = c_p (T - T_u) + Qy \tag{3.6}$$

For the one-dimensional planar flame; $e = c_p (T - T_u) + Qy = c_p (T_b^0 - T_u)(1 - e^{-xLe/\delta_T^0} + e^{-x/\delta_T^0})$ where $Qy_u = c_p (T_b^0 - T_u)$ by conservation of energy.

The temperature, mass fraction and enthalpy distributions for different Lewis numbers are shown in Figures 3.1, 3.2 and 3.3 respectively. The premixed flames are generally

divided into three zones as shown in Fig. 3.4; zone 1 is the fresh mixture zone, zone 2 is the flame zone, and zone 3 is the product zone. Zone 2 will be the control volume in the following analysis. At the boundary of zone 1 and zone 2, $T_1 = T_u$ and $u = S_u$, and at the boundary of zone 2 and zone 3, $T_3 = T_b$ and $u = S_b$; $m_1$ is the flow rate from zone 1 to zone 2; $m_2$ is the net flow rate out of zone 2 in the direction that is perpendicular to the diffusion direction, i.e. transverse direction; and $m_3$ is the flow rate from zone 2 to zone 3. Considering the conservation of mass and energy, we have the following equations.

$$m_1 = m_2 + m_3 \tag{3.7}$$

$$m_1 e_1 = m_2 e_2 + m_3 e_3 \tag{3.8}$$

$$e_1 = c_p (T_b^0 - T_u) \tag{3.9}$$

$$e_3 = c_p (T_b - T_u) \tag{3.10}$$

Substituting Eq. (3.7) into Eq. (3.8):

$$e_3 = e_1 + m_2 / m_3 \cdot (e_1 - e_2) \tag{3.11}$$

The above equation relates the flame temperature ($e_3$) to the adiabatic flame temperature ($e_1$), stretch rate ($m_2/m_3$) and Lewis number ($e_1$-$e_2$). For the one-dimensional planar flame, $m_2$ is zero, so $e_1 = e_3$ and the flame temperature is always the adiabatic flame temperature $T_b^0$; if $Le$ is more than one, $e_1 = e_3 < e_2$; if $Le$ equals to one, $e_1 = e_3 = e_2$ and if $Le$ is less than one, $e_1 = e_3 > e_2$.

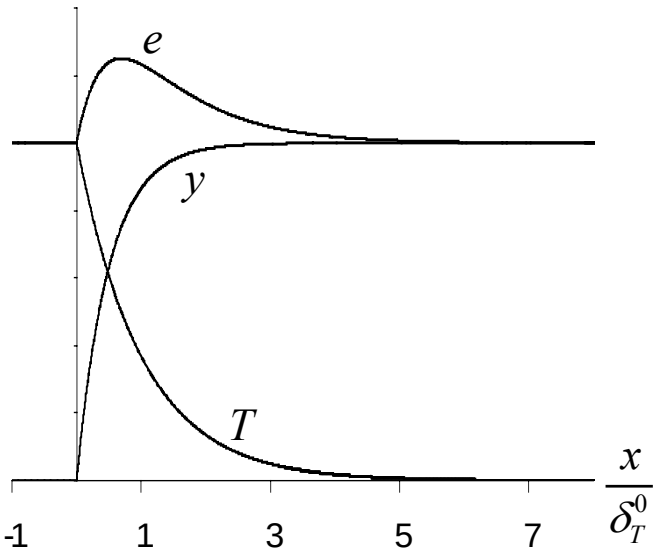


**Fig. 3.1**. One-dimensional planar flame structure in the case of *Le*=2.0.

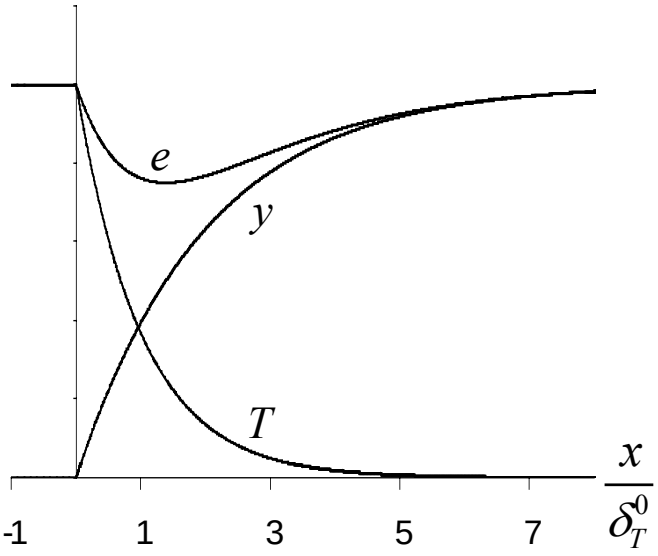


**Fig. 3.2**. One-dimensional planar flame structure in the case of *Le*=0.5.

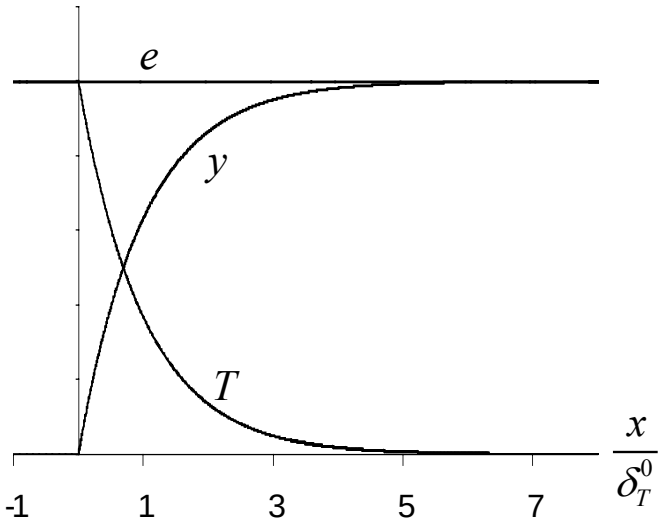


**Fig. 3.3**. One-dimensional planar flame structure in the case of *Le*=1.

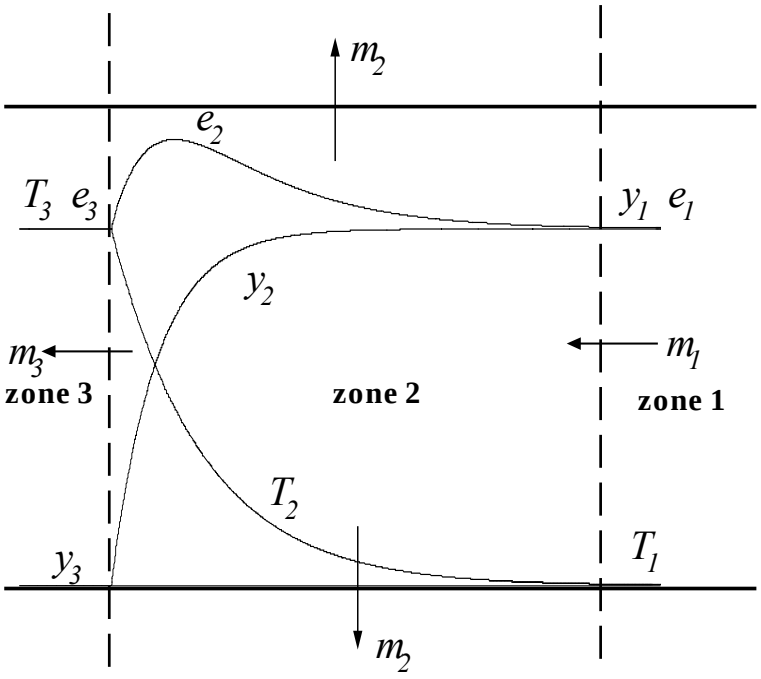


**Fig. 3.4**. The schematic of three zones.

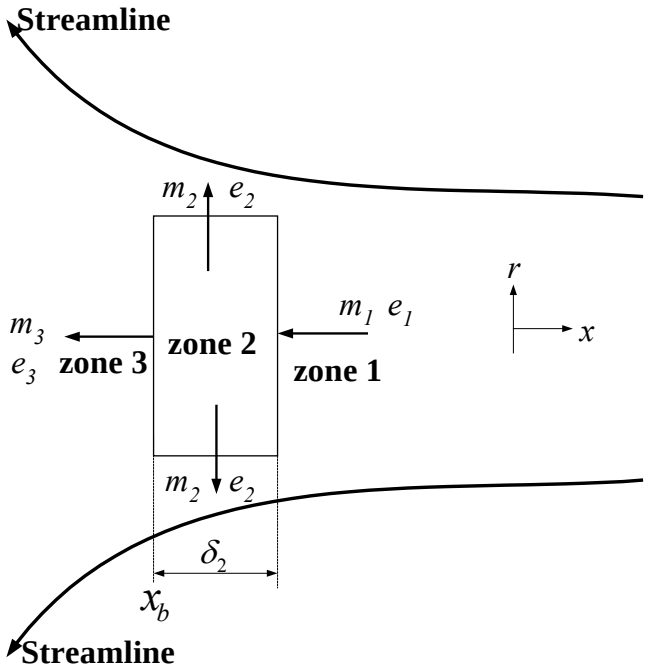


**Fig. 3.5**. Flame temperature analysis.

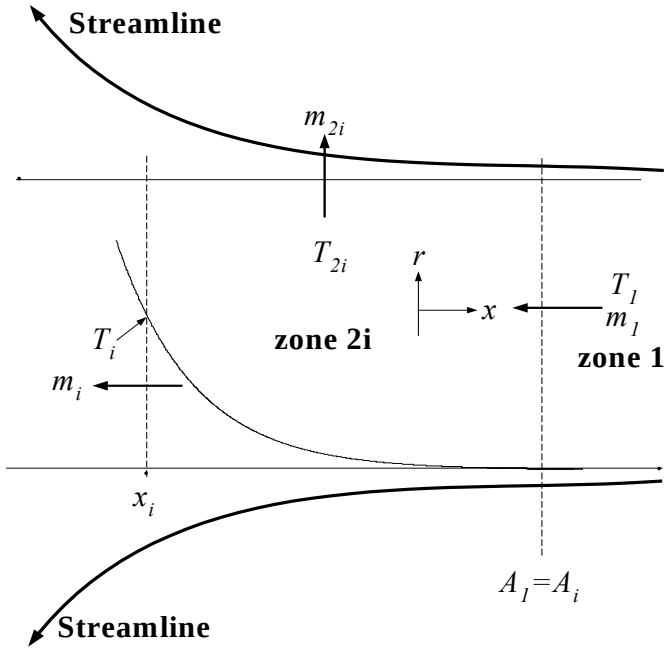


**Fig. 3.6**. Flame speed analysis.

**Opposed jet flame**

For the opposed jet flame, there is no diffusion in the radial direction, but there is convection in this direction, i.e. $m_2$ is not zero now as shown in Fig. 3.5. If *Le* is less than one, we have $e_1 > e_2$ for the one-dimensional planar flame; as the stretch rate increases from 0 to a small value, the flame structure has some variation by stretch; for example, the distributions of temperature and mass fraction are a little steeper, the average enthalpy of zone 2, i.e., $e_2$ would be different from that of the one-dimensional planar flame $e_2^0$; however, its value will still be less than $e_1$; to satisfy the energy equation Eq. (3.11), we must have $e_3 > e_1$, i.e. $T_b > T_b^0$; the increase of $e_3$ will cause the increase of $e_2$, i.e., $e_2 > e_2^0$, but $e_2$ is still less than $e_1$. As the stretch rate keeps increasing, the flame is pushing toward the stagnation plane, the flow divergence ratio $m_2/m_3$ and $e_2$ keep increasing, the product of $m_2/m_3 \cdot (e_1 - e_2)$ also increases which means the flame temperature $T_b$ increases with stretch rate continuously. When the stretch rate is high enough, the flame is pushed to the stagnation plane, $m_3$ is zero and $m_2/m_3$ is infinity, we must have $e_2 = e_1$ and the product of $m_2/m_3 \cdot (e_1 - e_2)$ is finite. Here, we can see that the preferential diffusion effect and flame temperature are related to the flow divergence ratio $m_2/m_3$. Vice versa, for *Le* larger than one, we have $T_b < T_b^0$; as the stretch rate increases from 0 to high values (the flame is pushed toward the stagnation plane), $m_2/m_3$ keeps increasing and $e_2$ keeps decreasing but $e_2 > e_1$, the product of $m_2/m_3 \cdot (e_1 - e_2)$ is negative and its absolute value increases which means the flame temperature $T_b$ decreases with stretch rate continuously. For *Le* is one, since

$e_1 = e_3 = e_2$ for the one-dimensional planar flame, the nonzero value of $m_2$ does not change the value of $e_3$, so the flame temperature is still the adiabatic flame temperature.

For the flame speed analysis, with certain premixed reactants, we assume there is a fixed ignition temperature $T_i$, above which the chemical reactions start (i.e., the Mallard and Le Chatelier theory. It is appropriate for the qualitative analysis) as shown in Fig. 3.6. Considering the energy conservation for zone 2i:

$$-\lambda A_i (dT / dx)|_{x_i} = m_i c_p (T_i - T_u) + m_{2i} c_p (T_{2i} - T_u) \tag{3.12}$$

where $T_{2i}$ is the average temperature for flow rate $m_{2i}$, and $T_u < T_{2i} < T_i$.

For the one-dimensional planar flame, $m_{2i}$ is zero

$$-\lambda A_i (dT / dx)|_{x_i}^0 = m_1^0 c_p (T_i - T_u) = m_i^0 c_p (T_i - T_u) \tag{3.13}$$

For the opposed jet flame, $m_{2i}$ is not zero and also the temperature gradient at $x_i$ changes with stretch rate. In general, for any premixed laminar flame, the convection in the reaction zone is negligible and the chemical heat release is balanced by the conduction; so the following relation holds (Glassman, 1996).

$$-\lambda \frac{dT}{dx}|_{x_i} \propto (2Q\lambda \int_{T_i}^{T_b} \omega dT)^{0.5} \tag{3.14}$$

The heat conduction at ignition point depends on the chemical heat release i.e. chemical reaction rate in the reaction zone $\omega$, which then depends on flame temperature. When *Le* is less than one, flame temperature is more than its adiabatic value; and so are the chemical reaction rate and temperature gradient at ignition point. For *Le* more than one, the temperature gradient at ignition point is less than its adiabatic value.

If *Le* <1;

$$m_1^0 c_p(T_i - T_u) = m_i^0 c_p(T_i - T_u) = -\lambda A_i \frac{dT}{dx}|_{x_i}^0 < -\lambda A_i \frac{dT}{dx}|_{x_i}$$
$$= m_i c_p(T_i - T_u) + m_{2i} c_p(T_{2i} - T_u) < m_1 c_p(T_i - T_u) \quad (3.15)$$

so we have $m_1^0 < m_1$ i.e. $S_u > S_u^0$; $S_i$ could be less, more than or equal to $S_i^0$. As the divergence ratio $m_{2i} / m_i$ increases, the flame temperature and temperature gradient increase; the ratio $\frac{m_i c_p(T_i - T_u) + m_{2i} c_p(T_{2i} - T_u)}{m_1 c_p(T_i - T_u)} = \frac{m_i}{m_1} + \frac{m_{2i}}{m_1} \frac{T_{2i} - T_u}{T_i - T_u}$ decreases; so the flame speed $S_u$ increases with the divergence ratio. We can see that the flame speed is also related to the flow divergence ratio.

If $Le$=1;

$$m_1^0 c_p(T_i - T_u) = m_i^0 c_p(T_i - T_u) = -\lambda A_i \frac{dT}{dx}|_{x_i}^0 = -\lambda A_i \frac{dT}{dx}|_{x_i}$$
$$= m_i c_p(T_i - T_u) + m_{2i} c_p(T_{2i} - T_u) < m_1 c_p(T_i - T_u) \quad (3.16)$$

we have $S_u > S_u^0$ and $m_i^0 > m_i$ i.e. $S_i < S_i^0$

If $Le$ >1;

$$m_1^0 c_p(T_i - T_u) = m_i^0 c_p(T_i - T_u) = -\lambda A_i \frac{dT}{dx}|_{x_i}^0 > -\lambda A_i \frac{dT}{dx}|_{x_i}$$
$$= m_i c_p(T_i - T_u) + m_{2i} c_p(T_{2i} - T_u) < m_1 c_p(T_i - T_u) \quad (3.17)$$

we have $S_i < S_i^0$; and $S_u$ could be less, more than or equal to $S_u^0$.

For the opposed jet flame, only when *Le* is larger than one, can increasing stretch rate decrease flame speed $S_u$. Thus the transition *Le* number *Le** (above which increasing stretch will decrease the flame speed $S_u$) is larger than one which is consistent with the analysis of Tien and Matalon (1991) and the experimental data of Law et al. (1986) in which the flame speed $S_u$ increases with stretch rate for rich and lean $CH_4$/air and $C_3H_8$/air opposed jet flames. Wu and Law (1984) also showed that the experiment flame

speed $S_u$ of lean $C_4H_{10}$-He-$O_2$ opposed jet flame, whose *Le* number is much larger than one, decreases with stretch rate.

If we assume $T_i \approx T_b$, then for *Le* greater than or equal to one, increasing stretch rate will decrease the flame speed $S_b$ and the transition Lewis number (below which increasing stretch will increase the flame speed $S_b$) is less than one which is consistent with Law and Sung (2000), Clavin and Williams (1982), Matalon and Matkowsky (1982). In Law and Sung (2000), the transition Lewis number $Le=1-2\varepsilon^0 < 1$ where $\varepsilon^0$ is the inverse of Zeldovich number.

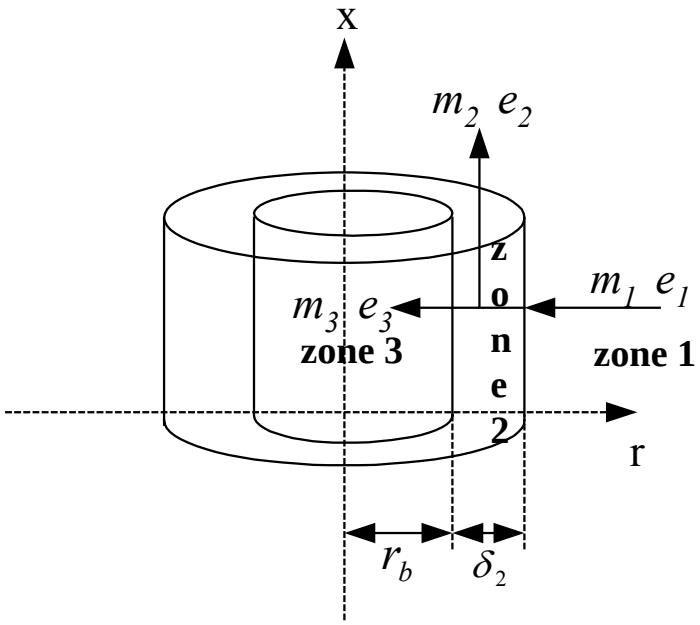


**Fig. 3.7**. Schematic of three zones in tubular flame.

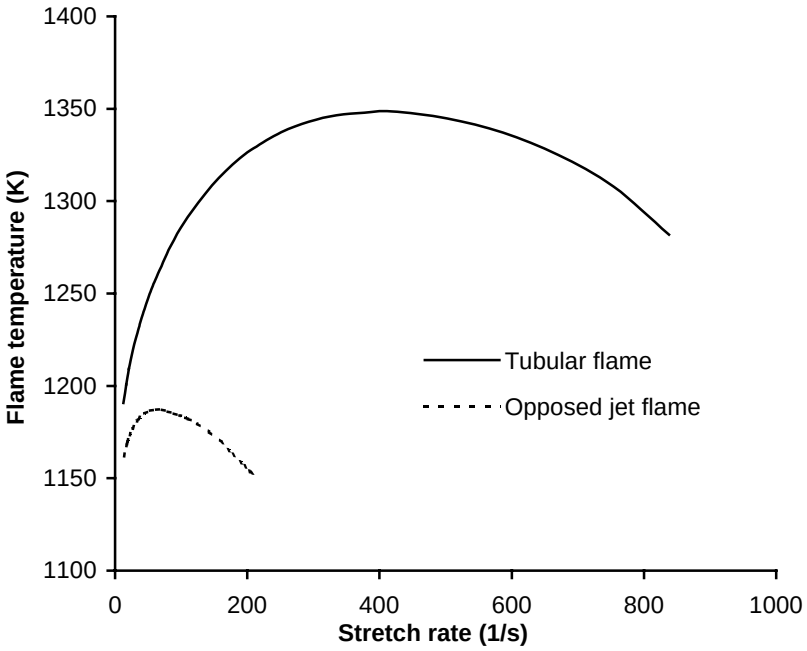


**Fig. 3.8**. Temperature variation with stretch rate for lean $H_2$/air flames, ϕ=0.1755 ($T_b^0 = 853$ K).

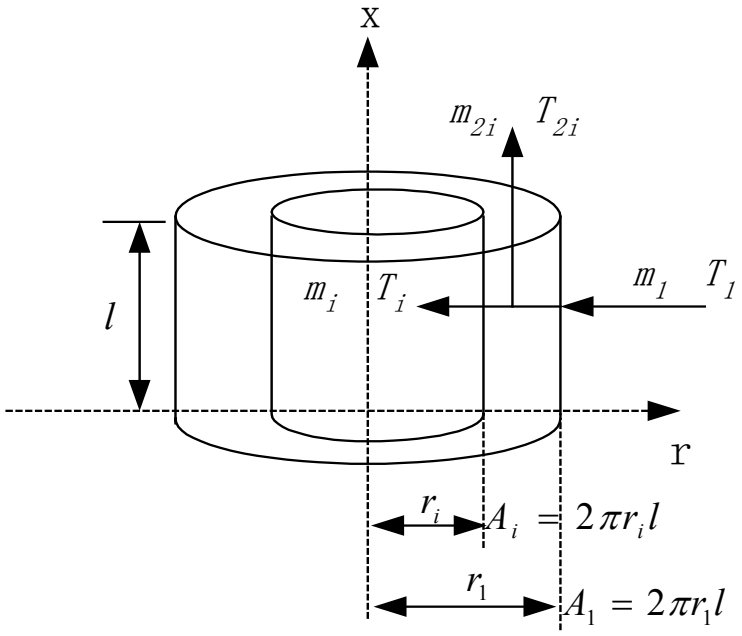


**Fig. 3.9**. Schematic of area difference of tubular flame.

**Tubular flame**

As can be seen from above analysis, flow divergence is critical to stretch effects. The following analysis shows how curvature affects the flow divergence ratio (The divergence ratio is defined as the flow rate ratio $m_2/m_3$).

For the opposed jet flame, assuming potential flow:

$$v_x = -\rho_u kx/\rho; \qquad v_r = \rho_u kr/(2\rho) \tag{3.18}$$

$$\frac{m_2}{m_3} = \frac{\rho_u k\delta_2}{\rho_u kx_b} = \frac{\delta_2}{x_b} = \frac{\rho_u k\delta_2}{\rho_b S_b} = \frac{\rho_u}{\rho_b} Ka \tag{3.19}$$

where $Ka$ is the Karlovitz number defined as $Ka = \delta_2 k / S_b$ and $k$ is the stretch rate.

For the tubular flame as shown in Fig. 3.7, assuming potential flow, we have:

$$v_r = -\rho_u kr/(2\rho), \qquad v_x = \rho_u kx/\rho \tag{3.20}$$

$$\frac{m_2}{m_3} = \frac{\rho_u k\pi[(r_b+\delta_2)^2 - r_b^{\,2}]}{\rho_u k\pi r_b^{\,2}} = \frac{2r_b\delta_2 + \delta_2^{\,2}}{r_b^{\,2}} = \frac{2\delta_2}{r_b} + \left(\frac{\delta_2}{r_b}\right)^2 = \frac{\rho_u}{\rho_b} Ka + \frac{\rho_u}{\rho_b} Ka\left(\frac{\delta_2}{2r_b}\right) \tag{3.21}$$

where $\delta_2$ is the flame thickness and $r_b$ is the flame radius.

The second term on the right hand side of Eq. (3.21) comes from the geometry, i.e. curvature. When $\delta_2 / r_b$ <<1, the second term is negligible. However, when $\delta_2 / r_b$ is on the order of unity, the second term is very important which is the case for tubular flames and some turbulent flames. The tubular flame (positively curved) strengthens the flow divergence and enhances the effects of stretch. On the other hand, for negatively curved flames (see Appendix), the negative curvature weakens the flow divergence and the stretch effects; the strengthening or weakening effect is proportional to the ratio of flame thickness to flame radius (radius of curvature, i.e., the reciprocal of curvature).

From above analysis, we understand that the change of tubular flame temperature due to stretch has the same trend as the opposed jet flame but is generally more obvious for the same stretch rate because of the strengthening of flow divergence. Fig. 3.8 shows the numerical result of the variation of flame temperature of a lean $H_2$/air flame with stretch rate for both the opposed jet flame (The chemical reaction mechanism is from Mueller et al. (1999)) and the tubular flame. The stretch rates adopted here are from Chapter II. The tubular flame has a higher flame temperature than the opposed jet flame for the lean $H_2$/air mixture ($Le \approx 0.33$) as shown in Fig. 3.8.

As for the flame speed response, the tubular flame has same equation as the opposed jet flame; but the area $A_i = 2\pi r_i l$ is less than $A_1 = 2\pi r_1 l$ as shown in Fig. 3.9, so even for the case of $Le \leq 1$ (Eq. (3.15) and Eq. (3.16)), the tubular flame has $m_1 > m_1^0$, the $S_u$ of the tubular flame could be less than $S_u^0$. Compared to the opposed jet flame, the tubular flame has a larger divergence ratio, so $m_1$ (corresponding to area $A_1$) of the tubular flame is greater than $m_1$ (corresponding to area $A_i$) of the opposed jet flame, the $S_u$ of the tubular flame may be less than the $S_u$ of the opposed jet flame for the same stretch rate. As for $S_i$ ($\approx S_b$, if $T_i \approx T_b$), there is no area problem, so all the conclusions about $S_i$ for the opposed jet flame (Eq. (3.16) and Eq. (3.17)) applies to the tubular flame and the $S_i$ of the tubular flame has more variation than that of the opposed jet flame.

The methodology of above analysis about flame temperature and flame speeds also can be used for outwardly and inwardly freely propagating spherical premixed flames. In those cases, the mass rate $m_2$ is not the transverse convection flow rate any more; it is the rate of mass variation within flame zone 2 i.e., $m_2 = d\left(\left|\int_{r_b}^{r_u} \rho 4\pi r^2 dr\right|\right) / dt$ .

From above analysis, we understand that the flame properties such as flame temperature and flame speed depend on the divergence ratio. The divergence ratio is not only a function of stretch rate but also a function of curvature. From the second term in the right hand side of Eq. (3.21) that is a product of Karlovitz number (proportional to stretch rate) and the ratio of flame thickness to flame radius, we understand that the curvature effects of stretched flames are not independent of stretch but coupled with it. Positive curvature strengthens preferential diffusion and negative curvature weakens preferential diffusion; the strengthening or weakening effect is proportional to the ratio of flame thickness to flame radius (radius of curvature).

**Extinction**

For a premixture with *Le* less than one, when the stretch rate increases, the flame temperature increases and at the same time, the flame diameter of tubular flame (or distance between two flames of opposed jet flame) decreases. The residence time of reactants in the flame zone also becomes shorter (Kobayashi and Kitano, 1991; $\tau \propto 1/k$ for both flames). When this time is less than the chemical reaction time, the chemical reactions are incomplete and temperature starts to decrease until it finally reaches extinction. The incompleteness of chemical reactions is the extinction mechanism of the flame whose *Le* is less than or equal to one, and the flame will be extinguished at the center of the burners. This result is shown numerically in Fig. 3.10 for the tubular $H_2$/air flame where the residual $H_2$ fuel is 11.1% at extinction ($k$=837$s^{-1}$). Comparing the tubular flame and the opposed jet flame, the tubular flame has a higher flame temperature; it can tolerate more incompleteness of chemical reactions and should be extinguished at a

higher stretch rate, as is the case of lean $H_2$/air flames shown in Fig. 3.11. The numerical and experimental extinction data have good agreement except for the tubular flame at high stretch rate; the large deviation at high stretch rate is caused by the turbulence that comes from high flow rate and correspondingly high inlet Reynolds number (Re=3120 at $k$=500$s^{-1}$).

For a premixture with *Le* more than one, increasing the stretch rate will decrease the flame temperature continuously until extinction; so the flame will be extinguished at a certain distance away from the center of the burners; the temperature decrease caused by preferential diffusion effect alone or with the incompleteness of chemical reactions is the extinction mechanism for the flame. Comparing the tubular flame and the opposed jet flame, the tubular flame has a lower flame temperature, it can tolerate less incompleteness of chemical reactions and should be extinguished at a lower stretch rate. This is consistent with the experimental extinction measurements of lean $C_3H_8$/air premixed flames by Kobayashi and Kitano (1989) (The comparison is based on the stretch rates $4V/L$ for the opposed jet flame and $\pi V/R$ for the tubular flame although the original comparison is based on the stretch rates of $2V/L$ and $V/R$).

As pointed out in Law (1988), the incompleteness of chemical reactions in the opposed jet flames is not the intrinsic character of stretch effects, it comes from the symmetry of the burner. In the real flames, the flames may propagate freely; the extinction caused by the incompleteness of chemical reactions is invalidated. However, the extinction caused by the preferential diffusion (i.e., the case where *Le* >1 and the extinction occurs at a certain distance away from the center of the burner) is an intrinsic

character of stretch effects; the extinction stretch rate predicted or measured from the opposed jet flame can be used in the real flames.

Above analysis on flame extinction is mainly based on flame temperature. For the mixture with Lewis number close to one, the curvature effect on flame temperature is minimal; then the curvature effects on other aspects such as the radical diffusion and distribution might play more important role than the flame temperature.

## Conclusion

An analysis using basic conservation equations to study stretch and curvature effects on premixed flames recovers the main conclusions from the literature. It overcomes the limit of the popularly used explanation of stretch and curvature effects on premixed flames that has difficulties with being applied to unstretched planar and curved flames. It also shows that the curvature effects are coupled with the stretch effects: The positive curvature strengthens the preferential diffusion and the negative curvature weakens the preferential diffusion; the strengthening or weakening effect is proportional to the ratio of flame thickness to flame radius (reciprocal of curvature).

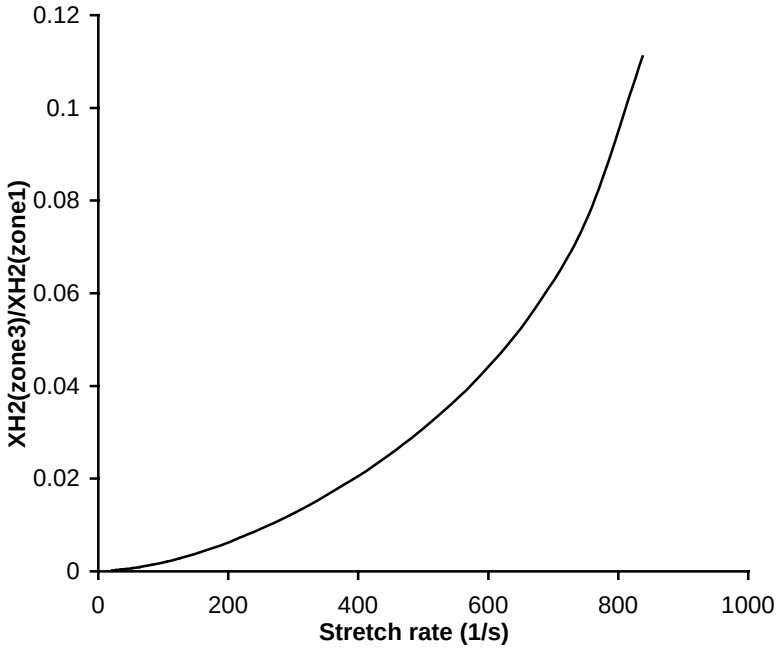


**Fig. 3.10**. Residual fuel vs. stretch rate of lean $H_2$/air tubular flame, $\phi$=0.1755.

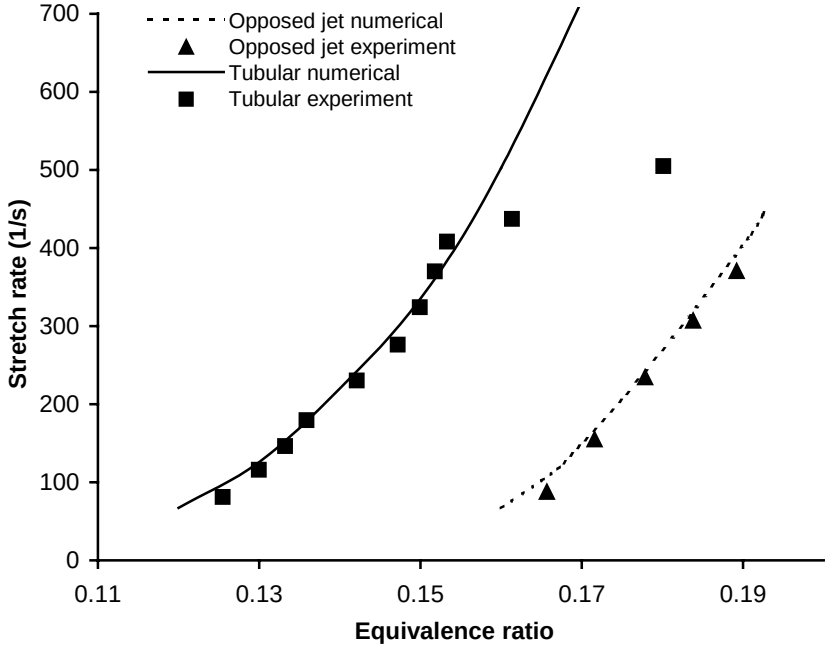


**Fig. 3.11**. Extinction stretch rates for lean $H_2$/air flames with Lewis number less than one.

# CHAPTER IV

# PREMIXED FLAME PARAMETERS FOR STRETCHED AND CURVED FLAMES

## Abstract

Based on a simple flow assumption and one-step high-activation energy chemistry, the flame speed and flame temperature of three specific stretched and curved premixed flames (the planar flame, the tubular flame, and the spherical flame) are predicted by asymptotic analysis. The expressions for flame speed and flame temperature are two coupled nonlinear equations and they can be solved easily with a simple numerical method. Unlike the previous asymptotic analyses, which are limited to small stretch rate, small curvature, and small Lewis number deviation, these expressions are for any range of stretch rate, curvature and Lewis numbers. The analytical solutions are compared to the numerical solutions with satisfactory results. To extend the solutions to generally curved flames, correlations on flame speed and flame temperature for the stretched and curved flame are given. With these correlations, we can predict the flame speed and flame temperature of any curved and stretched flame from information on stretched planar flames.

## Introduction

The laminar flame response of premixed flames to stretch has been studied for a long time by many researchers. Two review papers by Law and Sung (1998, 2000) have investigated stretch effects on premixed flames numerically and experimentally; analytical results by the integral method were given. The more rigorous analytical

solutions with asymptotic methods can be found in Sivashinsky (1976), Buckmaster (1977), Clavin and Williams (1982), and Matalon and Matkowsky (1982); they are reviewed in Clavin (1985). The advantage of these asymptotic analyses is that the analyses apply to the general flow field and they give explicit expressions for flame parameters. However, these asymptotic solutions are under the assumptions of small stretch rate (i.e., Karlovitz number much less than one), small curvature, or small Lewis number deviation that limit their range of usage. For the specific case of the opposed jet flow field, Tien and Matalon (1991) studied the flame speed response to stretch rate.

The above analyses emphasized the stretch effects on premixed flames. In this chapter, our emphasis is the curvature effect on flame properties. We study the curvature effect on premixed flame parameters with the asymptotic method and correlations. We derive the expressions for flame speed and flame temperature of three specific stretched flames, i.e. the planar, tubular and spherical flames. To extend the solutions to any curved flame, correlations on flame speed and flame temperature for the stretched and curved flames are given and they apply to any value of stretch rate, curvature, and Lewis number. With these correlations, we can predict the flame speed and flame temperature of curved and stretched flames from the information on stretched planar flames that is easily obtained.

## Reaction zone

In the reaction zone of any premixed flame, the convection is negligible and one assumes one-step chemistry.

$$v_1 m_1 + v_2 m_2 \rightarrow product$$

Here $v_1$ and $v_2$ are the stoichiometric coefficients, $m_1$ and $m_2$ are the reactants where $m_1$ is the deficient one; $y_1$ and $y_2$ are the mass fractions of species $m_1$ and $m_2$ respectively. $y_{10}$ and $y_{20}$ are the initial mass fractions of $y_1$ and $y_2$; $w_1$ and $w_2$ are the molecular masses of species $m_1$ and $m_2$.

$$y_{10}Q = c_p(T_b^0 - T_u) \tag{4.1}$$

$$\varpi = v_1 w_1 (\rho y_1 / w_1)^{n_1} (\rho y_2 / w_2)^{n_2} B(T) \exp(-T_a / T) \tag{4.2}$$

where $n_1$ and $n_2$ are the empirical reaction orders, and generally, $B(T) \propto T^m$.

$$T' = (T - T_u)/(T_b - T_u) = \theta / \theta_b; \qquad y' = 1 - y_1 / y_{10} \tag{4.3}$$

$$-\rho D_1 (d^2 y'/dx^2) - \varpi / y_{10} = 0 \tag{4.4}$$

$$-\rho a (T_b - T_u)/(T_b^0 - T_u) \cdot (d^2 T'/dx^2) - \varpi / y_{10} = 0 \tag{4.5}$$

From Eq. (4.4) and Eq. (4.5) where $\rho D$ and $\rho\alpha$ are constants:

$$\rho D_1 (d^2 y'/dx^2) = \rho a' (d^2 T'/dx^2) \tag{4.6}$$

where $a' = a(T_b - T_u)/(T_b^0 - T_u)$

Boundary conditions are: at the product side,

$$y' = T' = 1 \text{ and } dy'/dx = dT'/dx = 0 \tag{4.7}$$

By integrating Eq. (4.6) twice from the product side to the preheat side, we have

$$\rho D_1 (y' - 1) = \rho a' (T' - 1) \text{ i.e. } y_1 = y_{10} Le_1' (1 - T') \tag{4.8}$$

where $Le_1' = a'/D_1 = (T_b - T_u)/(T_b^0 - T_u) Le_1$

By the same procedure, $y_2 = y_2^* + (y_{20} - y_2^*) Le_2' (1 - T')$ where $y_2^*$ is the residual mass fraction of species $m_2$.

From Eq. (4.5), $d^2 T'/dx^2 = \varpi/(y_{10}\rho a') \Rightarrow \left(dT'/dx\right)^2\Big|_{reaction} = \int_{1^-}^{1} 2\varpi/(y_{10}\rho a') dT'$ where

$$2\varpi/(y_{10}\rho a') \approx 2v_1 w_1^{1-n_1} w_2^{-n_2} \rho_b^{n_1+n_2} y_{10}^{n_1} Le_1'^{n_1} (1-T')^{n_1} \cdot [y_2^* + (y_{20} - y_2^*) Le_2'(1-T')]^{n_2} \cdot B(T_b) \cdot \exp(-T_a/T_b) \cdot \exp[-T_a(T_b - T_u)\cdot(1-T')/T_b^2]/(y_{10}\rho a') \tag{4.9}$$

For the equivalence ratio $|\phi - 1| >> 1/\beta$ (Zeldovich number $\beta = T_a(T_b - T_u)/T_b^2$), the species mass fraction $y_2 = y_2^* + (y_{20} - y_2^*) Le_2'(1-T') \approx y_2^*$ can be recognized as a constant (this constant could be different from that of the classical one-dimensional unstretched adiabatic flame because of differential diffusion of species).

Defining: $\Omega = 2v_1 w_1^{1-n_1} w_2^{-n_2} \rho_b^{n_1+n_2} y_{10}^{n_1} Le_1'^{n_1} y_2^{*n_2} B(T_b) \exp(-T_a/T_b)/(y_{10}\rho a')$ (4.10)

$$(dT'/dx)^2\Big|_{reaction} = \Omega \int_{1^-}^{1} (1-T')^{n_1} \cdot \exp[-\beta(1-T')] dT' \approx \Omega/\beta^{n_1+1} \cdot \int_0^{\infty} X^{n_1} \exp(-X) dX = \Omega\Gamma_{n_1+1}/\beta^{n_1+1} \tag{4.11}$$

$$\lambda dT'/dx = \lambda(d\theta/dx)/\theta_b \Rightarrow |\lambda d\theta/dx| = |\lambda\theta_b dT'/dx| = \lambda\theta_b(\Omega\Gamma_{n_1+1}/\beta^{n_1+1})^{0.5} \tag{4.12}$$

For the curved flames such as the tubular flame and the spherical flame: $-\lambda/r^n d\left(r^n dT/dr\right)/dr - Q\varpi = 0$, $n$=1 for the tubular flame and $n$=2 for the spherical flame. Even if $\delta/r_b$ is on the order of unity, $\delta_r/\delta$ ($\delta_r$ is the thickness of reaction zone) is on the order of $1/\beta$, $\delta_r/r_b$ is on the order of $1/\beta$ which is much less than one. The radius can be recognized as constant in the reaction zone, i.e. $-\lambda/r^n d\left(r^n dT/dr\right)/dr = -\lambda d^2T/dr^2$ . For curved flames, we still get $|\lambda d\theta/dr| = \lambda\theta_b(\Omega\Gamma_{n_1+1}/\beta^{n_1+1})^{0.5}$.

**Stretched planar flame**

For the steady uniformly stretched planar premixed flame with constant stretch rate $k$ in cold flow, the $x$ coordinate is set to the diffusion direction; the flame parameters such as density, temperature, species concentration are just functions of $x$ coordinate.

The stretch rate without the expansion due to combustion heat release is: $k = k_y + k_z = \partial v/\partial y + \partial w/\partial z$ where $u$, $v$, $w$ are velocities in $x$, $y$, $z$ coordinates.

Mass conservation is given by:

$$\partial(\rho u)/\partial x + \partial(\rho v)/\partial y + \partial(\rho w)/\partial z = 0 \tag{4.13}$$

Considering the expansion due to heat release of combustion, we assume:

$$\partial(\rho v)/\partial y \cong \rho_u k_y ; \qquad \partial(\rho w)/\partial z \cong \rho_u k_z \tag{4.14}$$

where subscript $u$ denotes the unburned fresh mixture.

From Eq. (4.14), we can get:

$$\rho v = \rho_u k_y y + q_1(x,z) \text{ and } \rho w = \rho_u k_z z + q_2(x,y) \tag{4.15}$$

The stretch rate with expansion from Eq. (4.15) is:

$$K = \partial v/\partial y + \partial w/\partial z = (k_y + k_z)\rho_u/\rho = \rho_u k/\rho \tag{4.16}$$

Thus the stretch rate $K$ with expansion is $k$ times the density ratio and $k$ is the stretch rate at the unburned side. In this chapter, we mean $k$ when we refer the value of stretch rate. The above assumption for Eq. (4.14) may not be valid in the real flame, for example, as in Chapter II, the stretch rate varies with expansion by the power about 0.4~0.5 of the density ratio for the opposed jet flame, the tubular flame and the opposed tubular flame; however, this assumption reduced the flow field to a very simple form which makes the analytical solution possible.

From Eq. (4.13) and Eq. (4.14), we can get:

$$\rho u = -\rho_u k[x + q_3(y, z)] \tag{4.17}$$

In the preheat zone, the energy conservation is:

$$\rho c_p u(dT/dx) = \lambda(d^2T/dx^2) \tag{4.18}$$

where $c_p$ and $\lambda$ are the specific heat and thermal conductivity which are set to constants.

Substituting Eq. (4.17) to Eq. (4.18):

$$-\rho_u c_p k[x + q_3(y,z)](d\theta/dx) = \lambda(d^2\theta/dx^2) \tag{4.19}$$

Here, $\theta = T\text{-}T_u$ is the relative temperature and the function $q_3(y, z)$ is just a constant for Eq. (4.19); it will disappear with coordinate transformation so we set it to 0.

Then, Eq. (4.17) becomes:

$$u = -\rho_u kx / \rho \tag{4.20}$$

The energy conservation becomes:

$$d^2\theta/dx^2 + kx/a \cdot (d\theta/dx) = 0 \tag{4.21}$$

and for a positively stretched flame, the boundary conditions are:

$$x = \infty,\ \theta = 0 \quad d\theta/dx = 0 \text{ and } x = x_b,\ \theta = \theta_b \tag{4.22}$$

where $a = \lambda/(\rho_u c_p)$ is the thermal diffusivity, $x_b$ is the position of reaction surface, and $\theta_b = T_b - T_u$ where $T_b$ is the flame temperature.

The species conservation equation and boundary conditions are:

$$d^2f/dx^2 + kx/D \cdot (df/dx) = 0;\ x = \infty,\ f = f_0 \quad df/dx = 0; \quad x = x_b,\ f = 0 \tag{4.23}$$

where $f$ is the mass fraction of deficient species and $D$ is the mass diffusivity of deficient species ($\rho D$ is set to a constant).

The solutions for above conservation equations and boundary conditions are:

$$\theta = \theta_b[1 - erf(x\sqrt{k/2/a})]/[1 - erf(x_b\sqrt{k/2/a})] \tag{4.24}$$

$$f = f_0[erf(x\sqrt{kLe/2/a}) - erf(x_b\sqrt{kLe/2/a})]/[1 - erf(x_b\sqrt{kLe/2/a})] \tag{4.25}$$

Energy balance at flame surface is:

$$-\lambda(dT/dx)|_{x=x_b} = \rho DQ(df/dx)|_{x=x_b} \text{ with } f_0 Q = c_p\theta_b^0 \tag{4.26}$$

where $Q$ is the reaction heat of unit mass deficient species. We can get the flame temperature expression:

$$\theta_b/\theta_b^0 = 1/\sqrt{Le}\cdot\exp[kx_b{}^2(1-Le)/2/a]\cdot[1-erf(x_b\sqrt{k/2/a})]/[1-erf(x_b\sqrt{kLe/2/a})] \tag{4.27}$$

where superscript 0 means one-dimensional adiabatic planar flame and $Le = a/D$ has been used.

Here, we have two ways to solve for the flame speed:

1) We solve it directly. For the reaction zone, we know:

$$\lambda(dT'/dx)|_{x_b} = \lambda/\theta_b\cdot(d\theta/dx)|_{x_b} \Rightarrow \left|\lambda(d\theta/dx)|_{x_b}\right| = \left|\lambda\theta_b(dT'/dx)|_{x_b}\right| = \lambda\theta_b(\Omega\Gamma_{n_1+1}/\beta^{n_1+1})^{0.5} \tag{4.28}$$

Eq. (4.27) and Eq. (4.28) have two unknowns, i.e. $\theta_b$ and $x_b$; we can solve the two equations to get $\theta_b$ and $x_b$ and then get the flame speed at the product side, $S_b$ with Eq. (4.20). If we define the unburned flame speed $S_u$ at $\theta/\theta_b = 0.01$ as in Tien and Matalon (1991), we can get flame speed $S_u$ with Eq. (4.20) and Eq. (4.24).

2) We use the numerical and experimental data of the classic one-dimensional unstretched planar flame. Comparing to the one-dimensional planar flame, we can get the flame speed.

$$\rho_u S_u^0 c_p\theta_b^0 = \left|\lambda(d\theta/dx)\right|_{x=x_b}^0\right| = \lambda\theta_b^0(\Omega_0\Gamma_{n_1+1}/\beta_0{}^{n_1+1})^{0.5} \tag{4.29}$$

$$\left|\lambda(d\theta/dx)\right|_{x=x_b}\right| = \lambda\theta_b(\Omega\Gamma_{n_1+1}/\beta^{n_1+1})^{0.5} \tag{4.30}$$

$$\left|\lambda(d\theta/dx)|_{x_b}\right|/\left|\lambda(d\theta/dx)|_{x_b}^0\right| = \left|\lambda(d\theta/dx)|_{x_b}\right|/(\rho_u S_u^0 c_p\theta_b^0) = \theta_b/\theta_b^0\left[(\beta_0/\beta)^{n_1+1}\Omega/\Omega_0\right]^{0.5} \tag{4.31}$$

For a premixture whose equivalence ratio deviates from unity by the order of $1/\beta$,

$$\Omega/\Omega_0 = B(T_b)/B(T_b^0)\cdot\exp[-T_a(1/T_b - 1/T_b^0)]\cdot(T_b^0/T_b)^{n_1+n_2}(\theta_b/\theta_b^0)^{n_1-1} \tag{4.32}$$

where $T_a$ is the activation temperature, $B(T)$ is the frequency factor of chemical reaction rate and the Zeldovich number is $\beta = T_a\cdot(T_b - T_u)/T_b^2$; $n_1$ and $n_2$ are the empirical reaction orders for reactant 1 (deficient one) and reactant 2.

From equations (4.29)~(4.32), we can get:

$$\lambda\exp(-kLex_b^2/2/a)\cdot\sqrt{2kLe/a/\pi}/(\rho_u S_u^0 c_p Le)/[1-erf(x_b\sqrt{kLe/2/a})] = F(T_b) \tag{4.33}$$

$$F(T_b) = [B(T_b)/B(T_b^0)]^{0.5}\exp[-T_a/2\cdot(1/T_b - 1/T_b^0)](\beta_0/\beta)^{(n_1+1)/2}(\theta_b/\theta_b^0)^{(n_1+1)/2}(T_b^0/T_b)^{(n_1+n_2)/2} \tag{4.34}$$

Generally, $B(T)\propto T^m$ and the exponential term in function $F(T_b)$ dominates; the product of the other terms is close to one, i.e. $F(T_b)\approx\exp[-T_a/2\cdot(1/T_b - 1/T_b^0)]$.

The flame temperature $T_b$ and flame position $x_b$ can be obtained by solving Eq. (4.27) and Eq. (4.33) numerically. We can get the flame speed $S_u$ with Eq. (4.20) and Eq. (4.24). In this chapter, we use the second method.

For negatively stretched planar flame, the boundary conditions are different.

$$x = x_u,\ \theta = 0\quad d\theta/dx = 0\quad f = f_0\quad df/dx = 0 \text{ and } x = x_b,\ \theta = \theta_b\quad f = 0 \tag{4.35}$$

where $x_u$ is the position of fresh mixture origin. There is no value of $x_u$ satisfying both the conservation equations and adiabatic boundary conditions at the fresh mixture origin.

In fact, the negatively stretched planar flame is not a stable flame. With negative stretch rate, $du/dx = -(dv/dy + dw/dz) - u/\rho\cdot(d\rho/dx) = -k - u/\rho\cdot(d\rho/dx) > 0$ and suppose the flame is stabilized at some place at first; if the flow rate decreases a little, the flame speed is bigger than the flow speed, the flame will move to the position with

smaller flow speed and keep moving until being blown off; and vice versa. To get the stable, negatively stretched flame, we want $-(dv/dy + dw/dz) = -k > 0$ and $du/dx < 0$; the only way to satisfy these conditions is to negatively curve the flame. The steady stable negatively stretched premixed flame must be negatively curved. As we will see below, we can not get the solution satisfying the conservation equations and adiabatic boundary conditions for the positively curved flame under negative stretch.

**Stretched and curved flame (tubular flames)**

For the curved and positively stretched steady premixed flame such as a stretched cylindrical flame, i.e. the tubular flame, the diffusion direction is the *r* coordinate and the flame parameters such as density, temperature, species concentration are just functions of the *r* coordinate. The stretch is caused by the flow divergence in *z* and $\phi$ directions.

The stretch rate without the expansion due to combustion heat release is: $k = k_z + k_\phi = \partial v/\partial z + \partial w/\partial \phi / r$ where *u*, *v*, *w* are velocities in *r*, *z*, $\phi$ coordinates.

Mass conservation is given by:

$$\partial(\rho r u)/\partial r + \partial(\rho r v)/\partial z + \partial(\rho r w)/\partial \phi / r = 0 \tag{4.36}$$

We determine the stretch rate with the expansion due to combustion heat release as before:

$$\partial(\rho v r)/\partial z \cong \rho_u r k_z \text{ and } \partial(\rho w r)/\partial \phi / r \cong \rho_u r k_\phi \tag{4.37}$$

$$v = \rho_u k_z z/\rho + q_1(r,\phi) \text{ and } w = \rho_u k_\phi r\phi/\rho + q_2(r,z) \tag{4.38}$$

The stretch rate with expansion from Eq. (4.38) is:

$$K = \partial v/\partial z + \partial w/\partial \phi / r = (k_z + k_\phi)\rho_u/\rho = \rho_u k/\rho \tag{4.39}$$

$$\rho ru = -[\rho_u k r^2 / 2 + A + q_3(z,\phi)] \tag{4.40}$$

In Eq. (4.40), function $q_3$ is just a role of constant and we will include it in the constant $A$; the constant $A$ can be used to change the curvature of the flame while keeping the stretch rate constant (at $r = r_s = \sqrt{-2A/(\rho_u k)}$, $u = 0$; $r_s$ is the stagnation radius of the flow field).

$$\rho ru = -(\rho_u k r^2 / 2 + A) = -\rho_u k / 2 \cdot (r^2 - r_s^2) \tag{4.41}$$

Energy conservation:

$$\rho c_p u(d\theta / dr) = \lambda / r \cdot \left[d\left(rd\theta / dr\right)/ dr\right] \tag{4.42}$$

Substituting Eq. (4.41) to Eq. (4.42):

$$rd^2\theta / dr^2 + (kr^2 / 2 / a + Ac_p / \lambda + 1) \cdot (d\theta / dr) = 0 \tag{4.43}$$

Species conservation:

$$rd^2 f / dr^2 + (kr^2 / 2 / D + A / \rho_u / D + 1) \cdot (df / dr) = 0 \tag{4.44}$$

For the positively curved flame (flame surface is convex to the fresh mixture), the boundary conditions are:

$$r = \infty,\ \theta = 0 \quad d\theta / dx = 0 \quad f = f_0 \quad df / dx = 0 \text{ and } r = r_b,\ \theta = \theta_b \quad f = 0 \tag{4.45}$$

The solutions for above equations and boundary conditions are:

$$\theta = \theta_b \int_r^\infty r^{B1} \exp(-kr^2 / 4 / a) dr \,/ \int_{r_b}^\infty r^{B1} \exp(-kr^2 / 4 / a) dr \text{ with } B1 = -A / \rho_u / a - 1 \tag{4.46}$$

$$f = f_0 \int_{r_b}^r r^{B2} \exp(-Lekr^2 / 4 / a) dr \,/ \int_{r_b}^\infty r^{B2} \exp(-Lekr^2 / 4 / a) dr \tag{4.47}$$

with $B2 = -ALe / \rho_u / a - 1$.

According to Eq. (4.26), the flame temperature is:

$$\theta_b / \theta_b^0 = 1/Le \cdot r_b^{B2-B1} \exp[kr_b^2(1-Le)/4/a] \int_{r_b}^{\infty} r^{B1} \exp(-kr^2/4/a)dr / \int_{r_b}^{\infty} r^{B2} \exp(-Lekr^2/4/a)dr \quad (4.48)$$

Following the same procedure used to obtain Eq. (4.33), we can get

$$\lambda r_b^{B2} \exp[-kr_b^2 Le/4/a] / [\rho_u S_u^0 c_p Le \cdot \int_{r_b}^{\infty} r^{B2} \exp(-Lekr^2/4/a)dr] = F(T_b) \quad (4.49)$$

By solving Eq. (4.48) and Eq. (4.49), we can obtain flame temperature $T_b$ and flame position $r_b$; and we can determine the flame speed $S_b$ by substituting $r_b$ into Eq. (4.41). We can find $S_u$ at $\theta/\theta_b = 0.01$ with Eq. (4.41) and Eq. (4.46).

For the negatively curved flame (flame surface is concave to the fresh mixture), the boundary conditions are:

$$r = 0 \text{ (line source)},\ \theta = 0 \quad d\theta/dx = 0 \quad f = f_0 \quad df/dx = 0 \text{ and } r = r_b,\ \theta = \theta_b \quad f = 0 \quad (4.50)$$

The solutions for the negatively curved flames (apply to both positive stretch rate and negative stretch rate) are in the same form with Eq. (4.48) and Eq. (4.49) except that the integration range is from 0 to $r_b$, $B1 = -A/\rho_u/a - 1 > 0$ and $B2 = -ALe/\rho_u/a - 1 > 0$.

For the negatively stretched and positively curved tubular flame, The boundary conditions are as the following: $r = r_s > r_b > 0,\ \theta = 0 \quad d\theta/dx = 0 \quad f = f_0 \quad df/dx = 0$ and $r = r_b,\ \theta = \theta_b \quad f = 0$, where $r_s$ is the stagnation radius and also the position of fresh mixture origin here. There is no value of $r_s$ satisfying both the conservation equations and adiabatic boundary conditions at the fresh mixture origin.

**Stretched and curved flame (spherical flames)**

Following the same procedure as the tubular flame, we can determine the solutions for the stretched spherical flames. The solutions for the positively stretched and positively curved spherical flames are:

$$\rho r^2 u = -(\rho_u k r^3 / 3 + A) = -\rho_u k / 3 \cdot (r^3 - r_s^3) \tag{4.51}$$

$$\theta_b / \theta_b^0 = 1/Le \cdot \exp[\, kr_b{}^2 (1 - Le) / 6 / a + (B2 - B1) / r_b \,] \frac{\int_{r_b}^{\infty} r^{-2} \exp(-kr^2 / 6 / a + B1 / r) dr}{\int_{r_b}^{\infty} r^{-2} \exp(-Lekr^2 / 6 / a + B2 / r) dr} \tag{4.52}$$

$$\lambda r_b^{-2} \exp[-kr_b{}^2 Le / 6 / a + B2 / r_b \,] / [\rho_u S_u^0 c_p Le \cdot \int_{r_b}^{\infty} r^{-2} \exp(-Lekr^2 / 6 / a + B2 / r) dr] = F(T_b) \tag{4.53}$$

with $B1 = A/(\rho_u a)$, $B2 = ALe/(\rho_u a)$ and at $r = r_s = \sqrt[3]{-3A/(\rho_u k)}$, $u = 0$.

The solutions for the negatively curved flames (apply to both positive stretch rate and negative stretch rate) are in the same form with Eq. (4.52) and Eq. (4.53) except that the integration range is from 0 to $r_b$, $B1 = A/(\rho_u a) < 0$ and $B2 = ALe/(\rho_u a) < 0$.

There is no negatively stretched and positively curved spherical flame that satisfies the adiabatic boundary conditions.

## Correlations

In Chapter III, it is shown that the effect of stretch on premixed flames depends on the flow divergence ratio, which is proportional to $Ka = k\delta / S_b$ ($\delta$ is the flame thickness) for the planar flame. The positive or negative curvature tends to strengthen or weaken the stretch effects, and this strengthening or weakening effect is proportional to $\delta / r_b$. For a given fresh mixture, the flame temperature $T_b$ and flame speed $S_b$ should be a function of $Ka$ and $\delta / r_b$; we also determine the flow divergence ratio $m_2 / m_3 = (1 + 0.5\delta / r_b) Ka \rho_u / \rho_b$ for the tubular flame. For the more general case, we replace the reciprocal of flame radius with flame curvature and 0.5 with a positive

empirical constant $\alpha$ that depends on the fresh mixture and the method of determining flame radius and flame thickness. The divergence ratio becomes $m_2 / m_3 = [1 + \alpha\delta(\nabla \cdot \mathbf{n})]Ka\rho_u / \rho_b$ where **n** is the unit normal vector of flame surface; $\nabla \cdot \mathbf{n}$ has positive or negative values for positive or negative curvature respectively and is evaluated at $r = r_b$.

The premixed flame parameters depend on the divergence ratio, that is,

$$T_b = f_1\{[1 + \alpha\delta(\nabla \cdot \mathbf{n})]Ka\} \text{ and } S_b = f_2\{[1 + \alpha\delta(\nabla \cdot \mathbf{n})]Ka\} \tag{4.54}$$

For the flames with the same fresh mixture, if they have the same value of the corrected Karlovitz number $[1 + \alpha\delta(\nabla \cdot \mathbf{n})]Ka$, they almost have same flame temperature and flame speed $S_b$. For flame speed $S_u$, we have:

$$m_1 = \rho_u S_u A_u = m_2 + m_3 = \{\rho_u / \rho_b[1 + \alpha\delta(\nabla \cdot \mathbf{n})]Ka + 1\}m_3 = \{\rho_u / \rho_b[1 + \alpha\delta(\nabla \cdot \mathbf{n})]Ka + 1\}\rho_b S_b A_b$$

$$\text{i.e., } S_u A_u / A_b = \{[1 + \alpha\delta(\nabla \cdot \mathbf{n})]Ka + T_u / T_b\}S_b = f_3\{[1 + \alpha\delta(\nabla \cdot \mathbf{n})]Ka\} \tag{4.55}$$

where $A_u/A_b$ is the area ratio of the fresh mixture side to the product side; it is equal to one for the planar flame;

$A_u / A_b = r_u / r_b = 1 \pm \delta / r_b = 1 + \delta(\nabla \cdot \mathbf{n})$ for the tubular flame;

$A_u / A_b = (r_u / r_b)^2 = (1 \pm \delta / r_b)^2 = 1 + \delta(\nabla \cdot \mathbf{n}) + [\delta(\nabla \cdot \mathbf{n})]^2 / 4 \approx 1 + \delta(\nabla \cdot \mathbf{n})$ for the spherical flame;

$$A_u / A_b = 1 + \delta(\nabla \cdot \mathbf{n}) + \mathbf{o}[\delta(\nabla \cdot \mathbf{n})] \approx 1 + \delta(\nabla \cdot \mathbf{n}) \tag{4.56}$$

for generally curved flames.

Considering that the extent of the influence of the divergence ratio on flame temperature and flame speed may be different, the more general correlations would have the following expressions,

$$T_b \propto [1 + \alpha\delta(\nabla \cdot \mathbf{n})]Ka \tag{4.57}$$

$$S_u A_u / A_b \propto [1 + \beta\delta(\nabla \cdot \mathbf{n})]Ka \tag{4.58}$$

where $\alpha$ and $\beta$ are positive constants on the order of unity; their values depend on the fresh mixture and the method of determining the flame radius and flame thickness; they are independent of how the flame is curved and the degree of curvature.

If $A_u/A_b$ is not extremely large or small, i.e. the absolute value of curvature is not extremely large, the difference of $\delta / S_b$ between the curved flame and the planar flame is small and the small difference can be absorbed by the coefficients $\alpha$ and $\beta$. Then, the flame temperature and corrected flame speed $S_uA_u/A_b$ of the curved flame with stretch rate $k$ are almost equal to those of a stretched planar flame with the corrected stretch rates $[1 + \alpha\delta(\nabla \cdot \mathbf{n})]k$ and $[1 + \beta\delta(\nabla \cdot \mathbf{n})]k$ respectively.

$$T_b \propto [1 + \alpha\delta(\nabla \cdot \mathbf{n})]k \tag{4.59}$$

$$S_u A_u / A_b \propto [1 + \beta\delta(\nabla \cdot \mathbf{n})]k \tag{4.60}$$

The above equations are more convenient than its previous versions (Eq. (4.54), Eq. (4.55) and Eq. (4.57), Eq. (4.58)) because they do not require the value of $S_b$ that is hard to define and find in real flames. With above equations, we can estimate the flame temperature and flame speed of any curved flame. We can get the values of $\alpha$ and $\beta$ by comparing the opposed jet flame and any curved flame such as the tubular flame or the spherical flame.

## Calculation examples

Here, we give example calculations for stretched and curved flames burning a lean $H_2$/air mixture with an equivalence ratio of 0.4. According to Law and Sung (2000), the

activation temperature is $T_a \approx 18000$K and Lewis number is $Le \approx 0.33$. From the PREMIX program of CHEMKIN, $T_b^0 = 1418$K, $S_u^0 = 0.199$ m/s. The specific heat and heat conductivity are calculated with the average temperature and species of fresh mixture and product of the one-dimensional unstretched planar flame: $\lambda \approx 0.077$W/mK and $c_p \approx 1265$ J/Kg/K (the $c_p$ determined by this method also satisfies the energy conservation equation $c_p(T_b^0 - T_u) = Qf_0$ within 1% error); and set $m = 0$, $n_1 = 1$, $n_2 = 1$. Fig. 4.1 compares the flame temperatures of the analytical solutions of the planar stretched flame and the tubular flame with $r_s = 0$ to the numerical solutions of the opposed jet burner flame and the tubular burner flame. The numerical solution of the opposed jet flame is from OPPDIF of CHEMKIN and the numerical solution of the tubular flame is described in Chapter II; the chemical mechanism is from Mueller et al. (1999). In Fig. 4.1, there are two numerical solutions for the opposed jet flame, one is from the twin flame configuration and the other one is from the single flame configuration (premixed flame vs. hot nitrogen). The flame temperature of the single flame is quantified by the following way: when the hot nitrogen temperature is lower than the premixed flame temperature, there is a peak on the temperature curve; the nitrogen temperature is increased until the peak disappears at which point the temperature of the nitrogen is the flame temperature. The stretch rates adopted here are from Chapter II. At low stretch rate, the solutions of twin flame and single flame configurations have the same temperature; at high stretch rate, the twin flames approach the center of the burner and the chemical reactions become incomplete because of the symmetry and the flame temperature is lowered; however, for the single flame, it can move freely, the chemical reactions will be complete and its temperature will represent the real flame temperature

affected by stretch. As seen in Fig. 4.1, the flame temperatures of the numerical solutions and analytical solutions have good agreement. Fig. 2 shows the comparisons of flame speed. For the opposed jet flame, the analytical solution is about 30% higher than the numerical solution; for the tubular flame, the analytical solution is about 15% higher than the numerical solution. The difference comes from two parts: 1) the flow field, we assume a very simple flow field for the analytical solution which can represent the more complicated real flow field qualitatively but not quantitatively; 2) the chemistry, flame speed is sensitive to chemistry and the one-step chemistry is too simplified to predict the flame speed accurately. However, the accuracy of the analytical prediction of the flame speed is satisfied considering the simple chemistry and flow field assumptions.

To prove above correlations, we compare the planar, positively curved and negatively curved flames through Fig. 4.3 to Fig. 4.8 (+ denotes positively curved and – denotes negatively curved; positively and negatively curved tubular flames have $r_s = 0$ and $r_s =$ 1.75mm respectively； positively and negatively curved spherical flames have $r_s = 0.6$mm and $r_s = 2$mm respectively). Fig. 4.3 and Fig. 4.8 show the flame temperature and flame speed $S_u$ variation with stretch rate for these flames. Fig. 4.5 and Fig. 4.6 show the flame temperature and corrected flame speed comparisons based on the corrected Karlovitz number (the empirical constant is set $\alpha = \beta = 1$) while Fig. 4.7 and Fig. 4.8 are based on the corrected stretch rate. In Fig. 4.3 and Fig. 4.4, we can see that the five flames have significant differences, especially for the flame speed. The curves match very well in Fig. 4.5 and Fig. 4.6; for the same corrected Karlovitz number, different flames have almost the same flame temperature and corrected flame speed. The curves match very well in Fig. 4.7 and Fig. 4.8.

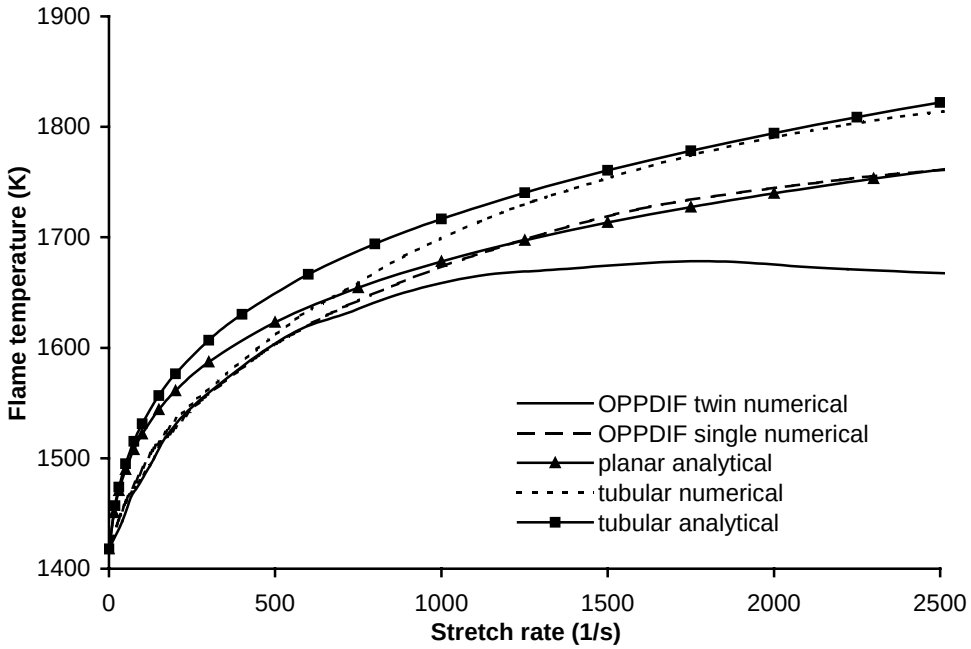


**Fig 4.1**. Flame temperature comparison of numerical and analytical solutions for the opposed jet flame and the tubular flame (lean $H_2$/Air premixed flame with equivalence ratio 0.4).

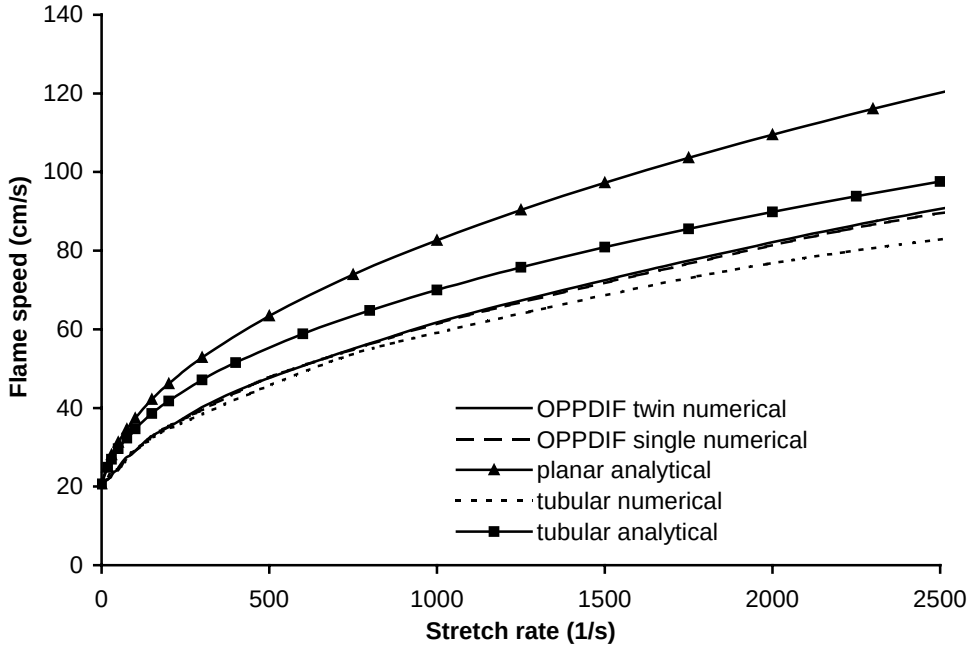


**Fig 4.2**. Flame speed $S_u$ comparison of numerical and analytical solutions for the opposed jet flame and the tubular flame (lean $H_2$/Air premixed flame with equivalence ratio 0.4).

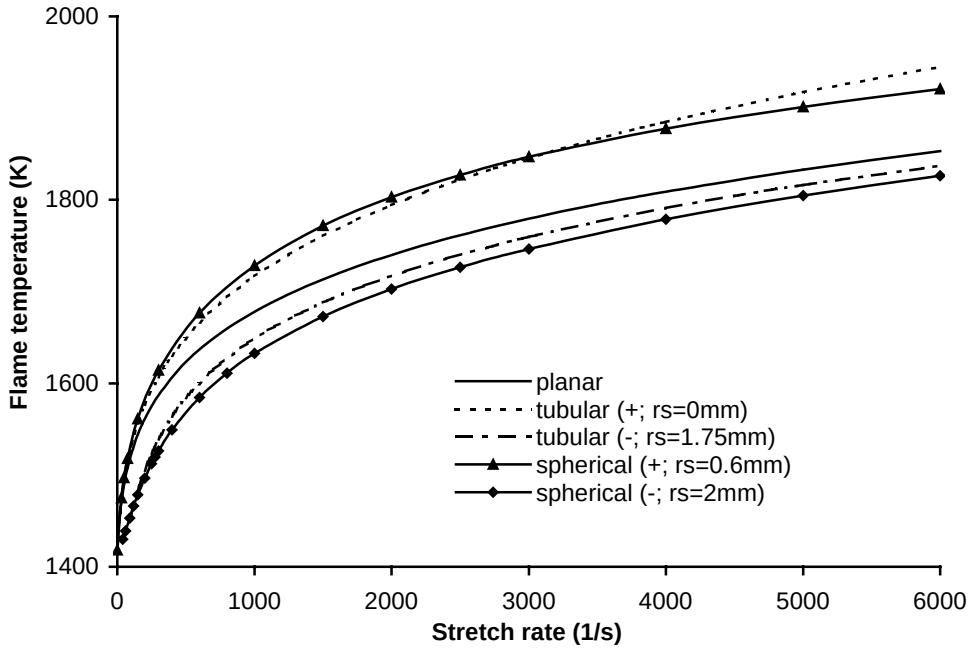


**Fig 4.3**. Analytical flame temperature variation with stretch rate for the planar and curved flames (lean $H_2$/Air premixed flame with equivalence ratio 0.4).

.

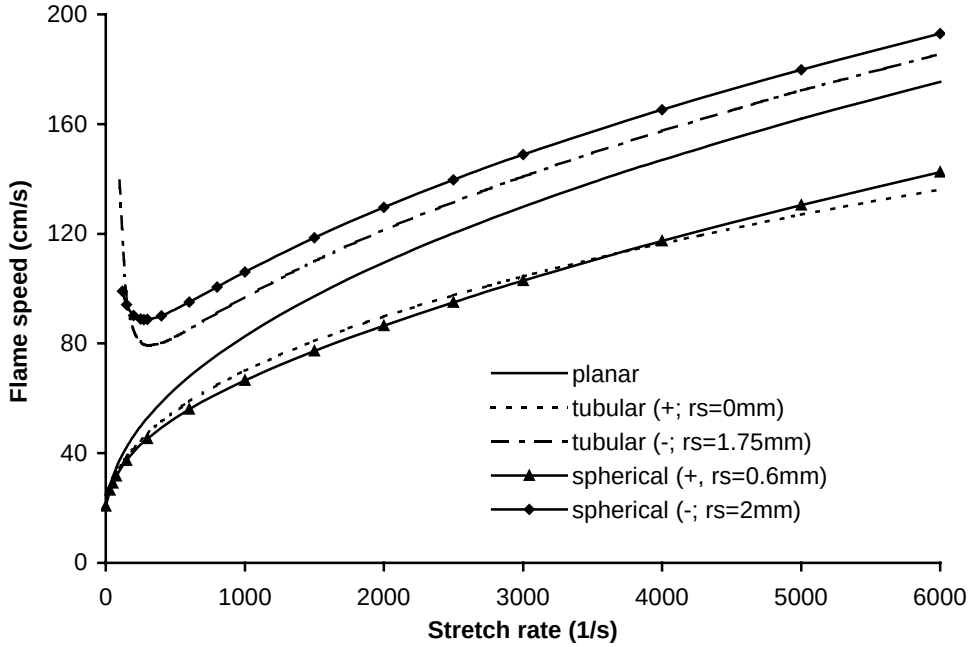


**Fig 4.4**. Analytical flame speed $S_u$ variation with stretch rate for the planar and curved flames (lean $H_2$/Air premixed flame with equivalence ratio 0.4).

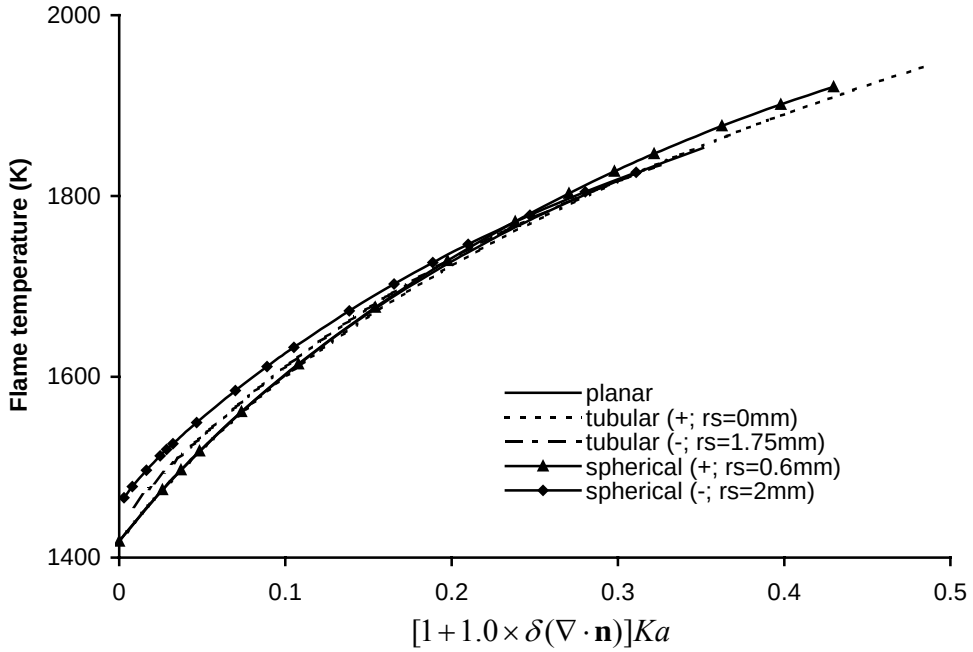


**Fig 4.5**. Analytical flame temperature variation with corrected Karlovitz number for the planar and curved flames (lean $H_2$/Air premixed flame with equivalence ratio 0.4).

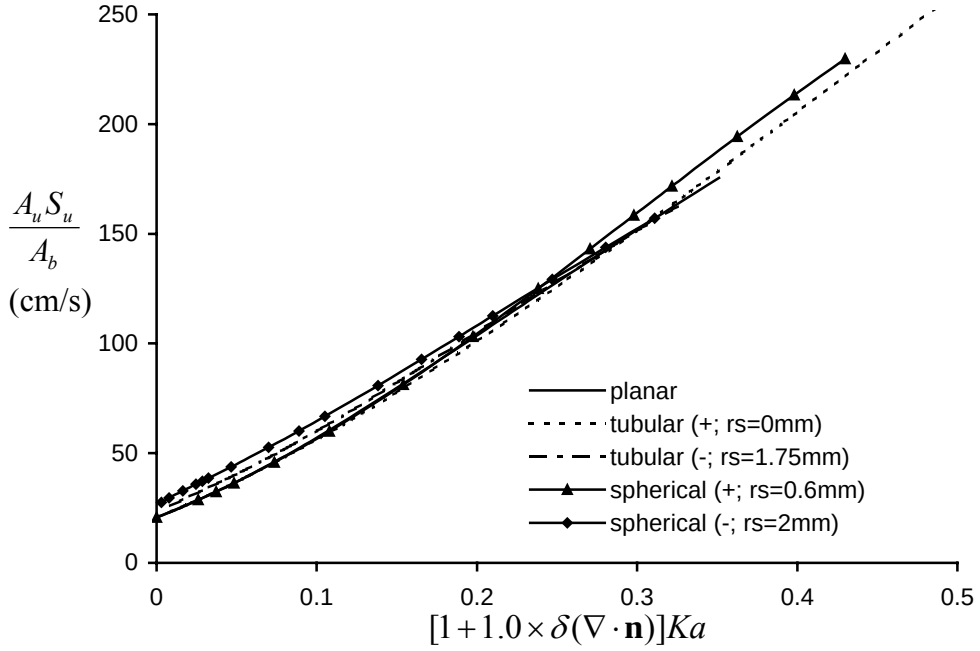


**Fig 4.6**. Analytical corrected flame speed variation with corrected Karlovitz number for the planar and curved flames (lean $H_2$/Air premixed flame with equivalence ratio 0.4).

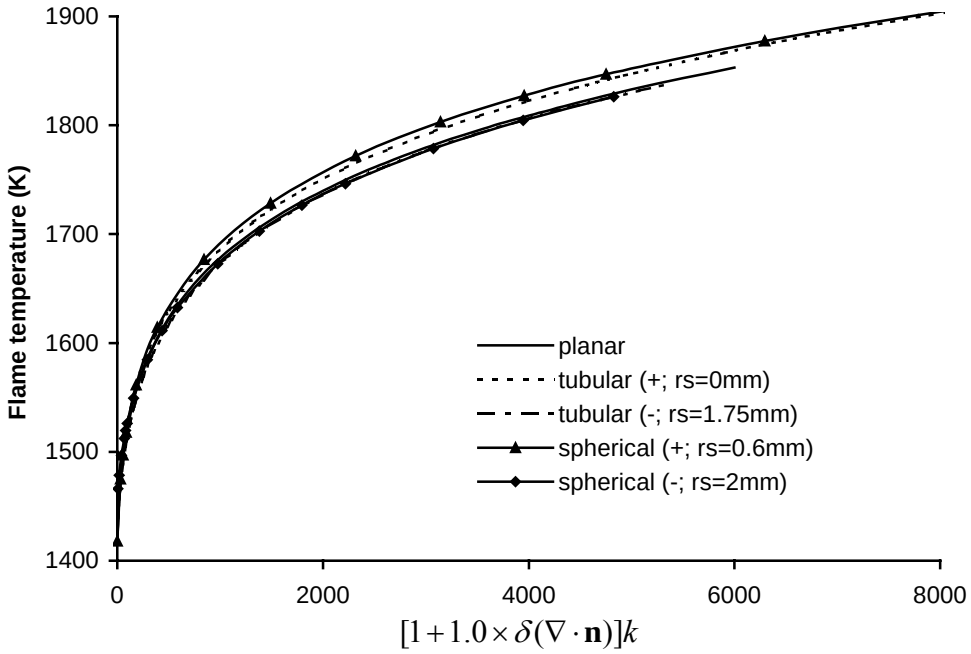


**Fig 4.7**. Analytical flame temperature variation with corrected stretch rate for the planar and curved flames (lean $H_2$/Air premixed flame with equivalence ratio 0.4).

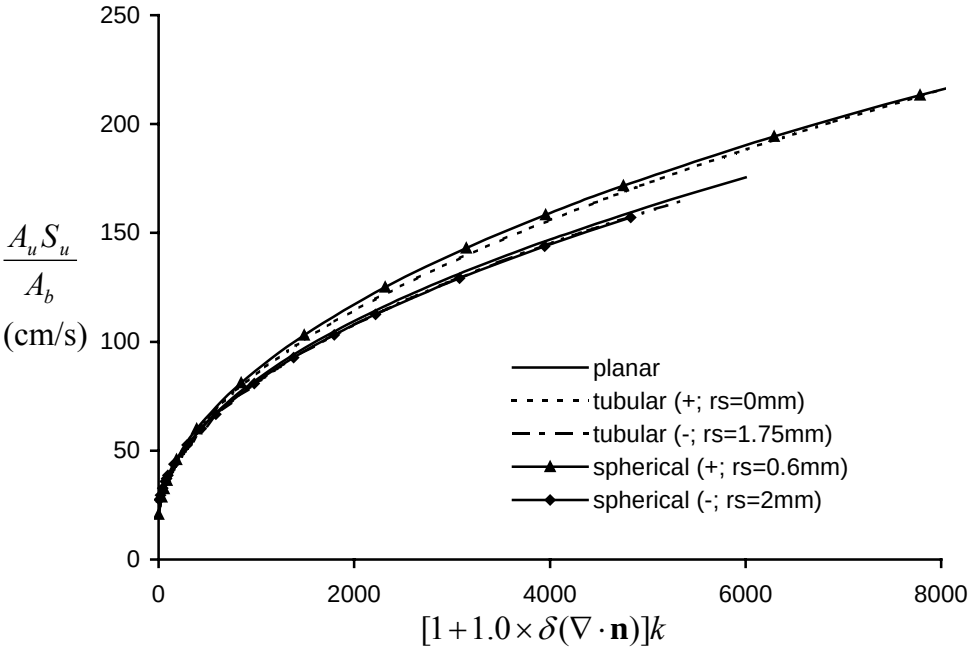


**Fig 4.8**. Analytical flame speed variation with corrected stretch rate for the planar and curved flames (lean $H_2$/Air premixed flame with equivalence ratio 0.4).

Another example is the rich $H_2$/air flame with an equivalence ratio of 4.0. According to Law and Sung (2000), the activation temperature is $T_a \approx 8300$K and Lewis number is $Le \approx 2.32$. From the PREMIX program of CHEMKIN, $T_b^0 = 1558$K, $S_u^0 = 1.7$ m/s. $\lambda \approx 0.1995$W/mK and $c_p \approx 2531$ J/Kg/K (the $c_p$ determined by this method also satisfies the energy conservation equation $c_p(T_b^0 - T_u) = Qf_0$ within 1% error); $m = 0$, $n_1 = 1$, $n_2 = 1$. Fig. 4.9 and Fig. 4.10 show the comparisons of the flame temperature and flame speed between the analytical solution and the numerical solution for the opposed jet twin flames. There are two numerical flame temperature curves in Fig. 4.9; one is the flame temperature of the twin flames; the other one is the equilibrium temperature at the symmetric plane of the twin flames and it is called OPPDIF twin product equilibrium temperature in Fig. 4.9; the product equilibrium temperature is the flame temperature with all the residual oxygen (deficient species) and radicals burned to equilibrium state and it is equivalent to the flame temperature of the single flame configuration. In Fig. 4.9, the difference between the analytical temperature and the equilibrium temperature is small and the result of the analytical solution is satisfied. The analytical solution predicts the extinction stretch rate $4679s^{-1}$; and the numerical solution predicts the extinction stretch rate $3870s^{-1}$. For the twin flames, the extinction is caused by the preferential diffusion and the incompleteness of chemical reactions. However, the extinction of the analytical solution is caused by the preferential diffusion only; it is natural that the extinction stretch rate of the analytical solution is higher than that of the numerical solution. In Fig. 4.10, the flame speed of the analytical solution is still about 30% higher than that of the numerical solution. The planar, positively curved and negatively curved flames are compared through Fig. 4.11 to Fig. 4.14. Fig. 4.11 and Fig. 4.12 shows the

flame temperature and flame speed $S_u$ variation with stretch rate for these flames. For $Le > 1$, the negatively curved flames have higher extinction stretch rate and the positively curved flames have lower extinction stretch rate which is consistent with the physical analysis in chapter III. Fig. 4.13 and Fig. 4.14 show the flame temperature and corrected flame speed comparisons based on the corrected stretch rate (the empirical constants are set to $\alpha = 0.7$ and $\beta = 1.2$). The five curves match very well in Fig. 13 and Fig. 14 although they are scattered in Fig. 4.11 and Fig. 4.12.

## Conclusion

We derived the coupled flame temperature and flame speed expressions with asymptotic analysis for the stretched planar, tubular and spherical flames. The comparisons between the numerical solutions and the analytical solutions are satisfied for $H_2$/Air premixed flames. Based on the physical analysis, correlations are given to calculate the flame temperature and flame speed of generally curved and stretched premixed flame from the information of stretched planar flames; which extend the usage of the asymptotic analysis. The correlations are validated for lean and rich curved $H_2$/air premixed flames. Using these correlations, one can predict the temperature and flame speed of any stretched and curved flame from the temperature and flame speed of the opposed jet planar flame.

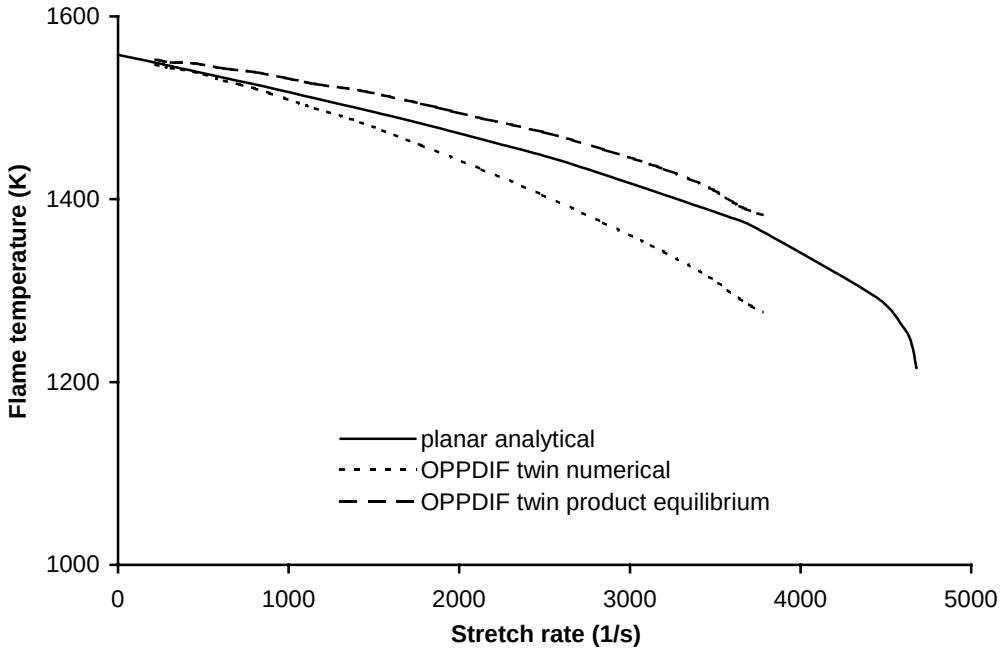


**Fig 4.9**. Flame temperature comparison of numerical and analytical solutions for the opposed jet flames (rich $H_2$/Air premixed flame with equivalence ratio 4.0).

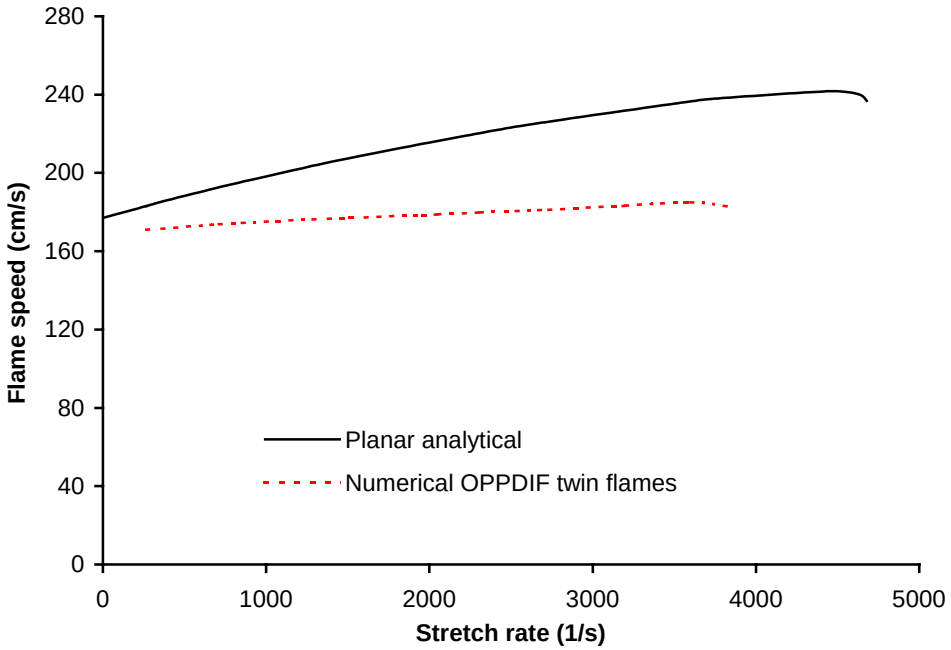


**Fig 4.10**. Flame speed $S_u$ comparison of numerical and analytical solutions for the opposed jet flames (rich $H_2$/Air premixed flame with equivalence ratio 4.0).

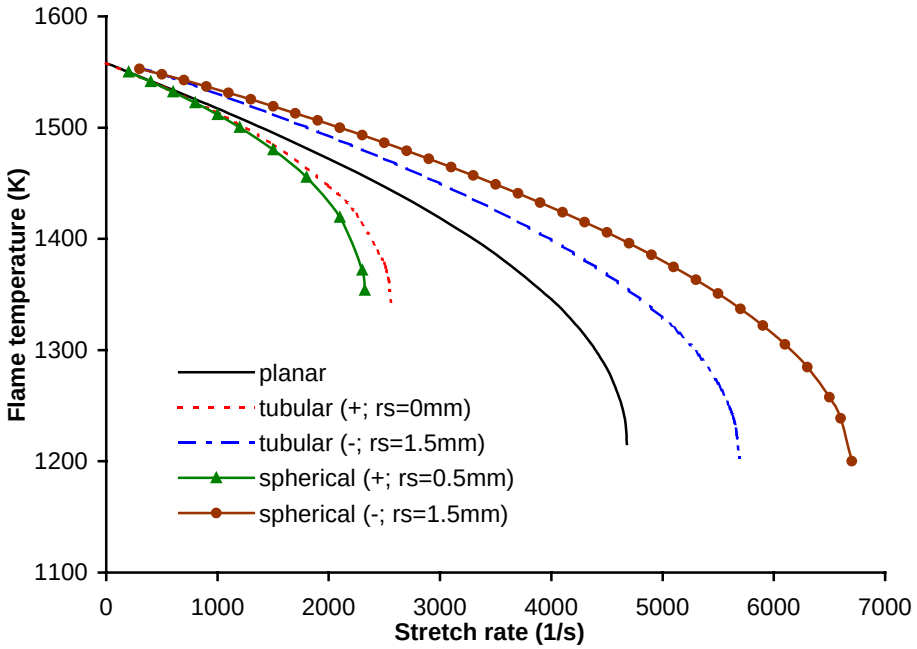


**Fig 4.11**. Analytical flame temperature variation with stretch rate for the planar and curved flames (rich $H_2$/Air premixed flame with equivalence ratio 4.0).

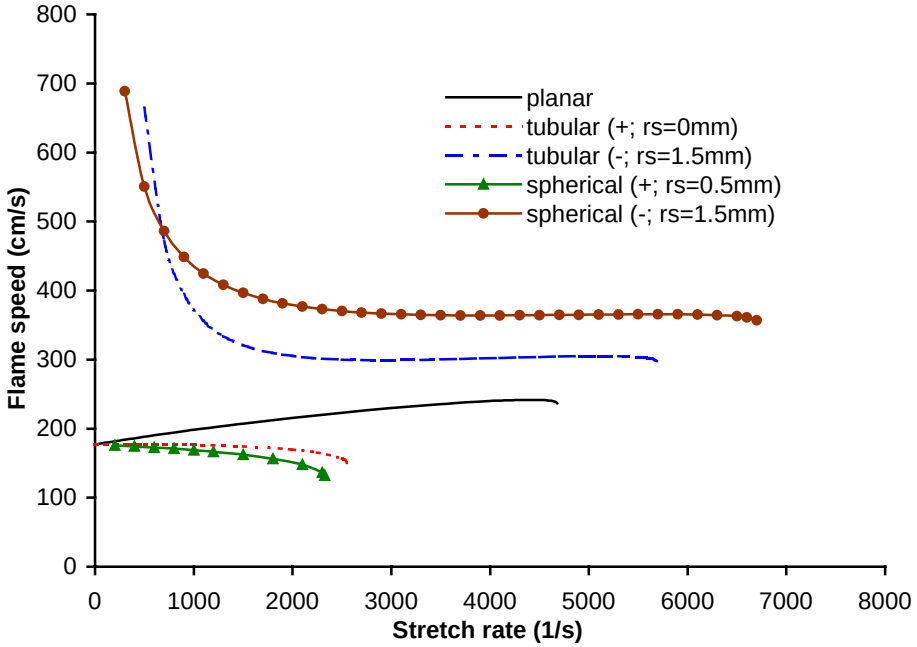


**Fig 4.12**. Analytical flame speed $S_u$ variation with stretch rate for the planar and curved flames (rich $H_2$/Air premixed flame with equivalence ratio 4.0).

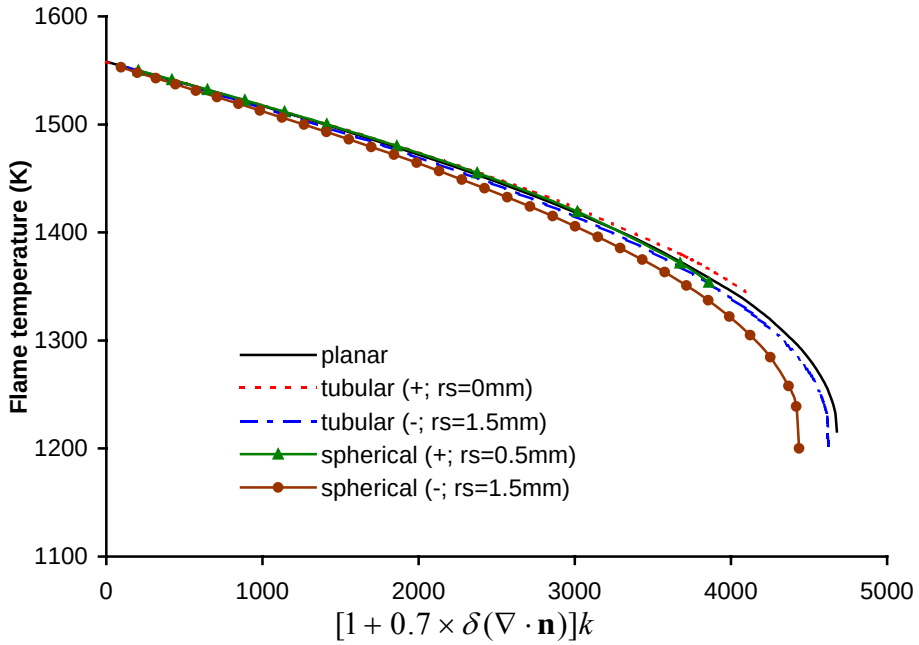


**Fig 4.13**. Analytical flame temperature variation with corrected stretch rate for the planar and curved flames (rich $H_2$/Air premixed flame with equivalence ratio 4.0).

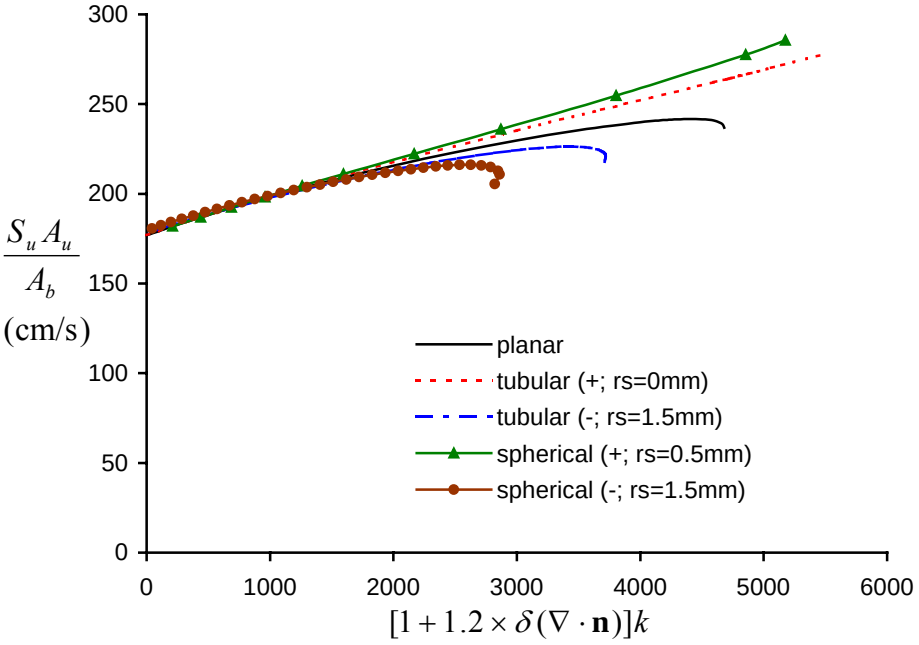


**Fig 4.14**. Analytical corrected flame speed variation with corrected stretch rate for the planar and curved flames (rich $H_2$/Air premixed flame with equivalence ratio 4.0).

# CHAPTER V

# NUMERICAL INVESTIGATION OF THE CURVATURE EFFECTS ON DIFFUSION FLAMES

## Abstract

In this chapter, tubular diffusion flames are compared with opposed jet diffusion flames numerically to show the effect of curvature on diffusion flames. The numerical results show that, as in premixed flames, positive curvature strengthens the preferential diffusion and negative curvature weakens the preferential diffusion; the strengthening or weakening effect is proportional to the ratio of flame thickness to flame radius. Since the flame temperature is related to the preferential diffusion, flame curvature affects flame temperature and extinction stretch rate. Since the flame thickness is related to pressure, the curvature effects also depend on pressure. $H_2/N_2$–air and $CH_4/N_2$–air diffusion flames with different flame radii and pressures are presented to verify the analysis.

## Introduction

Stretched planar laminar diffusion flames realized by the opposed jet burner shown in Fig. 2.1 have been studied broadly and numerical solutions using commercial software (e.g., OPPDIF of CHEMKIN) are available. Linan (1974) first studied this kind diffusion flame and obtained analytical expressions for the ignition and extinction. Chung and Law (1982, 1984), and Cuenot and Poinsot (1996) analyzed opposed jet diffusion flames with infinitely fast chemistry and non-unity Lewis numbers. It is shown that the preferential diffusion effect exists on both the fuel side and the oxidizer side of the flame. For example, when the Lewis number of the fuel or oxygen is less than one, the flame

temperature is higher than its adiabatic equilibrium temperature (With unity Lewis numbers, i.e., $Le_f = Le_o = 1$, the flame temperature is a constant under the infinitely fast chemistry assumption (Glassman, 1996) and is called the adiabatic equilibrium temperature); when the Lewis number of the fuel or oxygen is more than one, the flame temperature is less than its adiabatic equilibrium temperature; but the preferential diffusion effect is constant under infinitely fast chemistry, that is, the temperature increase or decrease is independent of stretch rate. With one-step high-activation-energy finite rate chemistry, Chung and Law (1983), and Cuenot and Poinsot (1996) gave the flame temperature and extinction variation with stretch rate and Lewis numbers. Sung et al. (1995) studied the opposed jet diffusion flame structure with complex chemistry and showed the influence of the chemical kinetics on the structure of the opposed jet flames. Brown et al. (1997) studied the flame structure and preferential diffusion for the opposed jet hydrogen diffusion flames. Both papers (Sung et al., 1995; Brown et al., 1997) showed that the flame thickness is inversely proportional to the square root of stretch rate.

The study of curvature effects on the diffusion flames basically focuses on two flames: the flame tip of the Burke-Schumann flames (Ishizuka and Sakai, 1983,1986; Im et al., 1990; Katta et al., 1994; Takagi et al., 1994, 1996a) and the perturbed opposed jet flames (Takagi et al., 1996b; Finke and Grünefeld, 2000; Yoshida and Takagi, 1998, 2003; Lee et al., 2000; Katta et al., 1998). Ishizuka and Sakai (1983, 1986) studied the extinction at the curved flame tip of Burke-Schumann flame experimentally; the local extinction at the tip was observed with the mixture of $H_2$ and $CO_2$ as the fuel stream. Im et al. (1990) also studied the flame tip theoretically and experimentally; the flame tip is negatively stretched which increases the residential time of reactants in the reaction zone; it makes

the flame tip stronger and harder to be extinguished. For a fuel stream with Lewis number less than one, the preferential diffusion results in low fuel concentration, low temperature and possible extinction at the flame tip. Katta et al. (1994) and Takagi et al. (1994, 1996a) also studied similar flames numerically. In Takagi et al. (1996a), the flame tip temperature is much lower than the adiabatic equilibrium temperature if the fuel ($H_2/N_2$, Lewis number less than one) comes from the inner nozzle, i.e. the flame is concave to the fuel stream and vice versa if the fuel comes from the outer nozzle; detailed numerical analysis on flame structure substantiated the preferential diffusion effect. Takagi et al. (1996b), Finke and Grünefeld (2000), and Lee et al., (2000) perturbed the opposed jet flow field to form curved flames with positive stretch; the results are consistent with those from Burke-Schumann flames. When the flame is concave to the fuel stream ($H_2/N_2$), the flame is weaker and the local extinction is observed; the flame is stronger if the flame is convex to the fuel stream. In Yoshida and Takagi (2003), for the same stretch rate, the flame has higher temperature if the flame is convex to the $H_2/N_2$ fuel stream and lower temperature if the flame is concave to the fuel stream; the temperature difference increases as the stretch rate decreases.

For the Burke-Schumann flames and perturbed opposed jet flames, the flames are multidimensional and it is hard to identify the values of stretch rate and curvature; and sometimes, it is hard to separate the effects of stretch and curvature since the stretch rate and curvature vary simultaneously when the operational conditions are varied. To overcome these difficulties, the opposed tubular burner as shown in Fig. 2.2 was built and has been tested by Wehrmeyer et al. (2001). The main advantages of this burner are: 1) the flame structure is one-dimensional; 2) the flame is uniformly stretched and curved; 3)

stretch rate and curvature can be varied independently. Here, we compare the opposed tubular flame with the opposed jet flame numerically to study the curvature effects on diffusion flames.

## Governing equations

The governing equations are the same as in Chapter II except the boundary condition.

$R=R_1,\ \ f = R_1\rho_1 V_1,\ \ g = 0,\ \ T = T_1,\ \ Y_i = Y_{i1}$

$R=R_2,\ \ f = R_2\rho_2 V_2,\ \ g = 0,\ \ T = T_2,\ \ Y_i = Y_{i2}$

The boundary condition specifies the mass fraction and temperature. Except convection, there is extra mass diffusion from the nozzles and extra heat conduction to the nozzles if the species and temperature gradients are not zero at the nozzle exits. The enthalpy gain from the extra mass diffusion and the heat loss from the extra conduction generally are not balanced; this makes flame temperature change and this change is not the result of stretch or curvature. We tried changing the boundary condition to specify the mass and thermal flux to eliminate the above problem; however, we found that the flame properties would be burner geometry dependent if temperature and species have gradients at the boundaries since only part of the diffusion flame structure exists in the flow field. In the following calculation, we did not include any results with either temperature or species gradients at the nozzle exits. The numerical solution has been validated by the experimental data in Hu et al. (2006); the measured and predicted flame temperature, flame position and flame structure have perfect agreement.

## Stretch rates of the flames

Stretch rates of the flames are calculated from the formulas in Chapter II. Since air is the oxidizer in the following study and there is little preferential diffusion effect in the oxidizer side ($Le_o \approx 1$), we will use the stretch rate in the fuel side as the stretch rate for both the opposed jet flame and the opposed tubular flame.

## Results and discussions

For premixed flames, the fuel and oxygen are mixed first, so the flame is curved to the premixture either positively (convex to the premixture) or negatively (concave to the premixture). For diffusion flames, the fuel and oxygen are in different sides of the curved flame surface, so the flame surface is positively curved to one stream and negatively curved to the other one. Since the curvature effects will be related to the preferential diffusion and the oxidizer is air ($Le_o \approx 1$) in the following calculation, the terms of "negatively curved" and "positively curved" refer to the curvature status of the fuel stream here; that is, "negatively curved flame" means that the flame surface is concave to the fuel stream; "positively curved flame" means that the flame surface is convex to the fuel stream.

Except stated otherwise, the following settings are used for $H_2$ diffusion flames. The fuel is 80%$N_2$ and 20% $H_2$; the oxidizer is air; the chemistry is from Mueller et al. (1999). For the opposed jet burner, the distance between two nozzles is set to 45mm and the equal velocities are used for the nozzles. For the opposed tubular burner, $R_1$ = 0.3mm and $R_2$ = 15mm. The velocities from both nozzles are chosen such that the stagnation radius

for both positively curved flames (fuel from the outer nozzle) and negatively curved flames (fuel from the inner nozzle) is 5mm. The pressure is atmospheric pressure.

The flame radius can be determined from the peak temperature position or the stoichiometric position that is different from the stagnation position. The distance between the stagnation position and the peak temperature position or the stoichiometric position decreases with stretch rate and is small compared to the stagnation radius for the cases we are studying here. For convenience, we choose the stagnation radius to represent the flame radius approximately.

First, we want to clarify that the diffusion flame parameters are functions of stretch rate and curvature only in the opposed tubular flame; they are independent of the burner geometry. Fig. 5.1 compares the flame temperature variation with stretch rate for different opposed tubular burner geometries and velocity ratios while keeping flame curvature constant (positively curved). For geometry one, $R_1$ = 0.3mm; $R_2$ = 15mm; $|V_1/V_2|$ = 5.538. For geometry two, $R_1$ = 1.5mm; $R_2$ = 25mm; $|V_1/V_2|$ = 0.562. For geometry three, $R_1$ = 1mm; $R_2$ = 20mm; $|V_1/V_2|$ = 1.138. All the three geometry and velocity ratio settings give the same constant curvature, i.e. $R_s$ = 5mm. From Fig. 5.1, we can see that the opposed tubular flames have same peak temperature for the same stretch rate and are extinguished at the same stretch rate ($1590s^{-1}$).

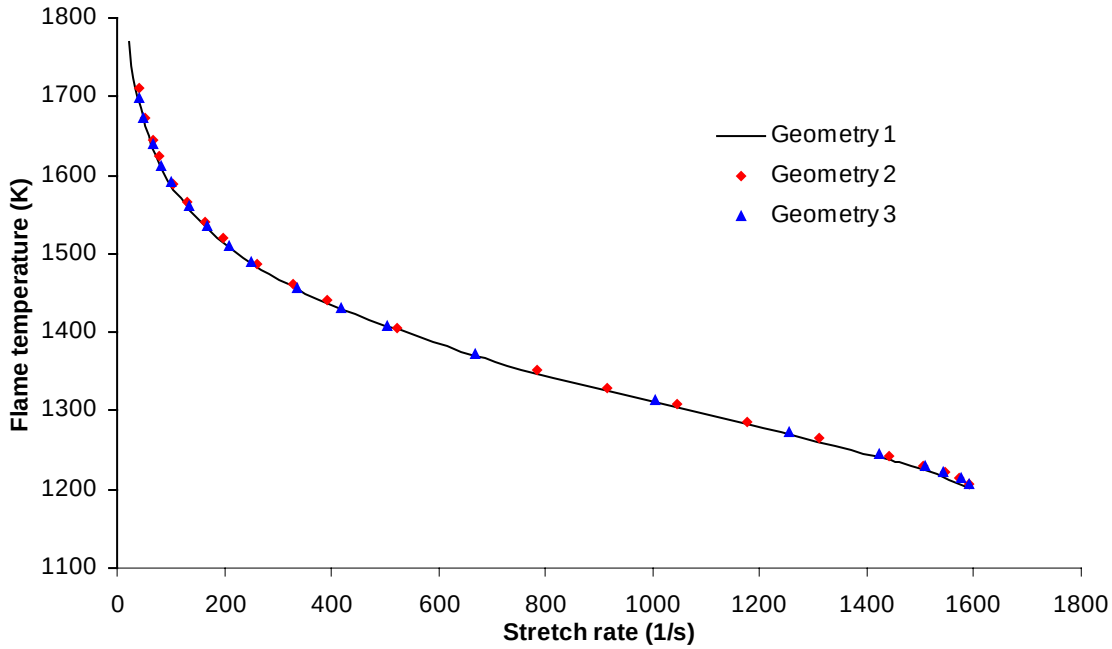


**Fig 5.1**. Flame temperature variation with stretch rate for the positively curved flames with different geometries.

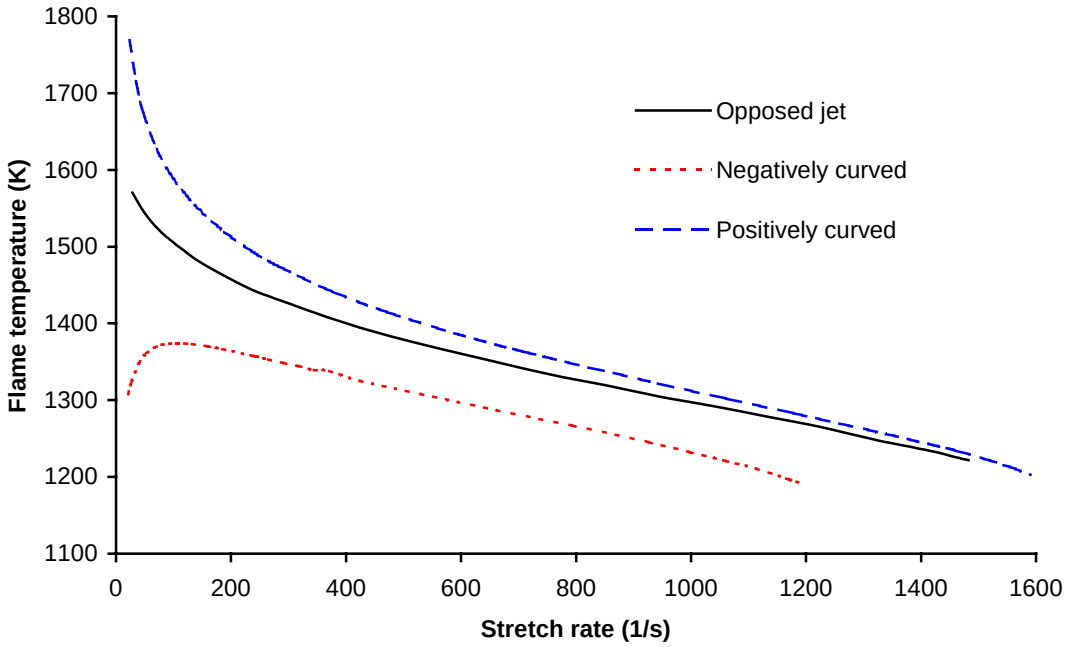


**Fig 5.2**. Flame temperature variation with stretch rate for the planar and curved flames.

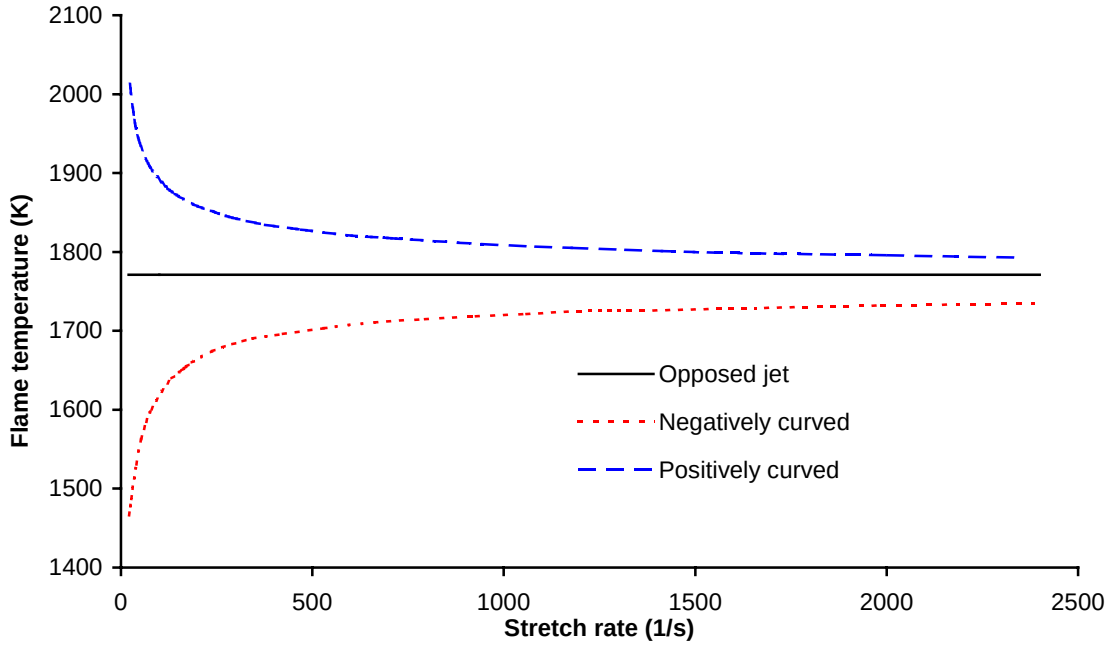


**Fig 5.3**. Flame temperature variation with stretch rate for the planar and curved flames (with infinitely fast chemistry).

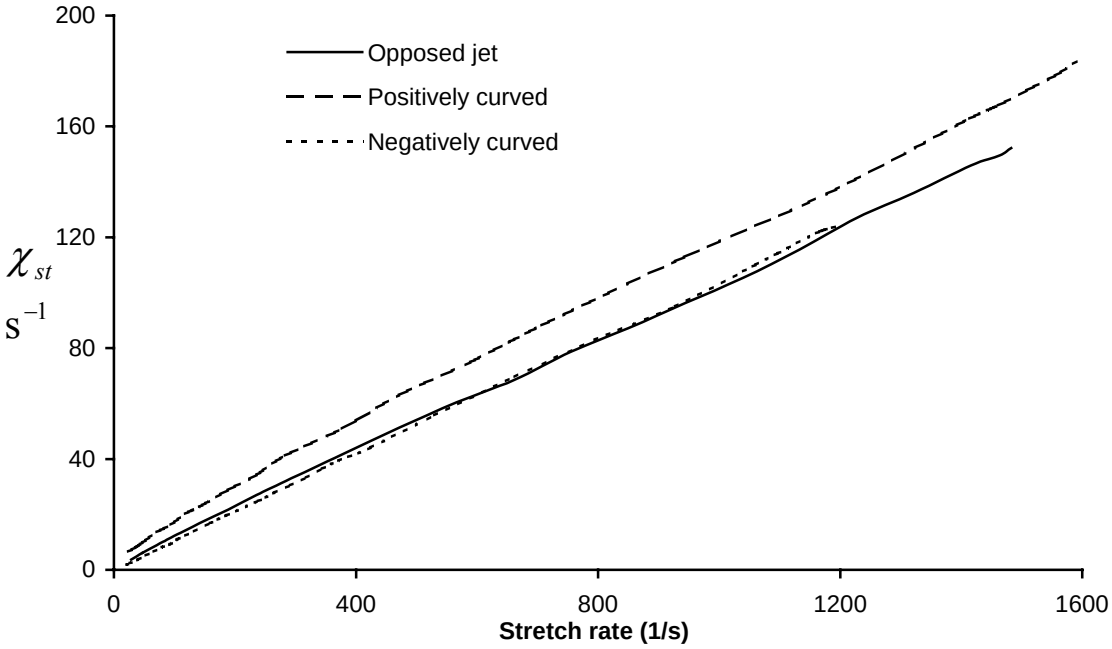


**Fig 5.4**. Scalar dissipation rate variation with stretch rate for the planar and curved flames.

Fig. 5.2 shows the comparison of the flame temperature variation with stretch rate for the planar and curved flames. For the opposed jet flame and positively curved flame, the flame temperature decreases monotonically with stretch rate; for the negatively curved flame, the flame temperature first increases and then decreases with stretch rate. The positively curved flame has higher flame temperature and a little bit higher extinction stretch rate ($1590s^{-1}$) than the opposed jet flame ($1482s^{-1}$); the temperature difference decreases with stretch rate. The negatively curved flame has lower flame temperature and extinction stretch rate ($1192s^{-1}$) than the opposed jet flame. As the stretch rate increases, the residence time of the reactants in the reaction zone decreases and the chemical reactions are more incomplete. It is the natural result that the flame temperature of diffusion flames decreases with stretch rate. The fact that the temperature increases with low values of stretch rate for the negatively curved flame is surprising and it must result from the curvature.

The flame temperature of diffusion flames is determined by two factors: the preferential diffusion and the completeness of chemical reactions that is related to Damköhler number. Damköhler number is defined as the ratio of the diffusion time to the chemical reaction time and it reflects the completeness of chemical reactions. For a second order reaction, $Da = \varpi/(\rho\chi)$ where $\varpi$ is the chemical reaction rate and $\chi = \alpha(\partial\xi/\partial x)^2$ is the scalar dissipation rate ($\alpha$ is the thermal diffusivity; $\xi$ is the mixture fraction; $x$ is axial coordinate for the opposed jet flame and radial coordinate for the opposed tubular flame).

To separate the effect of these two factors, we first set the chemistry to be infinitely fast, so that we can study the preferential diffusion effect independently. Fig. 5.3 shows

the flame temperature variation with stretch rate for the three flames with infinite chemistry (one-step irreversible reaction with a very high reaction rate). For the opposed jet flame, the flame temperature is constant (1771K) but higher than its adiabatic equilibrium value (1368.5K); this result is consistent with the previous analytical work by Chung and Law (1982,1984), and Cuenot and Poinsot (1996), the preferential diffusion increases the flame temperature. For the curved flames, we can see that the positive curvature strengthens the preferential diffusion (higher temperature) and the negative curvature weakens the preferential diffusion (lower temperature). As the stretch rate increases, the flames become thinner and the curvature effect on the preferential diffusion becomes smaller (smaller temperature difference). This means, for diffusion flames, positive curvature strengthens the preferential diffusion and negative curvature weakens the preferential diffusion; the strengthening or weakening effect is proportional to the ratio of flame thickness to flame radius (constant in this example). This result is similar to that of premixed flames.

Secondly the completeness of chemical reactions is related to the scalar dissipation rate. Fig. 5.4 shows the variation of $\chi_{st}$ with stretch rate for the three flames in Fig. 5.2; $\xi = (X_{O,2}/W_2\nu_O + X_F/W\nu_F - X_O/W\nu_O)/(X_{O,2}/W_2\nu_O + X_{F,1}/W_1\nu_F)$ (Williams, 1985); $\nu_O$ and $\nu_F$ are the stoichiometric coefficients for oxygen and fuel respectively; the subscripts $F$, $O$ refer to fuel and oxygen, the second subscripts 1, 2 means fuel and oxidizer stream boundaries. $\chi_{st}$ is evaluated at $\xi = \xi_{st} = 0.624$. For the same stretch rate, the negatively curved flame has almost the same scalar dissipation rate as the opposed jet flame; and the positively curved flame has higher value than the opposed jet flame, but the difference is small. So the flame temperature difference between the curved flames and the opposed jet

flame is mainly caused by the preferential diffusion (by two ways: directly from the preferential diffusion as shown in Fig. 5.3 and indirectly from Damköhler number through the reaction term).

The above analysis on the preferential diffusion is consistent with all the results of previous work (Ishizuka and Sakai, 1983,1986; Im et al., 1990; Katta et al., 1994, 1998; Takagi et al., 1994, 1996a, 1996b; Finke and Grünefeld, 2000; Yoshida and Takagi, 1998, 2003; Lee et al., 2000). For the perturbed opposed jet flames (Takagi et al., 1996b; Finke and Grünefeld, 2000; Yoshida and Takagi, 1998, 2003; Lee et al., 2000; Katta et al., 1998), the flames have lower flame temperature and can be extinguished if the $H_2/N_2$ fuel stream has negative curvature since the negative curvature weakens the preferential diffusion effect; vice versa, the flames have higher flame temperature if the $H_2/N_2$ fuel stream has positive curvature. It is observed that the preferential diffusion effect increases with decreasing the stretch rate in Yoshida and Takagi (2000); according our analysis, it results from the flame thickness increasing with decreasing the stretch rate.

To further prove the above analysis on the preferential diffusion, we change the flame thickness while keeping the flame curvature constant, and change the flame curvature while keeping the flame thickness constant. Fig. 5.5 shows the flame temperature variation with the flame radius for the curved flames with constant stretch rate ($200s^{-1}$). For constant stretch rate, the flame thickness is almost constant. As the flame radius decreases, the ratio of flame thickness to flame radius increases; the strengthening and weakening effect of the flame curvature to the preferential diffusion becomes stronger; the positively curved flame has higher temperature and the negatively curved flame has lower temperature. Fig. 5.6 shows the flame temperature variations with pressure for

constant stretch rate ($200s^{-1}$) and constant flame radius. Since Damköhler number is proportional to pressure for the second order reaction ($\varpi \propto P^2$ and $\rho\chi \propto P$, so $Da \propto P$); as the pressure increases, it becomes larger and the chemical reactions are more complete; so the flame temperature increases for all three flames. The trend and explanation of Fig. 5.6 are consistent with Chelliah et al. (1990). Fig. 5.7 shows the flame temperature difference (minus the flame temperature of the opposed jet flame) variations with pressure. As the pressure increases; the flames become thinner; the ratios of flame thickness to flame radius decrease and the flame temperature differences between the opposed jet flame and the curved flames become smaller.

As we have analyzed the mechanism of the curvature effects on diffusion flames, we now go back to Fig. 5.2. For the positively curved flame, as the stretch rate increases, both the preferential diffusion and incompleteness of chemical reactions cause the flame temperature decrease monotonically. For the negatively curved flame, as the stretch rate increases, the preferential diffusion tends to increase the flame temperature while the incompleteness of chemical reactions tends to decrease the flame temperature. At low stretch rate, the ratio of flame thickness to flame radius is large, the preferential diffusion effect dominates and the flame temperature increases with stretch rate; at high stretch rate, the ratio of flame thickness to flame radius is small, the incompleteness of chemical reactions dominates and the flame temperature decreases with stretch rate.

Fig. 5.8 shows the extinction stretch rate variations with curvature. The negatively curved flame extinguishes at lower stretch rate and the positively curved flame extinguishes at higher stretch rate than the opposed jet flame; the extinction stretch rate differences from that of the opposed jet flame decrease with the flame radius. This result

is consistent with the flame temperature analysis. Flame curvature plays important role in extinction if the Lewis numbers are far away from unity and the ratio of flame thickness to flame radius is large, i.e., on the order of unity.

For the $CH_4/N_2$-air diffusion flames, the temperature difference between the planar and curved flames should be small as shown in Fig. 5.9 (60%$CH_4$, 40%$N_2$; $R_1$=0.3mm, $R_2$=15mm, $R_s$=5mm; Kee et al. mechanism, 1985) since both the Lewis numbers of fuel and oxidizer streams are close to one; a little bit larger temperature difference close to extinction comes from the scalar dissipation rate. All three flames have the same extinction scalar dissipation rate $\chi_{st} = 19.36\text{s}^{-1}$ ($\xi_{st} = 0.112$); the flame curvature has little influence to the extinction scalar dissipation rate or Damköhler number if the Lewis numbers are close to one. For the same stretch rate, the planar flame has lower scalar dissipation rate than the curved flames leading to a higher flame temperature.

Although the above analysis comes from considering the fuel side only, it applies to the oxidizer side too. For negatively (positively) curved fuel stream with Lewis number less than one and positively (negatively) curved oxidizer stream with Lewis number more than one, curvature weakens (strengthens) the flame on both sides. For negatively curved fuel stream with Lewis number less (more) than one and positively curved oxidizer stream with Lewis number less (more) than one, curvature weakens (strengthens) the flame in the fuel side and strengthens (weakens) the flame in the oxidizer side, the comprehensive effect depends on the relative strength between weakening and strengthening.

## Conclusion

A new curved and stretched diffusion flame, i.e., opposed tubular flame that is uniformly stretched and curved, is studied numerically for the first time. The curvature effect is consistent with previous studies. Similar to premixed flames; for diffusion flames, the positive curvature strengthens the preferential diffusion and the negative curvature weakens the preferential diffusion; the strengthening or weakening effect is proportional to the ratio of flame thickness to flame radius. Resulting from the preferential diffusion, curvature has an important influence on extinction if the Lewis numbers are far away from unity and the ratio of flame thickness to flame radius is on the order of unity.

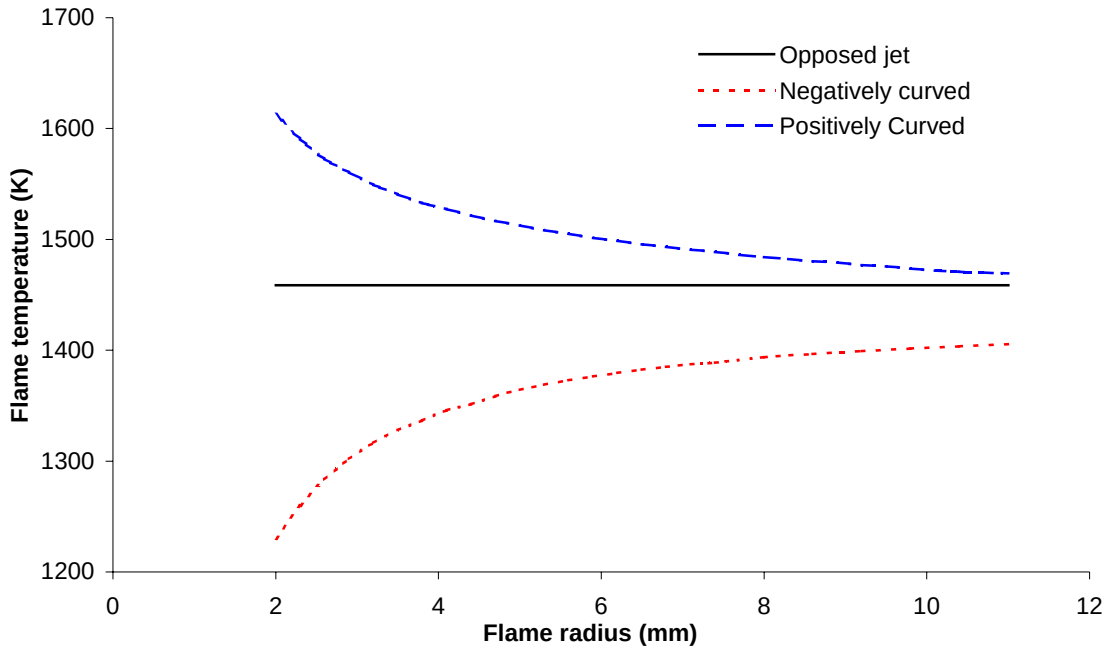


**Fig 5.5**. Flame temperature variation with flame radius for the curved flames with constant stretch rate ($k=200s^{-1}$).

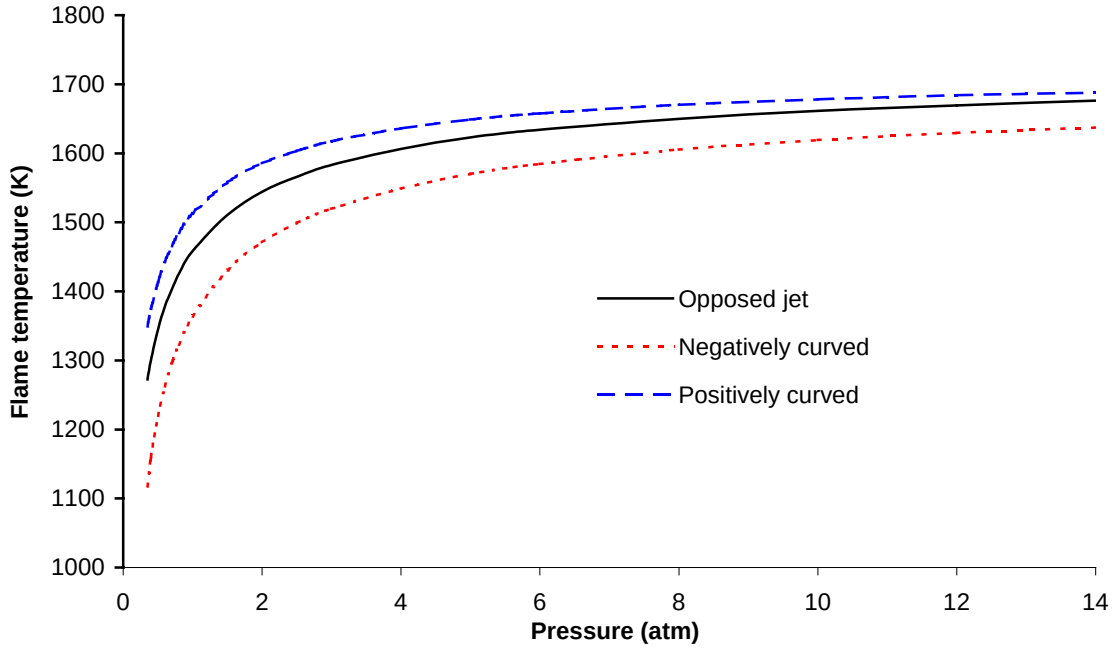


**Fig 5.6**. Flame temperature variation with pressure for the planar and curved flames with constant stretch rate ($k=200s^{-1}$).

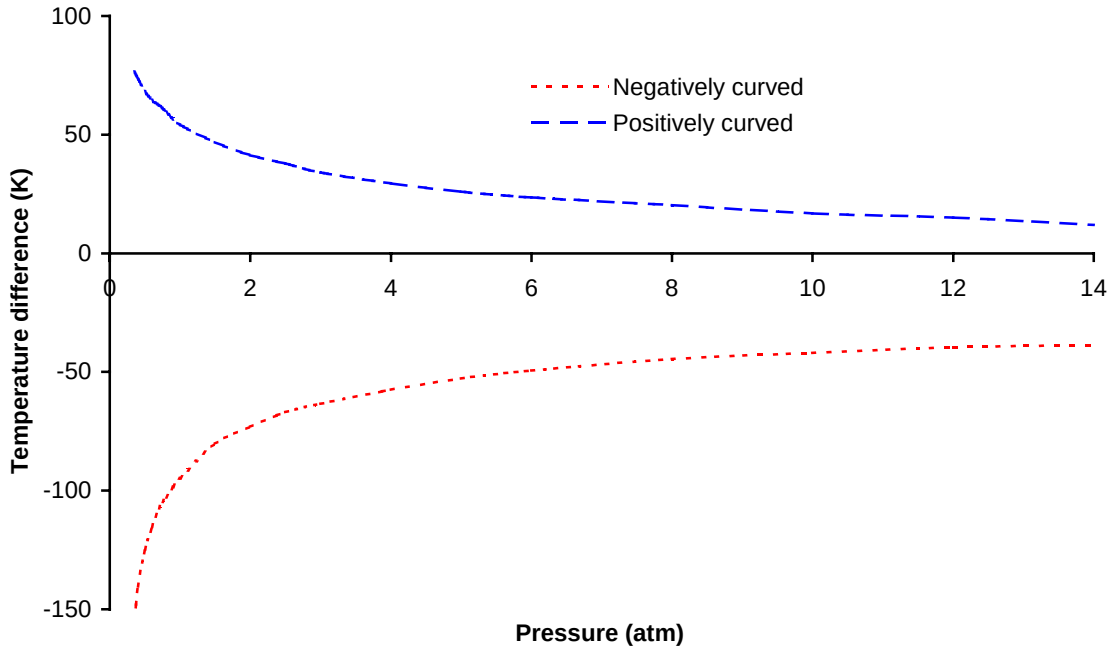


**Fig 5.7**. Flame temperature difference variation with pressure for the curved flames with constant stretch rate ($k=200s^{-1}$).

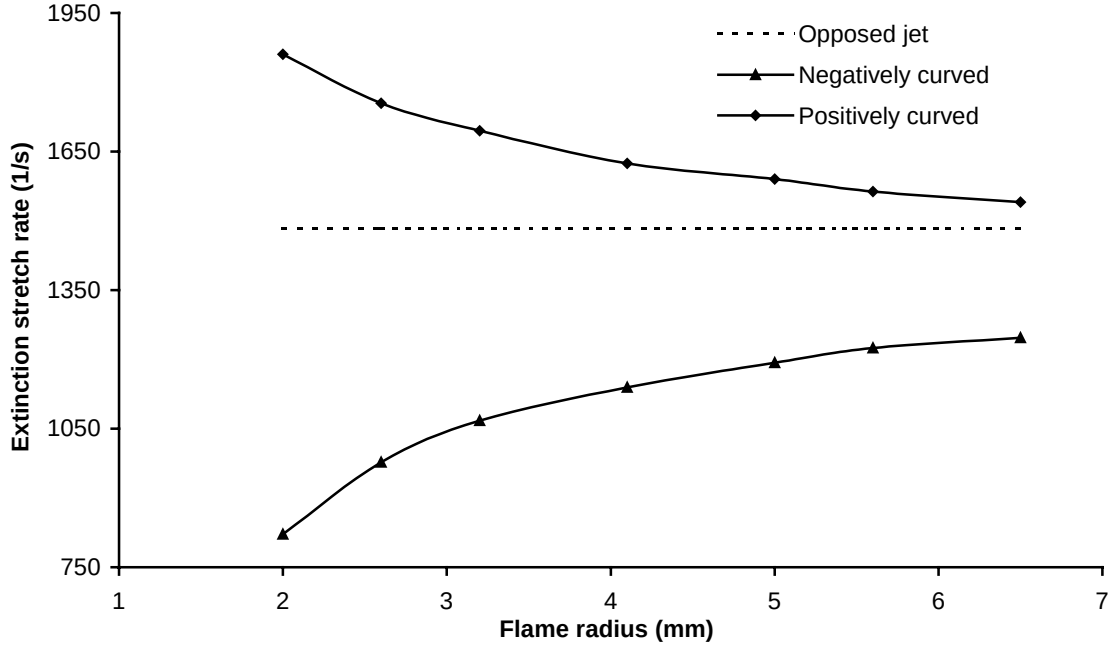


**Fig 5.8**. Extinction stretch rate variation with flame radius for the curved flames.

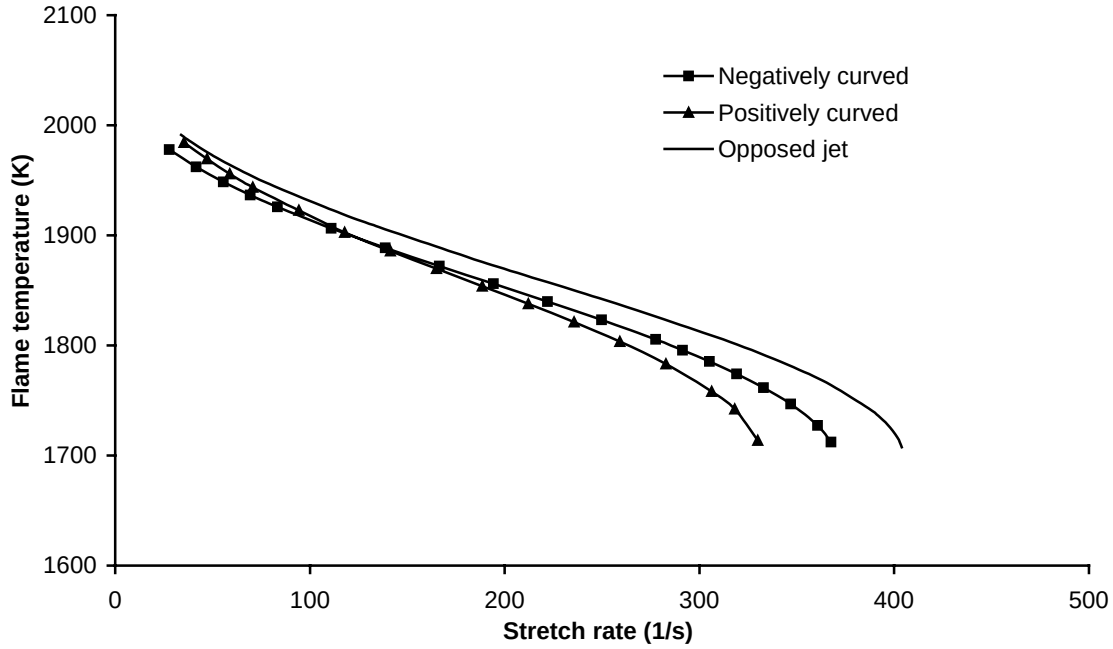


**Fig 5.9**. Flame temperature variation with stretch rate for the planar and curved $CH_4/N_2$ (60%$CH_4$, 40%$N_2$)-air flames.

# CHAPTER VI

## EXPERIMENTAL AND NUMERICAL STUDY OF TUBULAR PREMIXED HYDROCARBON FLAMES


### Abstract

This chapter investigates the tubular premixed flame structure experimentally with visible Raman scattering. The investigation covers the lean premixed flames of $H_2$, $CH_4$ and $C_3H_8$ whose Lewis numbers are less, close and more than one respectively. The premixed flame responses of different fuels to stretch and curvature are different because of the preferential diffusion effect: the lean $H_2$/air premixed flame temperature is much higher than the adiabatic equilibrium temperature; the lean $CH_4$/air premixed flame temperature is close to the adiabatic equilibrium value; the lean $C_3H_8$/air premixed flame temperature is lower than the adiabatic equilibrium value. The flame temperature, extinction and structure are also good criteria to judge the transport model and chemical kinetics used in the numerical simulations. The comparisons between the numerical and experimental data are carried out. It is shown that the multi-component transport model can capture the flame characteristics accurately. For $H_2$ and $CH_4$ flames, the predicted flame structure and temperature have very good agreement with measurement since the kinetics is relative simple and well understood; the simulation can even predict the accurate extinction stretch rate that is the most sensitive to chemical kinetics. For $C_3H_8$ flames, the measure flame temperature is lower than the adiabatic equilibrium temperature, which is consistent with the physical analysis.

## Introduction

Although there is some analytical and numerical study on tubular premixed flames, the experimental data is rare. Kobayashi and Kitano (1991) measured the flow field of the tubular burner with LDV; Kobayashi and Kitano (1989,1993) measured the extinction of the tubular premixed flames. The only experimental data of the tubular premixed flame structure is for the lean $H_2$/air premixed flame by Mosbacher et al. (2002). It is found that the experimental and numerical flame structure has a very good agreement at low stretch rate but shows obvious differences at high stretch rate especially close to extinction. A detailed analysis based on the chemical kinetics and the transport models is carried out; but no satisfactory explanation is determined. The present experiment work is a continuation of the previous work by Mosbacher et al. (2002). First we investigated the $H_2$ flame again and give an appropriate explanation to the difference between the numerical and experiment data. As an extension of previous study, we also studied the $CH_4$ and $C_3H_8$ flames.

## Experimental setup

Visible Raman spectroscopy is used to measure the temperature and concentrations of major species. The experimental system used previously (Mosbacher et al. 2002, Wehrmeyer et al. 2002) is modified to study the tubular premixed flame. A detailed schematic is shown in Fig. 6.1. The laser used in this work is a frequency-doubled, pulsed Nd:YAG laser (532 nm, 7 ns long @ 10 Hz). The laser beam passes through a zero order waveplate mounted at the exit of the laser followed by a thin film plate polarizer at its Brewster angle to enable continuous adjustment of the laser energy. The attenuated beam

then goes through a pulse stretcher (Kojima and Nguyen, 2002). By using 3 beamsplitters, the laser beam is split into 3 sets of beams trapped in the 3 optical ring cavities. Each beam experiences different amount of delay. A laser pulse of approximately 150 ns long (~140 mJ/pulse) is produced.

The laser light is focused by a 300 mm focal length lens. The beam diameter is measured to be 150 μm. The scattered Raman light is collected at 90º using a f/2 achromat (3" diameter) focused by a second achromat (f/7.5) onto the entrance slit of the spectrometer, Osborne et al. (2000). The focused signal is collimated by a 0.75 m defocusing mirror; then the signal is dispersed by a 600 groove/mm grating and focused to a liquid-nitrogen cooled, back-illuminated CCD camera (1024 × 1024 pixels) by a 0.65 m focusing mirror. Spatially resolved line imaging Raman signals are recorded. The sample volume passes through the symmetrical axis of the flame and is parallel to the temperature and species gradients. This sample volume is divided to 30 sections and the spatial resolution is 98 μm along the laser line. The resolving power of the system is sufficient to resolve 98 μm as determined by a 0.169 mm/pair Ronchi grating placed in the sample volume.

The CCD camera is gated by a DisplayTech ferroelectric liquid crystal shutter (45 μs) and a Uniblitz mechanical shutter (4.2 ms) to reduce the background flame emission. The Rayleigh scattered light is blocked by an OG-550 orange glass filter (Schott, 3mm thick). The flame illumination in the infrared region is blocked by an infrared filter (Dielectric shortpass filter, 750 nm cutoff). 1200 single-pulse Raman signals are integrated on the CCD chip to produce one Raman image. The tubular burner is translated a few times along the laser beam direction to cover the entire flame.

Calibration flames of the $H_2$/air, $H_2$/air/$CO_2$ and $H_2$/air/CO mixtures are produced using a Hencken multi-element burner (12.5 mm diameter multi-element matrix surrounded by a 4.3 mm wide $N_2$ co-flow annulus). The equilibrium condition is assumed where the laser beam passes and the adiabatic flame temperature is used to correlate the calibration factors for each individual species. The uncertainties of the mass flow meters used in the calibration are ± 1% of full scale. The accuracy of the temperature measurement is estimated to be less than ± 3% for $H_2$ flames by comparing the Raman derived temperature with the adiabatic equilibrium temperature in the calibration flames and ± 4% for $CH_4$ and $C_3H_8$ flames based on the RMS value of the measured temperature in the product zone. This increased uncertainty is due to the increased temperature and thereby reduced Raman signal.

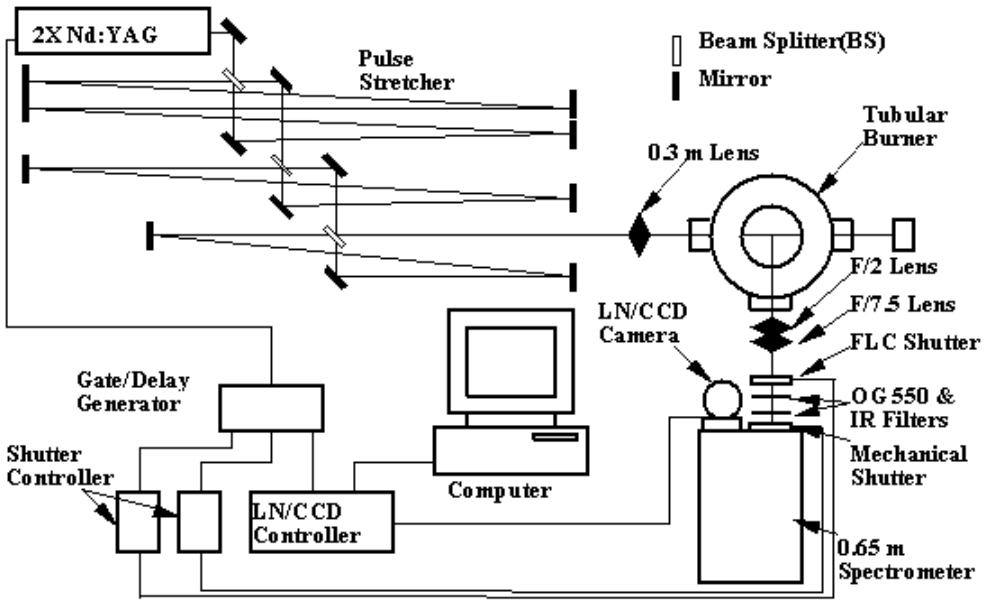


**Fig. 6.1**. Schematic of the visible Raman system.

## Results and discussion

Lean $H_2$/air premixed flames

Fig. 6.2 – Fig. 6.4 show the comparisons of numerical and experimental flame structure of the tubular $H_2$/air flame (equivalence ratio $\phi = 0.175$) with stretch rates k = 363, 293, 145 $s^{-1}$ respectively. The data from both sides of the flame centerline are plotted versus radius to show the axisymmetry of the flame. The numerical solution uses the multi-component transport model and Mueller mechanism, Mueller et al. (1999); the radiation heat loss from $H_2O$ is considered with optical thin assumption. The agreement between the numerical and experimental data is very good for all three stretch rates. However, in Mosbacher et al. (2002), the measurements are off the predictions when the stretch rate is higher than 199.5 $s^{-1}$. What are the differences between the previous and present work? There are two major differences; one is from the burner and the other one is from the numerical simulation. For the tubular burner, the premixture is introduced to the circular

chamber through 16 circumferentially spaced inlet port vertically; then the premixture diffuses through a packing of stainless steel wool and flow out in radial direction. The quality of the packing is very important for the uniformity of the flow field. At low stretch rates, the flow velocity in the contour tunnel is small and the viscous force makes the nozzle outlet velocity pretty uniform even when the velocity out of the steel wool packing is not quite uniform. At high stretch rates, the role of inertia is more important; the uniformity of the nozzle outlet velocity is more sensitive to the packing quality. A better packing quality is obtained for the present experiment than the previous one, so we get better experiment data at high stretch rates. For the numerical simulation, there are two kinds of transport models: the mixture-averaged and multi-component transport models. The mixture-averaged transport model calculates the diffusion velocities with a Fickian formula and uses mixture-averaged diffusion coefficients while the multi-component transport model solves the whole diffusion matrix to get the diffusion velocities. The mixture-averaged transport model runs much faster and converges easier while the multi-component model gives more accurate result and converges harder. Fig. 6.5 compares the difference of the two models for the $H_2$/air flame with equivalence ratio 0.175. At low stretch rates, the species gradients are relatively small, the mixture-averaged transport model predicts accurate flame temperature; at high stretch rates, the gradients are relatively large, the mixture-averaged transport model over predicts the flame temperature and extinction stretch rate. In Mosbacher et al (2002), the mixture-averaged transport model is used; part of the discrepancy between the prediction and experiment at high stretch rate comes from it. In the present study, we use the multi-component transport model. Fig. 6.6 compares the extinction stretch rate of the numerical

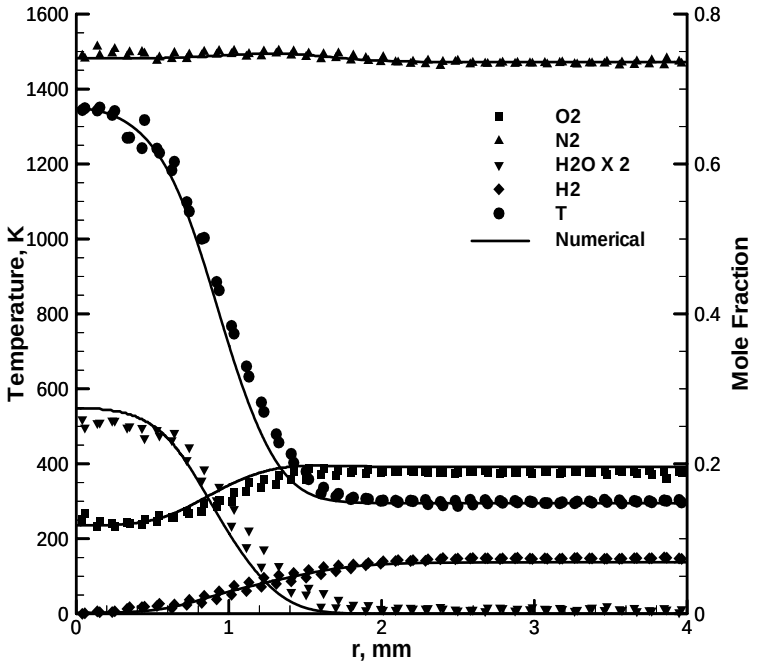


**Fig. 6.2**. Measured and calculated temperature and species profiles of the $H_2$/air premixed tubular flame with $\phi = 0.175$, k = 363 $s^{-1}$.

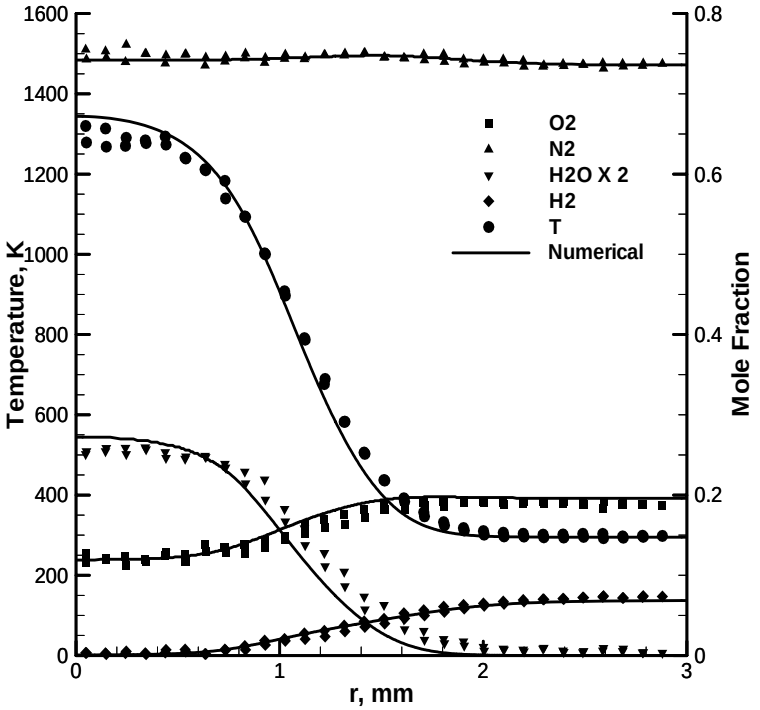


**Fig. 6.3**. Measured and calculated temperature and species profiles of the $H_2$/air premixed tubular flame with $\phi = 0.175$, k = 293 $s^{-1}$.

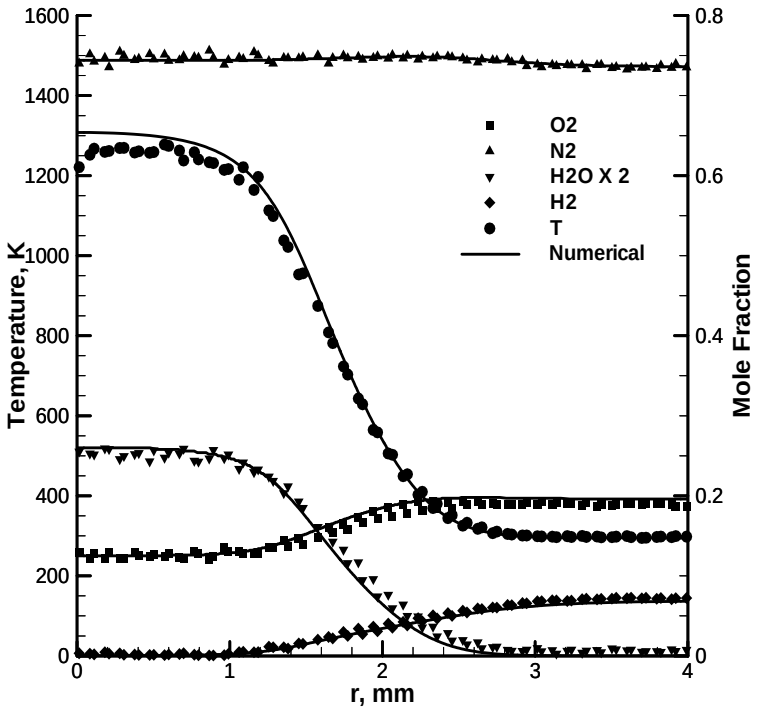


**Fig. 6.4**. Measured and calculated temperature and species profiles of the $H_2$/air premixed tubular flame with $\phi = 0.175$, k = 145 $s^{-1}$.

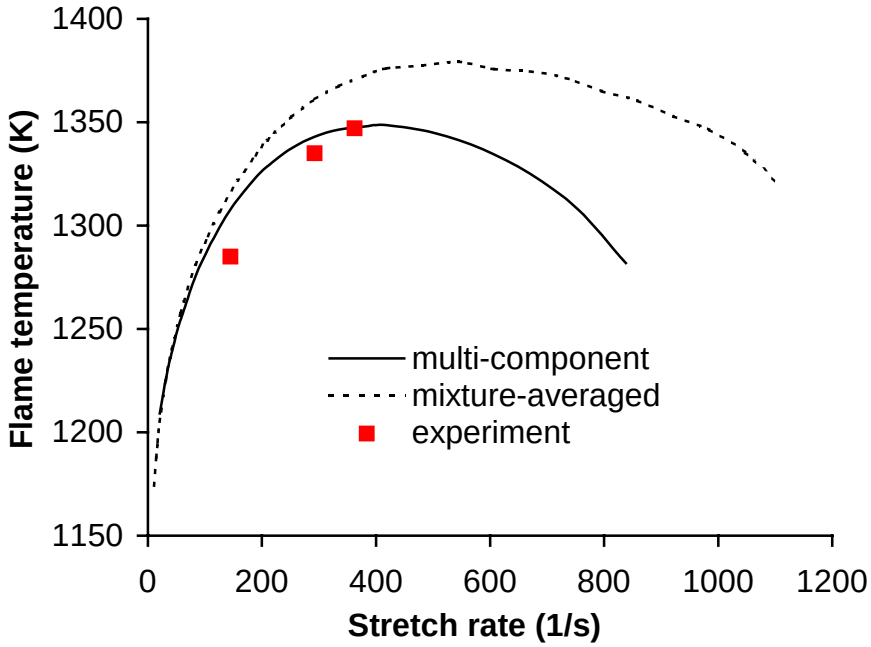


**Fig. 6.5**. Flame temperature variation with stretch rate for different transport models ($H_2$/air premixed flame with $\phi = 0.175$).

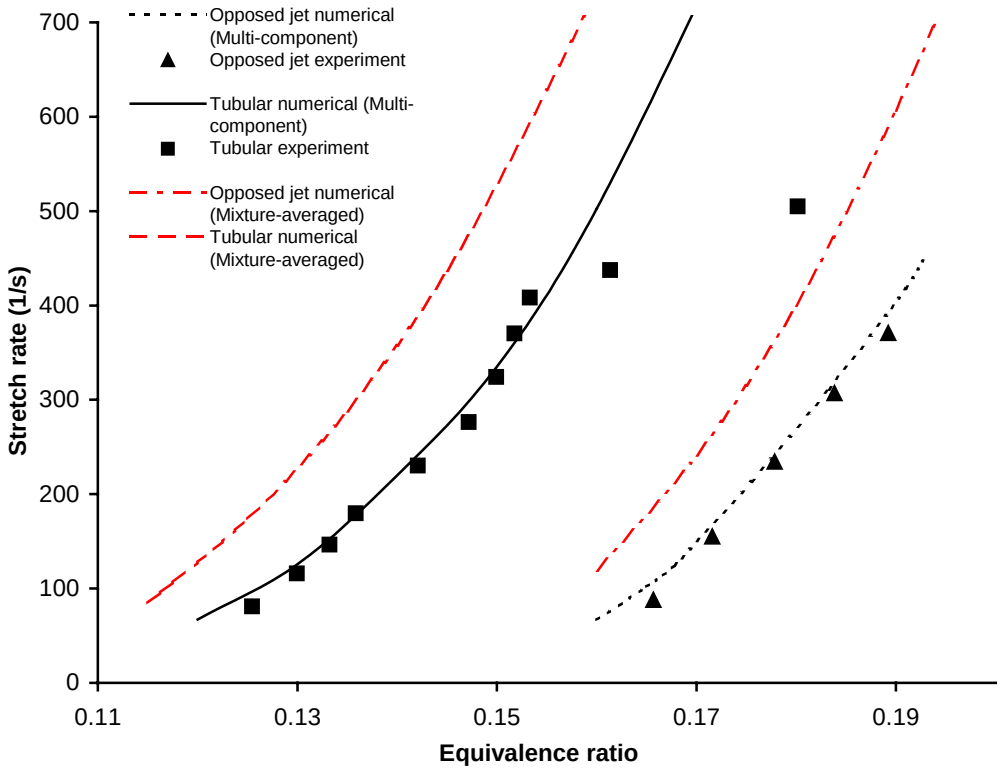


**Fig. 6. 6**. Extinction stretch rate comparison of experimental data and numerical data with different transport models.

data with different transport models and the experimental data; the mixture-averaged transport model always over predicts the extinction stretch rate. Among all the flame properties, extinction is most sensitive to the chemical kinetics and transport model. The chemical kinetics and transport model used here are so good that they can predict extinction accurately.

As we mentioned in Chapter III, further increase of stretch rate would cause turbulence that will destroy the laminar flame structure, so we can not study the flame structure near extinction for the equivalence ratio 0.175 since the predicted extinction stretch rate is as high as 838 $s^{-1}$. So we measured the $H_2$/air flames with equivalence ratio 0.152. At this equivalence ratio, the predicted extinction stretch rate is almost the same as

the measured value (370 $s^{-1}$). Fig. 6.7 – Fig. 6.11 show the comparisons of numerical and experimental flame structure of the tubular $H_2$/air flame ($\phi = 0.152$) with stretch rates k = 298, 257, 212, 168, 127 $s^{-1}$ respectively. The measured flame structure has a good agreement with the predicted structure even at high stretch rates close to extinction.

The measured and predicted flame temperature of the $H_2$/air flames is much higher than its adiabatic equilibrium value. This higher flame temperature is caused by the preferential diffusion effect that has been analyzed in Chapter III.

As a summary, since the $H_2$ flame kinetics is relatively simple and is well understood, the Mueller mechanism and multi-component transport model can predict the tubular flame temperature, structure and extinction rather accurately.

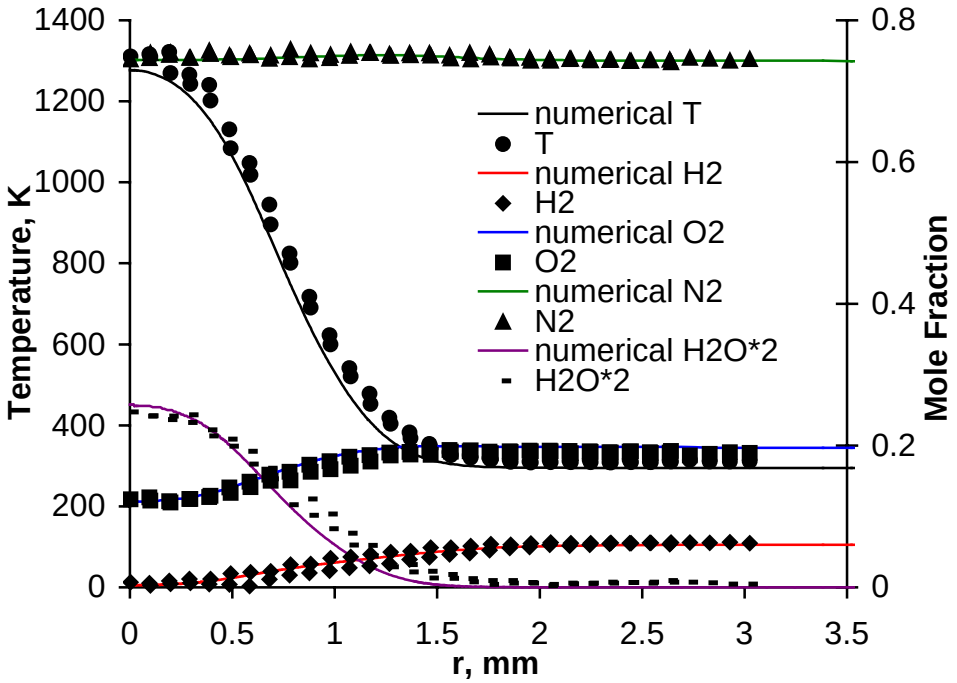


**Fig. 6.7**. Measured and calculated temperature and species profiles of the $H_2$/air premixed tubular flame with $\phi = 0.152$, k = 298 $s^{-1}$.

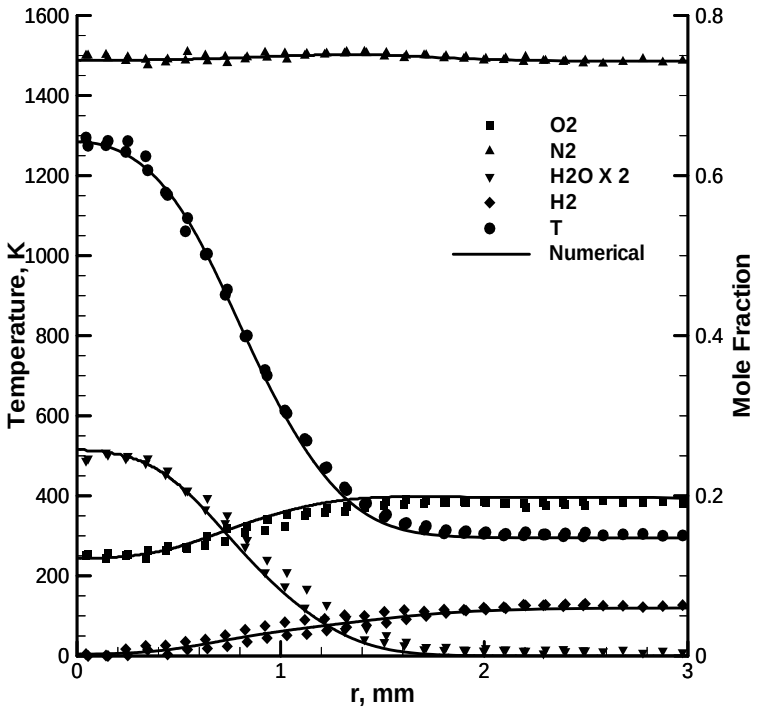


**Fig. 6.8**. Measured and calculated temperature and species profiles of the $H_2$/air premixed tubular flame with $\phi = 0.152$, k = 257 $s^{-1}$.

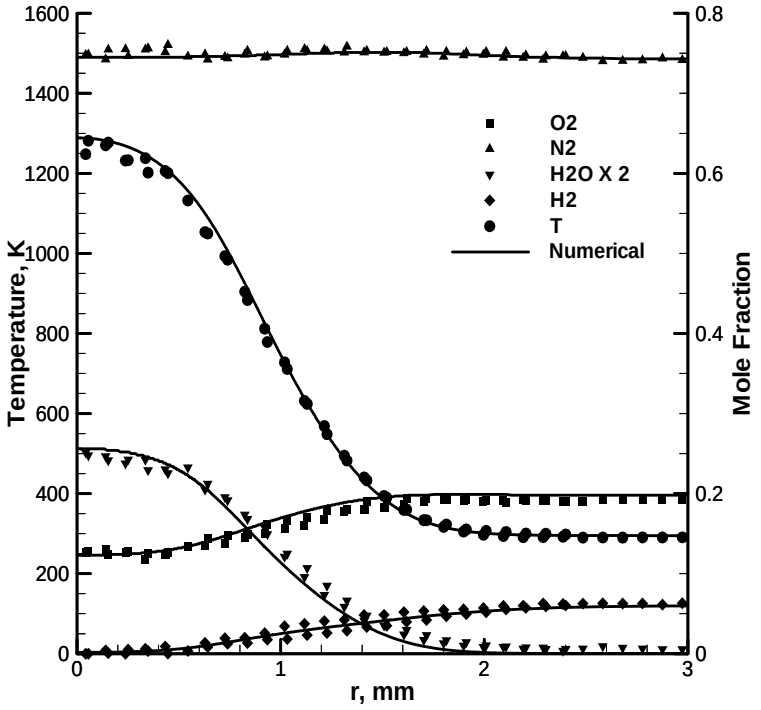


**Fig. 6.9**. Measured and calculated temperature and species profiles of the $H_2$/air premixed tubular flame with $\phi = 0.152$, k = 212 $s^{-1}$.

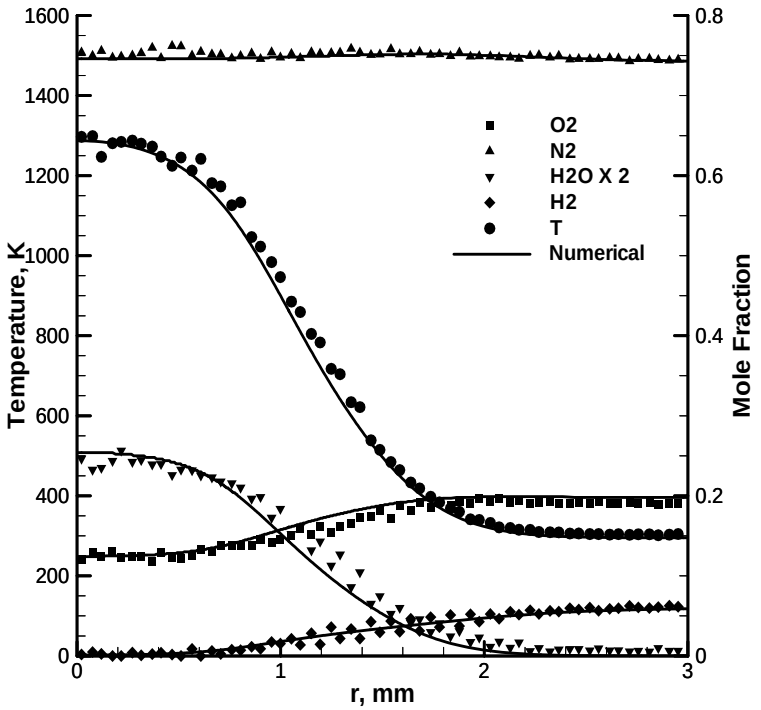


**Fig. 6.10**. Measured and calculated temperature and species profiles of the $H_2$/air premixed tubular flame with $\phi = 0.152$, k = 168 $s^{-1}$.

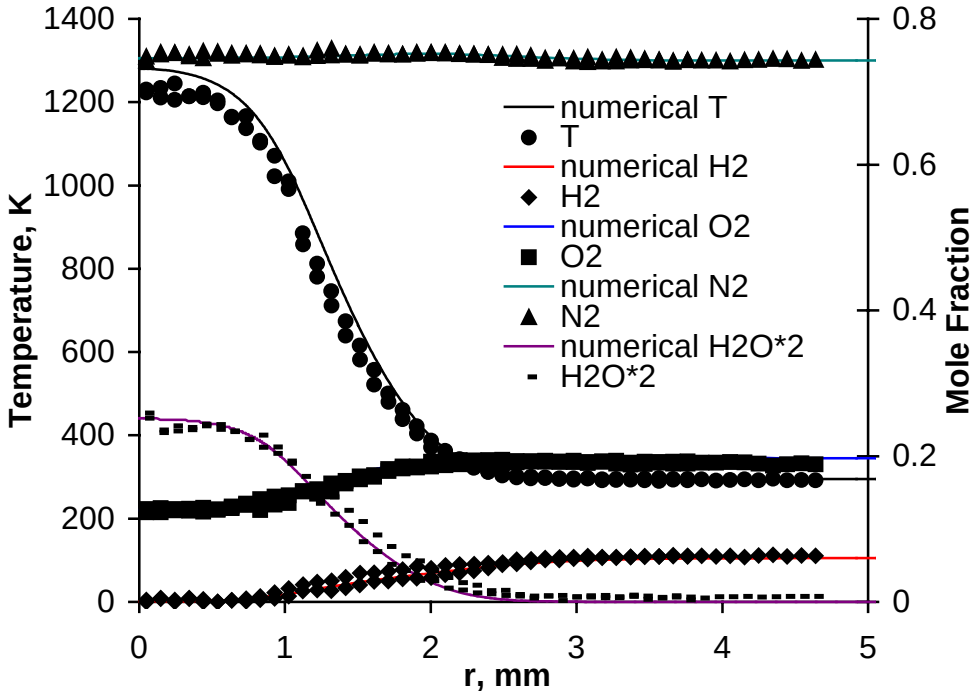


**Fig. 6.11**. Measured and calculated temperature and species profiles of the $H_2$/air premixed tubular flame with $\phi = 0.152$, k = 127 $s^{-1}$.

Lean $CH_4$/air premixed flames

Fig. 6.12 shows an example Raman spectra of $CH_4$/air flame at different radial positions. Due to the higher flame temperature of $CH_4$/air flame, the number density of species is lower than that of the $H_2$/air flames that leads to a little bit higher uncertainty. The uncertainty in high temperature zone is estimated to be about ±4%.

Fig. 6.13 and Fig. 6.14 show the comparisons of experimental and numerical flame structure for the $CH_4$/air flames ($\phi$ = 0.58) with stretch rates 166 $s^{-1}$ and 257 $s^{-1}$ respectively; the agreement is satisfied. The Kee mechanism (Kee et al., 1985) is used for the simulation. The Kee mechanism is a rather simple mechanism that has only 17 species (only one carbon species are considered) and 58 reactions; but it predicts flame structure very well. The mechanism also predicts the extinction stretch rate accurately; the measured value is 270.5 $s^{-1}$ and the predicted value is 273.5 $s^{-1}$. The measured flame temperature is close to the adiabatic equilibrium value (1626K) because there is little preferential diffusion effect for $CH_4$ flames whose Lewis number is close to one. This result is also consistent with the analysis in Chapter III. In the simulation of the hydrocarbon flames including $CH_4$ and $C_3H_8$ flames, the radiation heat loss from $H_2O$, CO and $CO_2$ are considered with optical thin assumption.

Fig. 6.15 shows the comparisons of experimental and numerical flame structure for the $CH_4$/air flames ($\phi$ = 0.54) with stretch rates 113 $s^{-1}$; the numerical curves are a little bit steeper than the experimental curves; but the difference is minimal and the comparison is satisfied. Some simulations with more complicated chemical mechanisms [C2 mechanism, Peters, 1992 (two carbon species are considered, 24 species and 81 steps); the San Diego mechanism, http://maeweb.ucsd.edu/~combustion/cermech/, 2005 (three

carbon species are considered, 40 species and 175 steps); the GRI-3.0 mechanism, Smith et al. (three carbon species are considered, 53 species and 325 steps)] are also carried out and shown in Fig. 6.16. It is found out that all the mechanisms predict the similar flame structure but with a little bit different flame positions.

As a summary, for very lean $CH_4$/air flames; the rather simple Kee mechanism can predict the tubular flame temperature, structure and extinction very accurately.

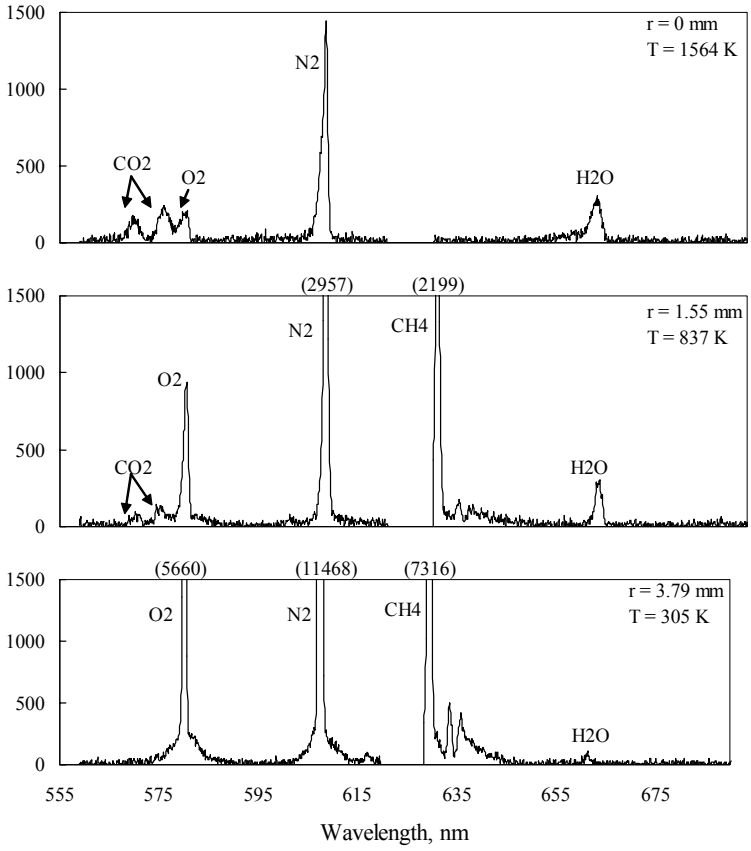


**Fig. 6.12**. Representative Raman spectra of a $\phi$ = 0.58, k =257 $s^{-1}$ $CH_4$/air premixed tubular flame at three radial locations.

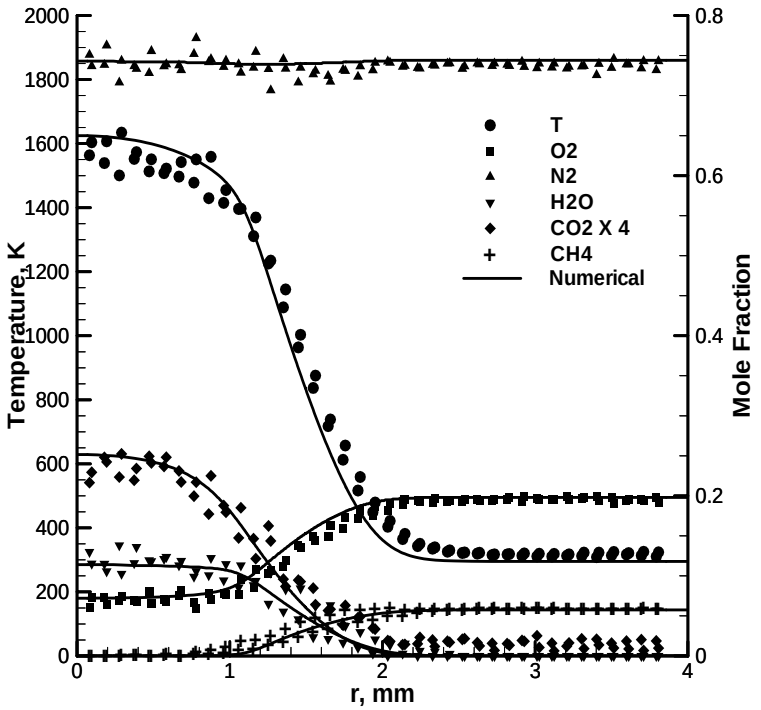


**Fig. 6.13**. Measured and calculated temperature and species profiles for a $\phi = 0.58$, k = 257 $s^{-1}$ $CH_4$/air premixed tubular flame.

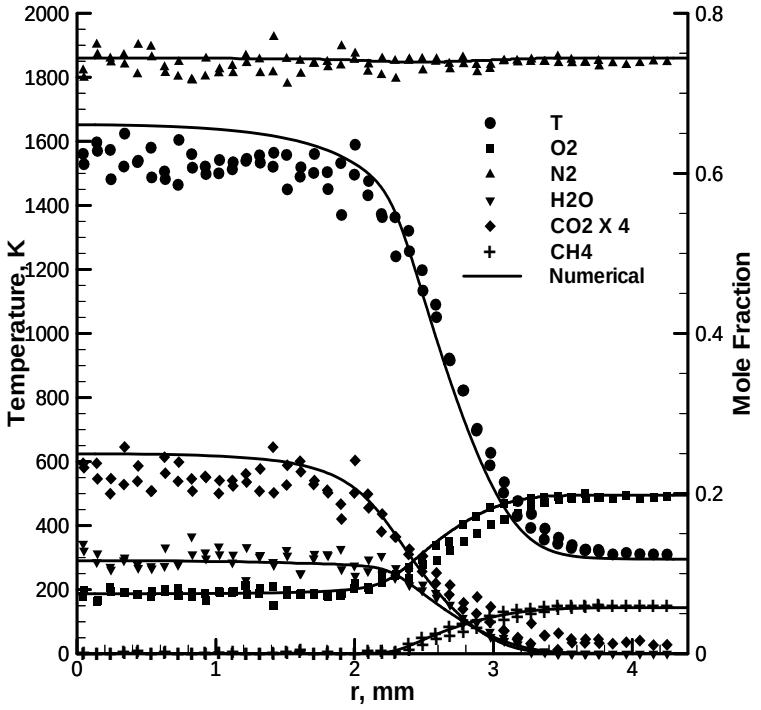


**Fig. 6.14**. Measured and calculated temperature and species profiles for a $\phi = 0.58$, k = 166 $s^{-1}$ $CH_4$/air premixed tubular flame.

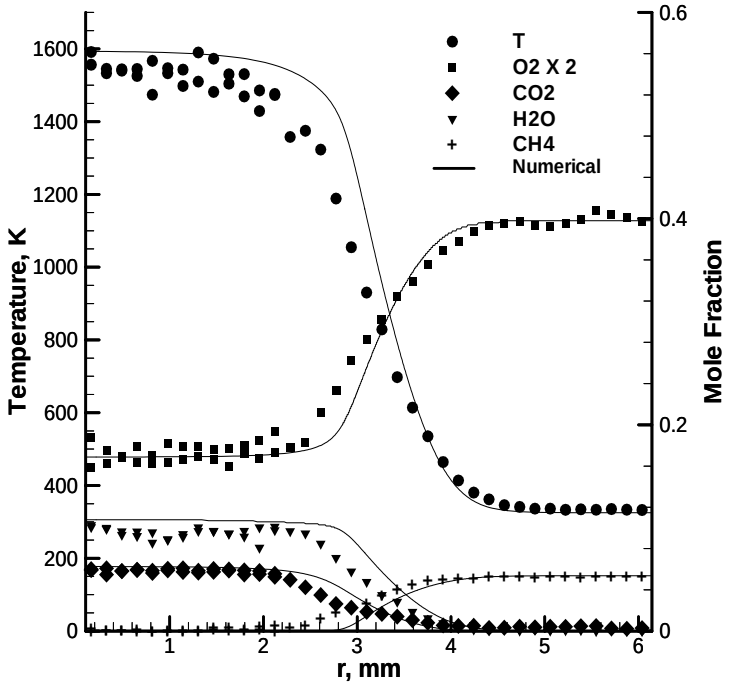


**Fig. 6.15**. Measured and calculated temperature and species profiles for a $\phi$ = 0.54, k =113 $s^{-1}$ $CH_4$/air premixed tubular flame.

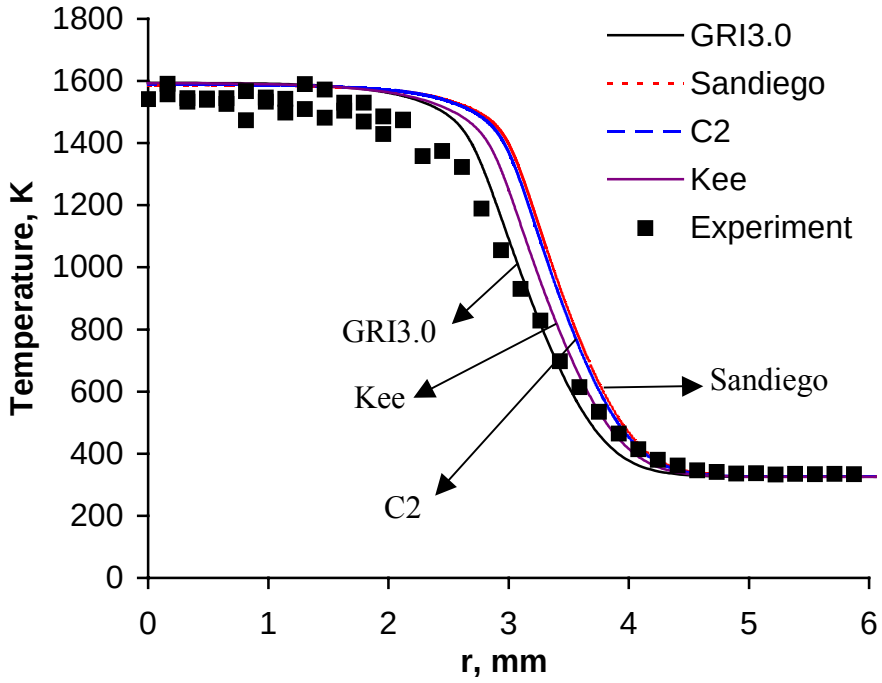


**Fig. 6.16**. Calculated temperature profile comparison with different chemical mechanisms for a $\phi$ = 0.54, k =113 $s^{-1}$ $CH_4$/air premixed tubular flame.

Lean $C_3H_8$/air premixed flames

Fig. 6.17 – Fig. 6.19 show the measured flame structure for $C_3H_8$/air flames ($\phi = 0.64$) with stretch rates 131, 168, 203 $s^{-1}$ respectively. In contrast to $CH_4$ flame, the $C_3H_8$/air flame is brighter which creates more noise for the Raman signal; the scatter of its experimental data is more serious than that of the $CH_4$ flames. The measured flame temperature is much less than the adiabatic equilibrium value (1771K), which is the result of preferential diffusion effect since the Lewis number is much larger than one (Le ~ 1.9). As we have discussed in Chapter III, unlike the $H_2$ and $CH_4$ flames that extinguish at the burner center, the lean $C_3H_8$ flames extinguish at certain distance from the burner center. So the measured $C_3H_8$ flames have large radius; the large flame shape is sensitive the packing quality of the burner, some non-circularity is observed for the $C_3H_8$ flames.

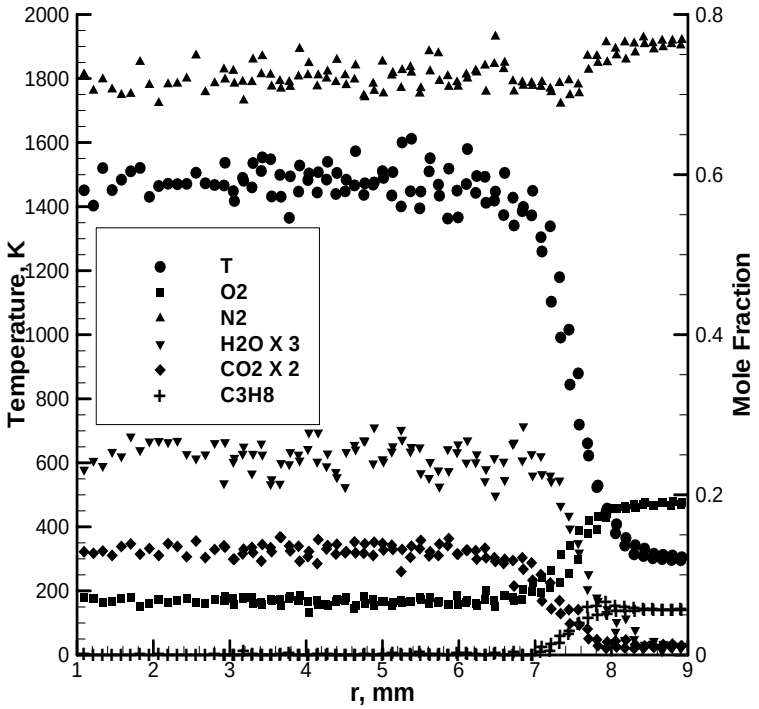


**Fig. 6.17**. Measured temperature and species profiles for a $\phi = 0.64$, k =131 $s^{-1}$ $C_3H_8$/air premixed tubular flame.

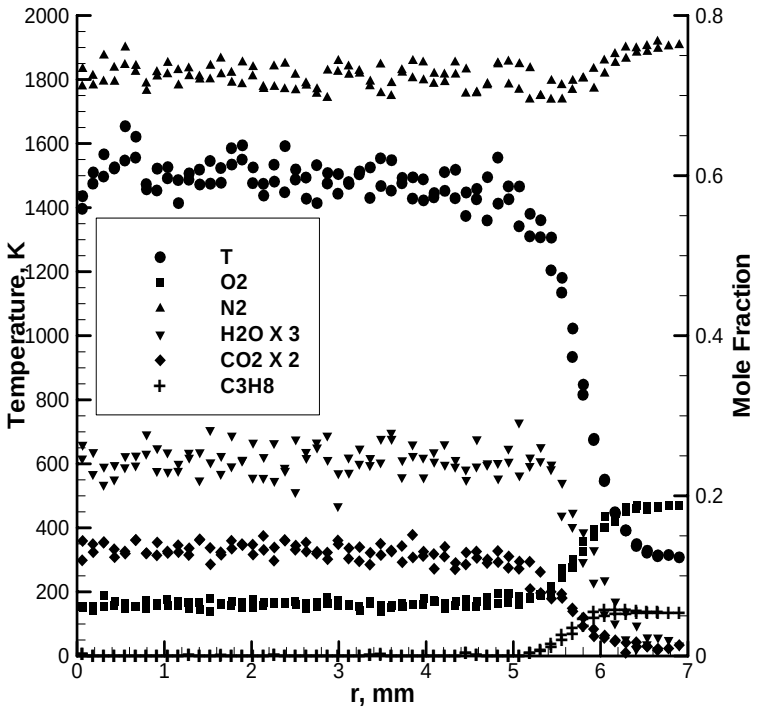


**Fig. 6.18**. Measured temperature and species profiles for a $\phi$ = 0.64, k =168 $s^{-1}$ $C_3H_8$/air premixed tubular flame.

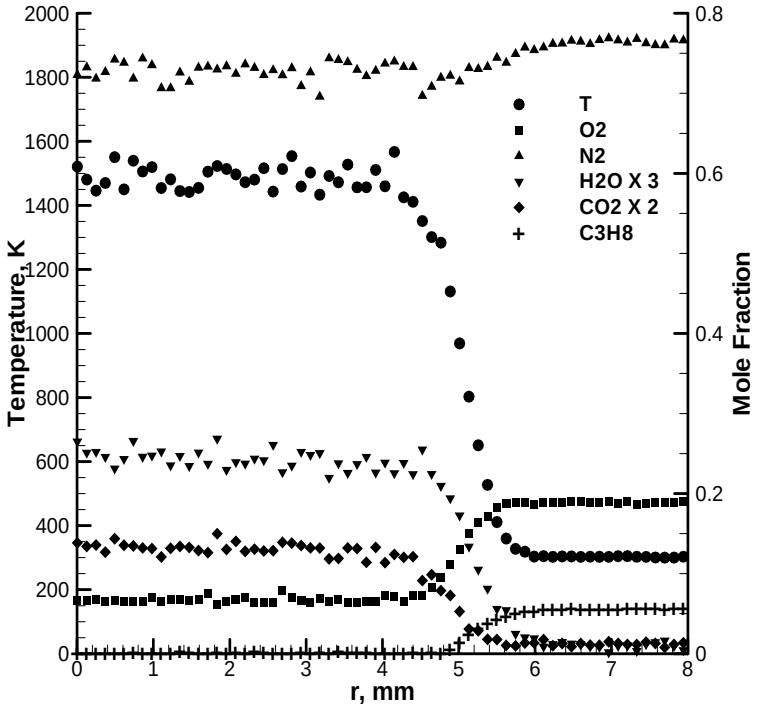


**Fig. 6.19**. Measured temperature and species profiles for a $\phi$ = 0.64, k =203 $s^{-1}$ $C_3H_8$/air premixed tubular flame.

## Conclusion

The flame structure of lean $H_2$/air, $CH_4$/air and $C_3H_8$/air flames are measured with visible Raman scattering and compared with numerical simulations. For transport models in simulation, the complicated multi-component model gives very accurate predictions. For $H_2$/air flames, the chemical mechanism is well understood and the Mueller mechanism gives good result for flame temperature, flame structure and extinction condition. For $CH_4$/air flames, the rather simple Kee mechanism gives a good result for flame temperature, flame structure and extinction condition. The measured and predicted flame temperatures of all three kinds of flames are consistent with the physical analysis on preferential diffusion effect.

# CHAPTER VII

# CONCLUSION AND FUTURE WORK

## Overview

The flames in the combustion chambers of most industry furnaces and engines consist of numerous turbulent flamelets that are stretched and curved. Fundamental study on the flame responses to stretch and curvature is important for understanding and modeling turbulent combustion. Although the stretch effects on flames are almost fully revealed, more work is needed to reveal the curvature effects on flames. The current research is to study the curvature effects on premixed flame responses including flame properties and flame structure in stretched flow field. In addition, a numerical study of curvature effects on diffusion flames is conducted.

## Conclusions

Comparisons between the tubular flames and the opposed jet flames are used to understand how curvature affects the properties of stretched flames. The cold flow field of the tubular burners is solved analytically and the appropriate choice of stretch rates for comparison of different flames is given. The analytical solutions are validated with numerical simulations.

A physical analysis of the stretch and curvature effects on the opposed jet and tubular premixed flames is given. It is revealed for the first time that the curvature effects are coupled with stretch effects: The positive curvature strengthens the preferential diffusion and the negative curvature weakens the preferential diffusion; the strengthening or

weakening effect is proportional to the ratio of flame thickness to flame radius. Based on the physical analysis, correlations are given to calculate the flame temperature and flame speed of curved premixed flames from the information of planar flames.

An asymptotic analysis is also given for the flame speed and flame temperature of three specific stretched and curved premixed flames: the opposed jet flame, the tubular flame, and the spherical flame. The comparison between the asymptotic solutions and the numerical solutions is satisfied. With the above correlations, the asymptotic solutions can be extended to any curved flame. Unlike the previous asymptotic analyses from the literature, which are limited to small stretch rate, small curvature or small Lewis number deviation, the present asymptotic solutions and correlations have no such limitations.

The curvature effect theory is extended to diffusion flames and the application is proved to be correct by numerical analysis; the curvature affects diffusion flames by the same way as premixed flames (i.e. by strengthening or weakening the preferential diffusion). This means the curvature theory is a universal theory and it works for both premixed and diffusion flames.

## Future work

Two objectives needed to be met in order to perfect the curvature theory:

1. Quantify the coefficients in the correlations for the premixed flame temperature and flame speed with different fuels and equivalence ratios numerically and experimentally. After this is accomplished, the correlations are ready to be used in turbulent modeling and other applications.

2. Quantify the extinction scalar dissipation rate under curvature and non-unity Lewis

numbers. In the present turbulent flamelet modeling for diffusion flames, the flame extinction is related to the scalar dissipation rate only and curvature is assumed to have no influence on it. This is correct only for small curvature or Lewis numbers close to unity; otherwise, curvature has important influence on the value of extinction scalar dissipation rate. Quantifying the scalar dissipation rate under curvature and non-unity Lewis numbers is very important for improving the turbulent modeling of diffusion flames.

## APPENDIX A

## DIVERGENCE RATIO ANALYSIS

For the steady planar stretched flame as shown in Fig. A1, set the diffusion direction as $z$ coordinate; the flow divergence exists in the $x$ and $y$ directions which makes net flow rates $m_{2x}$ in $x$ direction and $m_{2y}$ in $y$ direction out of the control volume.

Stretch rate $k = k_y + k_x = \dfrac{\partial u_y}{\partial y} + \dfrac{\partial u_x}{\partial x}$ (A1)

With constant density assumption;

$$\nabla \cdot \mathbf{U} = \frac{\partial u_y}{\partial y} + \frac{\partial u_x}{\partial x} + \frac{\partial u_z}{\partial z} = 0 \quad \text{i.e. } \frac{\partial u_z}{\partial z} = -k \tag{A2}$$

$$\int_{z_1}^{z_3} \frac{\partial u_z}{\partial z} dz = u_{z,3} - u_{z,1} = -k(z_3 - z_1) = -k\delta \tag{A3}$$

where $\delta$ is the flame thickness.

$$m_3 = \rho u_{z,3} \Delta y \Delta x \qquad m_1 = \rho u_{z,1} \Delta y \Delta x$$

$$m_2 = m_{2x} + m_{2y} = m_1 - m_3 = -\rho(u_{z,3} - u_{z,1})\Delta x \Delta y = \rho k \delta \Delta x \Delta y \tag{A4}$$

So the divergence ratio is:

$$\frac{m_2}{m_3} = \frac{\delta}{u_{z,3}} k = \frac{\delta}{S_b} k = Ka \tag{A5}$$

where $S_b$ is the flame speed at product side.

For the steady positively curved tubular flame as shown in Fig. A2, set the diffusion direction as $r$ coordinate. The flow divergence exists in $z$ and $\theta$ direction which makes net flow rates $m_{2z}$ in $z$ direction and $m_{2\theta}$ in $\theta$ direction out of the control volume.

$$k = k_z + k_\theta = \frac{\partial u_z}{\partial z} + \frac{\partial u_\theta}{r\partial \theta} \tag{A6}$$

With constant density assumption,

$$\nabla \cdot \mathbf{U} = \frac{1}{r}\frac{\partial r u_r}{\partial r} + \frac{\partial u_\theta}{r\partial \theta} + \frac{\partial u_z}{\partial z} = 0 \quad \text{i.e. } \frac{1}{r}\frac{\partial r u_r}{\partial r} = -k \tag{A7}$$

$$\int_{r_1}^{r_3} \frac{\partial r u_r}{\partial r} dr = r_3 u_{r,3} - r_1 u_{r,1} = -\frac{1}{2}k(r_3^{\,2} - r_1^{\,2}) = k\delta(r_3 + \frac{\delta}{2}) \tag{A8}$$

$$m_3 = -\rho u_{r,3} r_3 \Delta z \Delta\theta \quad m_1 = -\rho u_{r,1} r_1 \Delta z \Delta\theta$$

$$m_2 = m_{2z} + m_{2\theta} = m_1 - m_3 = -\rho(r_1 u_{r,1} - r_3 u_{r,3})\Delta z \Delta\theta = \rho k\delta(r_3 + 0.5\delta)\Delta z \Delta\theta \tag{A9}$$

So the divergence ratio is:

$$\frac{m_2}{m_3} = \frac{\delta}{u_{r,3}} k(1 + \frac{\delta}{2r_3}) = (1 + \frac{\delta}{2r_b})\frac{\delta}{S_b} k = Ka(1 + \frac{\delta}{2r_b}) \tag{A10}$$

where $r_b$ is the flame radius at product side.

The second term on the right hand side of Eq. (A10) comes from the geometry, i.e. curvature. The positive curvature will strengthen the effects of stretch on flames and the strengthening effect depends the ratio of flame thickness to flame radius.

For the steady negatively curved tubular flame as shown in Fig. A3.

$$\frac{m_2}{m_3} = Ka(1 - \frac{\delta}{2r_b}) \tag{A11}$$

The negative curvature will weaken the effects of stretch on flames and the weakening effect still depends the ratio of flame thickness to flame radius.

For the steady negatively curved spherical flame as shown in Fig. A4, set the diffusion direction as $r$ coordinate. The flow divergence exists in $\phi$ and $\theta$ direction which makes net flow rates $m_{2\phi}$ in $\phi$ direction and $m_{2\theta}$ in $\theta$ direction out of the control volume.

From mass conservation $\nabla \cdot \mathbf{U} = \nabla \cdot (u_r \mathbf{e_r} + \mathbf{U_t}) = 0$, we can get

$$\frac{1}{r^2}\frac{\partial (r^2 u_r)}{\partial r} = -k \tag{A12}$$

where $\mathbf{U_t}$ is the tangential velocity vector and $\nabla \cdot \mathbf{U_t} = k$ has been used.

Integrating Eq. (A12) from fresh mixture side to product side,

$$\int_{r_1}^{r_3} \frac{\partial r^2 u_r}{\partial r} dr = r_3^2 u_{r,3} - r_1^2 u_{r,1} = -\frac{1}{3}k(r_3^3 - r_1^3) = -k r_3^2 \delta \left(1 - \frac{\delta}{r_3} + \frac{1}{3}\left(\frac{\delta}{r_2}\right)^2\right) \tag{A13}$$

$$\frac{m_2}{m_3} = \frac{m_1 - m_3}{m_3} = k r_3^2 \delta \left(1 - \frac{\delta}{r_3} + \frac{1}{3}\left(\frac{\delta}{r_2}\right)^2\right) \cdot \Delta\theta \cdot \Delta\phi / (u_{r,3} r_3^2 \Delta\theta \cdot \Delta\phi) = Ka\left(1 - \frac{\delta}{r_b} + \frac{1}{3}\left(\frac{\delta}{r_b}\right)^2\right) \tag{A14}$$

That is, for the negatively curved spherical flame,

$$\frac{m_2}{m_3} = Ka\left(1 - \frac{\delta}{r_b} + \frac{1}{3}\left(\frac{\delta}{r_b}\right)^2\right) \approx Ka\left(1 - \frac{\delta}{2(r_b/2)}\right) \approx Ka[1 - \frac{\delta}{2r_{b,c}}] \tag{A15}$$

In the above equation, the square term of the ratio of flame thickness to flame radius is negligible since the ratio is less than one and the square term divided by 3 is much less than the other two terms. In the right hand side of Eq. (A15), the flame radius is replaced by the curvature radius.

Following the same procedure, we deduced the divergence ratio for the positively curved spherical flames.

$$\frac{m_2}{m_3} \approx Ka[1 + \frac{\delta}{2r_{b,c}}] \tag{A16}$$

The spherical and tubular flames have the same expression of divergence ratio; so the expression can be extended to generally curved flames.

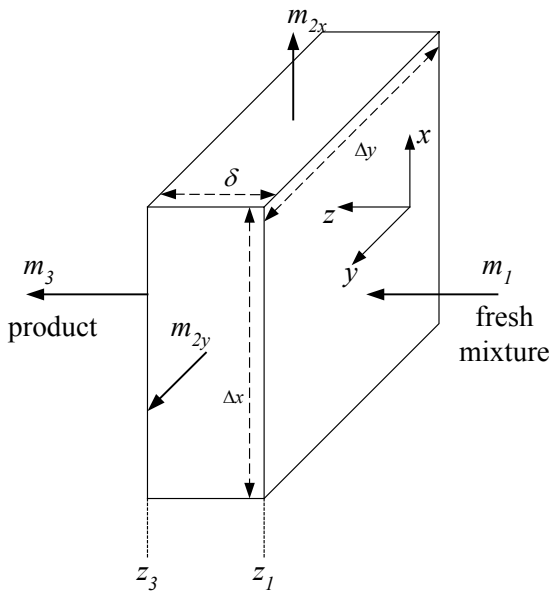


**Fig. A. 1**. Control volume schematic of steady stretched planar flame.

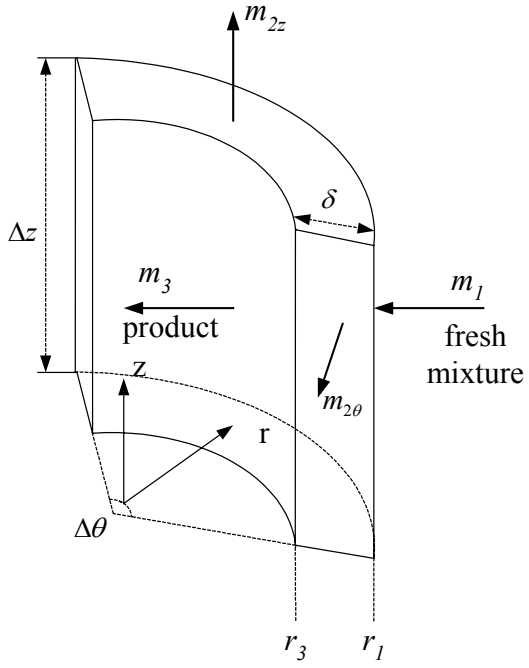


**Fig. A. 2**. Control volume schematic of steady positively curved tubular flame.

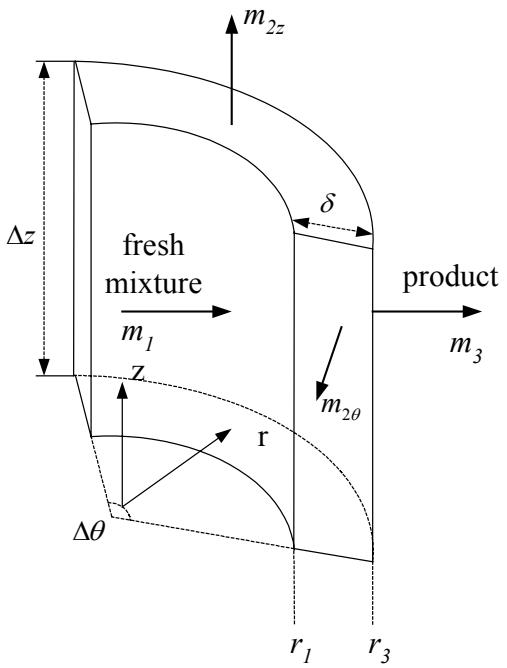


**Fig. A. 3**. Control volume schematic of steady negatively curved tubular flame.

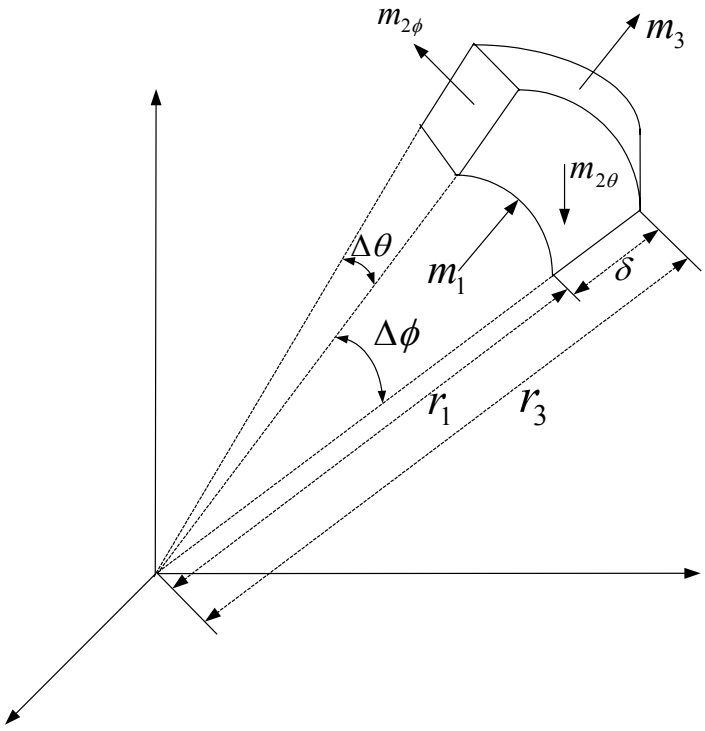


**Fig. A. 4**. Control volume schematic of steady negatively curved spherical flame.

## REFERENCE


Bird R. B., Stewart W. E., Lightfoot E. N. (1960) *Transport Phenomena*, John Wiley and Sons, New York.

Brown T.M., Tanoff M.A., Osborne R.J., Pitz R.W., Smooke M.D. (1997), "Experimental and Numerical Investigation of Laminar Hydrogen-Air Counterflow Diffusion Flames", *Combustion Science and Technology*, **129**, 71-88.

Buckmaster J.D. (1977) "Slowly Varying Laminar Flames", *Combustion and Flame*, **28**, 225.

Chelliah H.K., Law C.K., Smooke M.D., Williams F.A. (1990) "An Experimental and Theoretical Investigation of the Dilution, Pressure and Flow-Field Effects on the Extinction Condition of Methane-Air-Nitrogen Diffusion Flames", *Proceedings of the Combustion Institute*, **23**, 503-511.

CHEMKIN Collection (2000) Kee R. J., Rupley F., Miller J., Coltrin M., Grcar J., Meeks E., Moffat H., Lutz A., Dixon-Lewis G., Smooke M., Warnatz J., Evans G., Larson R., Mitchell R., Petzold L., Reynolds L., Caracotsios M., Stewart W., Glarborg P., Wang C., Adigun O., Release 3.6, Reaction Design, Inc., San Diego, CA.

Cheng Z., Wehrmeyer J.A., Pitz R.W. (2004) "Lean or Ultra Lean Stretched Planar Methane/Air Flames", *Proceedings of the Combustion Institute*, **30**, 285-293.

Cheng Z, Wehrmerer J. A., Pitz R. W. (2006) "Experimental and Numerical studies of Opposed Jet Oxygen-Enhanced Methane Diffusion Flames" *Combustion, Science and Technology* (accepted).

Chung S.H., Law C.K. (1983) "Structure and Extinction of Convective Diffusion Flames with General Lewis Number", *Combustion and Flame*, **52**, 59-79.

Chung S.H., Law C.K. (1984) "On the Flame-Sheet Assumption and Flame Temperature Determination in Combustion Modeling", *Combustion Science and Technology*, **35**, 297-310.

Chung S.H., Law C.K. (1988) "An Integral Analysis of the Structure and Propagation of Stretched Premixed Flames", *Combustion and Flame*, **72**, 325-336.

Clavin P., Williams F.A. (1982) "Effects of Molecular Diffusion and of Thermal Expansion on the Structure and Dynamics of Premixed Flames in Turbulent Flows of Large Scale and Low Intensity", *Journal of Fluid Mechanics*, **116**, 251.

Clavin P. (1985) "Dynamic Behavior of Premixed Flame Fronts in Laminar and Turbulent Flows", *Progress in Energy and Combustion Science.*, **11** (1), 1.

Cuenot B., Poinsot T. (1996) "Asymptotic and Numerical Study of Diffusion Flames with Variable Lewis Number and Finite Rate Chemistry", *Combustion and Flame*, **104**, 111-137.

Dixon-Lewis G., Giovangigli V., Kee R.J., Miller,J.A., Rogg B., Smooke M.D., Stahl G., Warnatz J. (1991) "Numerical Modeling of the Structure and Properties of Tubular Laminar Premixed Flames", *Progress in Astronautics and Aeronautics*, **131**, 125-144.

Dixion-Lewis G. (1990) "Structure of Laminar Flames", *Proceedings of Combustion Institute*, **23**, 305-324.

Finke H., Grünefeld G. (2000) "An Experimental Investigation of Extinction of Curved Laminar Hydrogen Diffusion Flames", *Proceedings of Combustion Institute*, **28**, 2133-2140.

Giovangigli V., Smooke M.D. (1987) "Extinction of Strained Premixed Laminar Flames with Complex Chemistry", *Combustion Science and Technology*, **53**, 23.

Glassman I. (1996) *Combustion*, 3rd ed., Academic Press, San Diego CA.

Guo H., Ju Y., Maruta K., Niioka T., Liu F. (1997) "Radiation Extinction Limit of Counterflow Premixed Lean Methane-Air Flames", *Combustion and Flame*, **109**, 639-646.

Hilbert R., Tap F., El-Rabii H., Thévenin D. (2004) "Impact of Detailed Chemistry and Transport Models on Turbulent Combustion Simulations", *Progress in Energy and Combustion Science*, **30**, 61-117.

Hu S., Wang P., Pitz R.W., Smooke M.D. (2006) "Experimental and Numerical Investigation of Non-Premixed Tubular Flames", accepted to the 31st Symposium of Combustion Institute.

Im H.G., Law C.K., Axelbaum R.L. (1990) "Opening of the Burke-Schumann Flame Tip and the Effects of Curvature on Diffusion Flame Extinction", *Proceedings of the Combustion Institute*, **23**, 551-558.

Ishizuka S. (1983) "An Experiment Study on the Opening of Laminar Diffusion Flame Tips", *Proceedings of the Combustion Institute*, **19**, 319-326.

Ishizuka S. (1984) "On the Behavior of Premixed Flames in a Rotating Flow Field: Establishment of Tubular Flames", *Proceedings of the Combustion Institute*, **20**, 287-294.

Ishizuka S., Sakai Y. (1986) "Structure and Tip-Opening of Laminar Diffusion Flames", *Proceedings of the Combustion Institute*, **21**, 1821-1828.

Ishizuka S. (1989) "An Experiment Study on Extinction and Stability of Tubular Flames",

*Combustion and Flame*, **75**, 367-379.

Ishizuka S. (1993) "Characteristics of Tubular Flames", *Progress in Energy and Combustion Science*, **19**, 187-226.

Ju Y., Guo H., Maruta K., Liu F. (1997) "On the Extinction Limit and Flammability Limit of Non-Adiabatic Stretched Methane-Air Premixed Flames", *Journal of Fluid Mechanics*, **342**, 315-342.

Ju Y.G., Matsumi H., Takita K., Masuya G. (1999) "Combined Effects of Radiation, Flame Curvature, and Stretch on the Extinction and Bifurcations of Cylindrical $CH_4$/Air Premixed Flame", *Combustion and Flame*, **116**, 580-592.

Katta V.R., Goss L.P., Roquemore W.M. (1994) "Effect of Nonunity Lewis Number and Finite-Rate Chemistry on the Dynamics of a Hydrogen-Air Jet Diffusion Flame", *Combustion and Flame*, **96**, 60-74.

Katta V.R., Carter C.D., Fiechtner G.J., Roquemore W.M., Gord J.R., Rolon J.C. (1998) "Interaction of Vortex with a Flat Flame Formed Between Opposing Jets of Hydrogen and Air", *Proceedings of the Combustion Institute*, **27**, 587-594.

Karlovitz B., Denniston D.W., Jr. Knappschaefer D.H., Wells F.E. (1953) "Studies on Turbulent Flames", *Proceedings of the Combustion Institute*, **4**, 613.

Kee R.J., Grcar J.F., Smooke M.D., Miller J.A. (1985) Sandia Report 85-8240, Sandia National Laboratories.

Kee R.J., Miller J.A., Evans G., Dixon-Lewis G. (1988) "A Computational Model of the Structure and Extinction of Stained, Opposed Flow, Premixed Methane-Air Flames", *Proceedings of the Combustion Institute*, **22**, 1479-1494.

Klimov A.M., Lebedev V.N. (1983) "Limiting Phenomena in Turbulent Combustion", *Fizika Goreniya Vzryva*, **19**, 7-9.

Kobayshi H., Kitano M., Otsuka Y. (1988) "An Analysis of Stretched Cylindrical Premixed Flame", *Combustion Science and Technology*, **57**, 17.

Kobayashi H., Kitano M. (1989) "Extinction Characteristics of a Stretched Cylindrical Premixed Flame", *Combustion and Flame*, **76**, 285.

Kobayashi H., Kitano M. (1991) "Flow Fields and Extinction of Stretched Cylindrical Premixed Flames", *Combustion Science and Technology*, **75**, 227.

Kobayashi H., Kitano M. (1993) "Effects of Equivalence Ratio on the Extinction Stretch Rate of Cylindrical Premixed Flames", *Combustion Science and Technology*, **89**, 253.

Kojima, J., Nguyen, Q. V., "Laser Pulse-Stretching with Multiple Optical Ring Cavities", *Applied Optics*, **41** (30), 2002, 6360-6370.

Law C.K., Chung S.H. (1982) "Steady State Diffusion Flame Structure with Lewis Number Variation", *Combustion Science Technology*, **29**, 129-145.

Law C.K., Zhu D.L., Yu, G. (1986) "Propagation and Extinction of Stretched Premixed Flames", *Proceedings of the Combustion Institute*, **21**, 1419-1426.

Law C.K. (1988) "Dynamics of Stretched Flames", *Proceedings of the Combustion Institute*, **22**, 1381.

Law C.K., Sung C.J., Yu G, Axelbaum R.L. (1994) "On the Structural Sensitivity of Purely Strained Planar Premixed Flames of Strain Rate Variations", *Combustion and Flame*, **98**, 139-154.

Law C.K., Sung C.J. (2000) "Structure, Aerodynamics, and Geometry of Premixed Flamelets", *Progress in Energy and Combustion Science*, **26**, 459.

Lee J.C., Frouzakis S., Boulouchos K. (2000) "Numerical Study of Opposed-Jet $H_2$/Air Diffusion Flame – Vortex Interactions", *Combustion Science and Technology*, **158**, 365.

Liñan A. (1974) "The Asymptotic Structure of Counterflow Diffusion Flames for Large Activation Energies", *Acta Astronautica*, **1**, 1007-1039.

Libby P.A., Peters N., Williams F.A. (1989) "Cylindrical Premixed Laminar Flames", *Combustion and Flame*, **75**, 265-280.

Matalon M., Matkowsky B.J. (1982) "Flames as Gasdynamic Discontinuities", *Journal of Fluid Mechanics*, **124**, 239.

Matalon M. (1983) "On Flame Stretch", *Combustion Science and Technology*, **31**, 169.

Mosbacher D.M., Wehrmeyer J.A., Pitz R.W., Sung C.J., Byrd J.L. (2002) "Experimental and Numerical Investigation of Premixed Tubular Flames", *Proceedings of the Combustion Institute*, **29**, 1479.

Mueller M. A., Kim T. J., Yetter R. A., Dryer F.L. (1999) "Flow Reactor Studies and Kinetic Modeling of the $H_2/O_2$ Reaction", *International Journal of Chemical Kinetics*, **31**, 113.

Nishioka M., Takeno T., Ishizuka S. (1988) "Effect of Variable Density on a Tubular Flame", *Combustion and Flame*, **73**, 287-301.

Nishioka M., Inagaki K., Ishizuka S., Takeno T. (1991) "Effect of Pressure on Structure and Extinction of Tubular Flame", *Combustion and Flame*, **86**, 90-100.

Osborne R.J., Brown T. M., Pitz R. W., Tanoff M., Smooke M. (1996) "Study of the Structure and Emission of Partially-Premixed Methane Flames in Laminar Counterflow", 34th Aerospace Sciences Meeting, Reno, NV, AIAA96-0212.

Osborne R. J., Wehrmeyer J. A., Pitz, R. W. (2000) "A Comparison of UV Raman and Visible Raman Techniques for Measuring Non-Sooting Partially Premixed Hydrocarbon Flames", 38th Aerospace Sciences Meeting, Reno, NV, AIAA2000-0776.

Peters N. (1983) "Local Quenching due to Flame Stretch and Non-Premixed Turbulent Combustion", *Combustion Science and Technology*, **30**, 1-17.

Peters N. (1986) "Laminar Flamelet Concepts in Turbulent Combustion", *Proceeding of Combustion Institute*, **21**, 1231-1250.

Peters N. (1992) "Flame Calculations with Reduced Mechanism - An Outline", Springer-Verlag, Berlin, **M15**, 3-12.

Peters N. (2000) *Turbulent Combustion*, Cambridge University Press, Cambridge, UK.

Seshadri K., Williams F.A. (1978) "Laminar Flow between Parallel Plates with Injection of a Reactant at High Reynolds Number", *International Journal of Heat and Mass Transfer*, **21**, 251-253.

Sivashinsky G. I. (1976) "On a Distorted Flame Front as a Hydrodynamic Discontinuity", *Acta Astronautica*, **3**, 889.

Smith G. P., Golden D. M., Frenklach M., Moriarty N. W., Eiteneer B., Goldenberg M., Bowman C. T., Hanson R. K., Song S., Jr. W. C. G., Lissianski V. V., Qin Z., Gas Research Institute, Chicago, Illinois, *http://www.me.berkeley.edu/gri_mech/*.

Smooke M.D., Giovangigli V. (1990) "Extinction of Tubular Premixed Laminar Flames with Complex Chemistry", *Proceedings of the Combustion Institute*, **23**, 447-454.

Sung C.J., Law C.K., Axelbaum R.L. (1994) "Thermophoretic Effects on Seeding Particles in LDV Measurements of Flames", *Combustion Science and Technology*, **99**, 119-132.

Sun C.J., Sung C.J., He L., Law C.K. (1999) "Dynamics of Weakly Stretched Flames: Quantitative Description and Extraction of Global Flame Parameters", *Combustion and Flame*, **118**, 108-128.

Sung C.J., Liu J.B., Law C.K. (1995) "Structural Response of Counterflow Diffusion Flames to Strain Rate Variations", *Combustion and Flame*, **102**, 481-492.

Sung C.J., Liu J.B., Law C.K. (1996) "On the Scalar Structure of Nonequidiffusive

Premixed Flames in Counterflow", *Combustion and Flame*, **106**, 168-183.

Sung C.J., Law C.K. (1996) "Extinction Mechanism of Near-Limit Premixed Flames and Extended Limits of Flammability", *Proceeding of the Combustion Institute*, **26**, 865.

Takeno T., Ishizuka S. (1986a) "A Tubular Flame Theory", *Combustion and Flame*, **64**, 83-98.

Takeno T., Nishioka M., Ishizuka S. (1986b) "A Theoretical Study of Extinction of a Tubular Flame", *Combustion and Flame*, **66**, 271-283.

Talbot L., Cheng R.K., Schefer R.W., Willis D.R. (1980) "Thermophoresis of Particles in a Heated Boundary Layer", *Journal of Fluid Mechanics*, **101**, 737-758.

Takagi T., Xu Z. (1994) "Numerical-Analysis of Laminar Diffusion Flames – Effects of Preferential Diffusion of Heat and Species", *Combustion and Flame*, **96**, 50-59.

Takagi T., Xu Z., Komiyama M. (1996a) "Preferential Diffusion Effects on the Temperature in Usual and Inverse Diffusion Flames", *Combustion and Flame*, **106**, 252-260.

Takagi T., Yoshikawa Y., Komiyama M., Kinoshita S. (1996b) "Studies on Strained Non-Premixed Flames Affected by Flame Curvature and Preferential Diffusion", *Proceeding of the Combustion Institute*, **26**, 1103-1110.

Tien J.H., Matalon M. (1991) "On the Burning Velocity of Stretched Flames", *Combustion and Flame*, **84**, 238.

Wehrmeyer J.A., Osborne R.J., Mosbacher D. M., Cheng Z., Pitz R.W., Sung C.J. (2001) "Investigation of Partially Premixed Propane-Air Flames with Flame Curvature", 39th AIAA Aerospace Sciences Meeting and Exhibit, Reno, NV, 8–11 January, 2001, AIAA paper No. 2001-1083.

Wehrmeyer J. A., Cheng Z., Mosbacher D. M., Pitz R. W., Osborne R. J. (2002) "Opposed Jet Flames of Lean or Rich Premixed Propane-Air Reactants Versus Hot Products", *Combustion and Flame*, **128**, 232.

Williams F.A. (1975) "A Review of Some Theoretical Considerations of Turbulent Flame Structure", *AGARD Conference Proceedings*, **164** Paris, II 1-25.

Williams F.A. (1985) *Combustion Theory*, 2nd ed., Addison-Wesley, Menlo Park, CA.

Wu C.K., Law C.K. (1984) "On the Determination of Laminar Flame Speeds from Stretched Flames", *Proceedings of the Combustion Institute*, **20**, 1941.

Yamamoto K., Ishizuka S., Hirano T. (1994) "Effects of Rotation on Stability and

Structure of Tubular Flame", *Proceedings of the Combustion Institute*, **25**, 1399-1406.

Yamamoto K., Hirano T., Ishizuka S. (1996) "Effect of Pressure Diffusion on the Characteristics of Tubular Flames", *Proceedings of the Combustion Institute*, **26**, 1129-1135.

Yoshida K., Takagi T. (1998) "Transient Local Extinction and Reignition Behavior of Diffusion Flames Affected by Flame Curvature and Preferential Diffusion", *Proceedings of the Combustion Institute*, **27**, 685-692.

Yoshida K., Takagi T. (2003) "Structural Studies of Locally Strained Diffusion Flames", *JSME International Journal Series B – Fluids and Thermal Engineering*, **46**, 190-197.

Yuan S.W., Finkelstein A.B. (1956) "Laminar Pipe Flow with Injection and Suction Through a Porous Wall", *Transactions of ASME*, **78**, 719-724.